A PZT-coated cantilever for simultaneous sensing and actuating in dynamic testing of structures

Wang, Deyang

2007

Wang, D. Y. (2007). PZT-coated cantilever for simultaneous sensing and actuating in dynamic testing of structures. Doctoral thesis, Nanyang Technological University, Singapore.

https://hdl.handle.net/10356/6555

https://doi.org/10.32657/10356/6555

A PZT-COATED CANTILEVER FOR SIMULTANEOUS SENSING AND ACTUATING IN DYNAMIC TESTING OF STRUCTURES

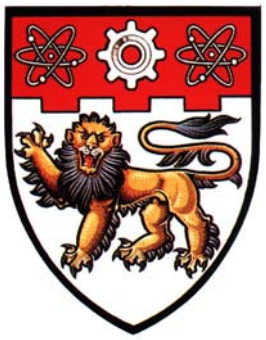

Submitted by

WANG DEYANG

School of Mechanical & Aerospace Engineering

NANYANG TECHNOLOGICAL UNIVERSITY

2007

A PZT-COATED CANTILEVER FOR SIMULTANEOUS SENSING AND ACTUATING IN DYNAMIC TESTING OF STRUCTURES

Submitted by

WANG DEYANG

School of Mechanical & Aerospace Engineering

NANYANG TECHNOLOGICAL UNIVERSITY

A thesis submitted to Nanyang Technological University

in partial fulfillment for the requirement of

Doctor of Philosophy

2007

ABSTRACT

Pseudo mechanical impedance, as one of frequency response functions, characterizes the dynamic behavior of a mechanical system and is useful for applications for applications such as modal testing, mechanical design, vibration monitoring and control, structural coupling and theoretical model modifications. Dynamic measurement of impedance, however, is difficult to be practiced for miniature or micro systems because of the very limited space available to install actuators and sensors and very large loading effects introduced by these transducers. To overcome the difficulties, simultaneous sensing and actuating (SSA) technique, which utilizes an existing or newly introduced actuator for sensing simultaneously, could be of use.

The aim of this research is to design a PZT-coated cantilever utilized as a transducer for simultaneous sensing and actuating in dynamic testing of miniature or microscale structures. In the study, the cantilever is viewed as an electromechanical system having a single electrical input port and a single mechanical output port. The relationship between the input electrical variables and output mechanical variables is then described by a two by two matrix. This matrix, termed as transduction matrix, completely characterizes the forward actuating and backward sensing functions of the cantilever transducer. Utilizing the transduction matrix, the mechanical impedance at the output port can be evaluated from the electrical impedance measured at the input port. As such, the cantilever transducer performs both actuating and sensing simultaneously in a dynamic testing of structures.

In this thesis, dynamics of a PZT-coated cantilever transducer was thoroughly studied firstly and the possibility of cantilever transducer for mechanical impedance measurement is also investigated numerically. The transduction matrix of cantilever transducer is firstly

obtained by solving the coupled equations governing the piezo-electric-mechanical behavior of the cantilever in close form. Next, to explore the potential of the proposed transducer, the obtained transduction matrix is utilized in a numerical experiment where the mechanical impedance at the tip of a test cantilever beam was simultaneously measured while excited by a cantilever transducer. After that, an optimization strategy was created and carried out to achieve the best performances of cantilever transducer for simultaneous sensing and actuating. Numerical simulation shows that the designed cantilever transducer is a good actuator with relative high sensitivity, which validates the optimization strategy.

Furthermore, experimental study has been done to examine the proposed optimization. Before use, calibration of cantilever transducer is necessary, which the transduction functions are obtained numerically and experimentally. After that, case studies including rigid block and beam structure are successfully carried out, which confirm the capability of designed cantilever transducer for simultaneous sensing and actuating. In order to further explore the applicability of the optimization, finally, a mini cantilever is designed and utilized to drive and sense mini dynamic systems. After the performances and transduction functions of the designed transducer are numerically analyzed and experimentally calibrated respectively, the feasibility of the proposed transducer for mechanical impedance measurement of mini structures is demonstrated experimentally. The detected experimental results agree well with the numerical results obtained by the finite element simulation, which examines the applicability of the design method.

In general, a PZT-coated cantilever has been successfully developed for best simultaneous sensing and actuating in dynamic testing of structures. Through the dynamic modeling, optimization design, numerical simulations and experimental studies, it is shown that the resulted prototype cantilever performs well in measuring mechanical impedance of miniature or micro scale structures.

ACKNOWLEDGEMENT

I would like to express my sincere appreciation to my doctoral supervisor, Professor Dr Ling Shih-Fu, for his invaluable advice and guidance and constant support and encouragement throughout my study and research.

Acknowledgements are also extended to Dr Fu Lianyu, Ms Yin Yanling, Dr. Liang Fenggang, Ms Lu Bei, Ms Hou Xiaoyan and other members of our research group, for their kind help, support and useful discussions; Thanks also go to all staff members, students and technicians in the Center for Mechanics of Micro-Systems (CMMS) and Mechanics of Machines (MOM) Lab, for their termless support; Gratitude is also given to Nanyang Technological University, for awarding full Research Scholarship to support the author's studies.

Finally, I am grateful to my beloved family, especially my parents, my wife and my brother, for their understanding, encouragement, and unconditional support.

TABLE OF CONTENTS

LIST OF FIGURES

LIST OF TABLES

LIST OF SYMBOLS

$[B_f], [B_q]$	force matrices
$[C_p]$	piezoelectric capacitance matrix
c_{11}^E	elastic modulus
d	piezoelectric constants
E	voltage or Young's modulus
$\{E\}$	potential vector
e_{in}, e_{out}	input and output effort
F	force
$\{F\}$	force vector
$\overline{F}$	mean value of output force over a specified frequency range
f_{in}, f_{out}	input and output flow
I, i	current
K	sensitivity
$[K_p]$	stiffness matrix for piezoelectric patch
$[K_s]$	stiffness matrix for the structure
L	length
$[M_p]$	mass matrix for piezoelectric patch
$[M_s]$	mass matrix for the structure

P_{in}, P_{out}	input and output power
$\{q\}$	charge vector
$\{r\}$	generalized displacement coordinates of the assumed modes
T	thickness
$[T]$	transduction matrix
$\|T\|$	determinant of transduction matrix
t_{11}	transfer function of voltage to force
t_{12}	transfer function of current to force
t_{21}	transfer function of voltage to velocity
t_{22}	transfer function of current to velocity
V, v	velocity
W	width
Y	admittance
Z_A	transducer output impedance
Z_e	electrical impedance
Z_{ec}	electrical impedance of SSA transducer under clamped condition
Z_{ef}	electrical impedance of SSA transducer under free condition
Z_m	mechanical impedance
Z_{mo}	mechanical impedance of SSA transducer under open-circuited condition
ε	dielectric constants
$[\Phi]$	eigenvector
$[\Theta]$	electromechanical coupling matrix
ρ	density
υ	Poisson's ratio
ω_n	natural frequency
ξ	damping ratio
ψ	energy efficiency
$\psi_n(x)$	assume mode function

CHAPTER 1

INTRODUCTION

1.1 Background

Point mechanical impedance, as one of frequency response functions (FRFs), characterizes the dynamic behaviour of a mechanical system and does not change with external excitation. It is defined as the ratio of the exciting force at one point to the velocity at the same point of system [1, 2]. It is measured for purposes such as material characterization, structural identification or health monitoring under dynamic excitations [3]. Due to its extensive applications, point mechanical impedance of various structures has been widely investigated in both theoretical modelling and experimental studies.

The most common way to measure mechanical impedance is to excite the structure using an actuator and measure the excitation force and responded motion by a load cell and an accelerometer respectively[4]. In this conventional measurement system, three transducers including exciter, force sensor and accelerometer, are needed. In the process, the measurement accuracy is often affected by the loading effects introduced by these devices.

In addition, installing the exciter and the sensors onto structures on site and ensuring true driving-point measurement are another two big problems to be overcome. When measuring mechanical impedance of miniature or micro scale structures, conventional sensors introduce excessive loading effect which causes big errors. Besides these, the installation of the conventional transducers becomes very difficult or impossible due to the very limited available space. Although the availability of Laser Doppler Vibrometer (LDV) makes it easier to obtain the response of small systems, the space required for actuators and its associated force transducers remains a major obstacle to applying conventional dynamic testing techniques to miniature or micro scale systems.

In addition to the above method using conventional transducers, in the last decade, researchers have devoted to developing transducers for mechanical impedance measurement using piezoelectric materials. For instance, Liang and his group utilize one or more PZT patches to obtain FRFs of structures based on the coupling of electro-mechanical impedance between piezoelective materials and structures [5-7]. Variation of the mechanical impedance of the structure is evaluated by measuring and comparing the electrical impedance of PZT. A one-dimensional model governing the electro-mechanical coupling was successfully developed. In these approaches, however, piezoceramic material patches are permanently bonded on or embedded into structure under test and cannot be moved or detached without destroying the structure. In order to provide strong enough excitation or to accurately sense the motion response, the contact area between the bonded PZT patches and the host structure can not be too small. However, big contact area hardly produces a point measurement. The measured results are only the average of the mechanical impedance over the area. Besides, this method relies on the closed-form

analytical solutions of the structural impedance, which often needs a complex process to be determined. Therefore, in applications, the method introduced is not only difficult to apply, but most significantly, calibrating the measurement system is inherently impossible due to the constitution of the measurement system.

As described above, existing methods and equipments are inconvenient and sometimes inaccurate in measuring mechanical impedance. New transducers and sensing techniques for mechanical impedance measurement are required. In the past decade, simultaneous sensing and actuating (SSA) technique has been developed for such purpose[8-10]. As we known that electromechanical actuators convert electrical into mechanical power in order to drive an attached mechanical system. Because of internal electromechanical interaction, the voltage and current at the input ports of these actuators vary if load driven by the transducer at the output port changes. If the relationship between the input variables and the output variables is made known, we then can obtain the output mechanical variables by detecting the input electrical variables. Among the input electrical variables and the output mechanical variables, four frequency response functions exist and together form a two-by-two matrix. This matrix completely characterizes the forward actuating and backward sensing functions of the cantilever transducer and thus is termed a transduction matrix. Using the transduction matrix, the mechanical impedance at the output port can also be evaluated from the electrical impedance measured at the input port. As such, mechanical impedance measurement is then turned to electrical impedance measurement, which is very convenient to achieve. An electromechanical transducer, therefore, performs both actuating and sensing simultaneously, eliminating or reducing the difficulties discussed earlier.

1.2 Objectives and Scope

Facing the above problems, means of transducer for simultaneous sensing and actuating should be developed. The focus of the research work is to design a PZT-coated cantilever utilized as a transducer for simultaneous sensing and actuating in view of its potential applications in dynamic measurement of miniature or microscale system. After dynamics of the cantilever transducer have been thoroughly studied, an optimization will be carried out to improve the performances of cantilever transducer for best simultaneous sensing and actuating. The improved cantilever transducer will then be realized and utilized to measure mechanical impedance of mini systems of interest. Hence, the scope of this research can be summarized in the following aspects.

1. Modelling and characterizing a PZT-coated actuating cantilever for sensing simultaneously.

2. Validating the feasibility of cantilever transducer in detecting mechanical impedance of system, which is excited by the cantilever transducer simultaneously.

3. Investigating and determining performance indices indicating sensing and actuating capability of cantilever transducer.

4. Optimizing cantilever transducer for best simultaneous sensing and actuating.

5. Verifying the validity of proposed optimization by numerical simulation and experiments.

6. Designing a mini cantilever transducer for mechanical impedance measurement of mini system and experimentally examining the applicability of optimization.

1.3 Outline of the Thesis

To trace the recent development on methods or techniques for measuring mechanical impedance, some representative works on relevant scientific literature are reviewed in Chapter 2. Introduction of mechanical impedance and its extensive application will be briefly presented. Followed by conventional methods for detecting mechanical impedance of system of interest. Disadvantages or difficulties of above methods for mechanical impedance measurement will be also discussed. A simultaneous sensing and actuating (SSA) method, which utilizes actuator for sensing simultaneously, is then introduced to overcome these difficulties. Furthermore, simultaneous sensing and actuating technique based on transduction matrix is reported. Newly developed SSA transducers utilizing transduction matrix to convert mechanical impedance measurement into electrical impedance measurement are listed and applications of transduction matrix are also reported in detail.

In Chapter 3, dynamics of a PZT-coated cantilever utilized as a transducer for simultaneous sensing and actuating is investigated because of its potential applications in dynamic measurement of miniature or micro systems. In this study, the cantilever is viewed as an electromechanical system with an electrical input port and a mechanical output port. Among the input electrical voltage and current and the output mechanical force and motion at the output port, four frequency response functions exist and together

form a two-by-two matrix. This matrix is termed a transduction matrix as it completely characterizes the forward actuating and backward sensing functions of the cantilever transducer. To derive the four components of the transduction matrix, the coupled equations governing the piezo-electric-mechanical behavior of the cantilever are solved in close form. It is then proved that the determinant of the matrix is in general unity, as it should be for linear and reciprocal dynamic systems without internal energy generation and consumption. To explore the potential of the proposed transducer, the obtained transduction matrix is then utilized in a numerical experiment where the mechanical impedance at the tip of a test cantilever beam was simultaneously measured while excited by a PZT-coated cantilever.

As the characteristics of the cantilever transducer have been thoroughly studied, performance indices indicating sensing and actuating capability of cantilever transducer, such as sensitivity, effective dynamic frequency range, energy efficiency, output force, and so on, will be investigated and determined in Chapter 4. Based on this, an optimization will be carried out to improve the capability of the cantilever transducer utilizing these performance indices to balance its sensing and actuating capability. A comparison of performances between the new and original cantilever transducer will then be done by numerical simulation.

To verify the validity of the proposed optimization, furthermore, experimental studies will be described in Chapter 5. A cantilever transducer will be designed by the proposed optimization strategy and then utilized in the experiments for the mechanical impedance measurement. Before the cantilever transducer is used, calibration of cantilever transducer

is necessary and a method, which selects several rigid masses as the load of cantilever transducer, will be proposed to calibrate the intrinsic attributes Z_{mo}, Z_{ec} and Z_{ef}. In the calibration, Z_{ef} will be measured directly from the SI Impedance Analyzer, when the transducer is under free condition. The other two impedances Z_{mo} and Z_{ec} will be evaluated by the proposed method and all these experimental results will be compared with the numerical results evaluated from the equations derived in Chapter 3. After calibration, case studies including rigid block and beam structure will then be carried out to further verify the feasibility of the designed cantilever transducer in mechanical impedance measurement and the validity of the optimization method.

To further explore the applicability of the optimization, in Chapter 6, a mini cantilever will be realized and utilized to drive and sense mini dynamic systems. Firstly, dimensions and system parameters of a cantilever transducer will be derived through the optimization. Followed, numerical simulation will be carried out to analyze the performances of the designed transducer and the transducer will be calibrated experimentally. Transduction matrix of the cantilever transducer calibrated experimentally will be compared to that obtained by numerical methods. After that, the mini cantilever transducer will be utilized to drive a hard disk suspension beam and detect its mechanical impedance by measuring input electrical impedance through obtained transduction matrix. The feasibility of proposed transducer for mechanical impedance measurement of mini structures will then be demonstrated experimentally.

Finally, conclusions of the thesis and recommendations related to the current research topic are given in Chapter 7.

CHAPTER 2

LITERATURE REVIEW

In this chapter, literature review in four areas will be presented. Firstly, mechanical impedance and its extensive applications are introduced briefly. Followed, conventional methods for detection of mechanical impedance are reviewed. After that, disadvantages or difficulties of above methods for mechanical impedance measurement are summarized. To overcome these difficulties, simultaneous sensing and actuating (SSA) method, which utilizes actuator for sensing simultaneously, are reported in the following section. Beside these, a SSA method based on transduction matrix proposed by Prof. Ling's group is presented. Application of this technique and newly developed transducers for such purpose are also discussed. However, sensing and actuating capability of the SSA devices are not studied in their works. In order to further explore the performances of proposed transducers, a PZT driven actuating cantilever for sensing simultaneously is selected for investigation because of the convenience of making it in miniature or micro dimensions.

2.1 Introduction

There are many different definitions of transducers in use. A transducer is a device that converts energy from one form into another [11-13]. A transducer is defined as a multiport device in which the input impedance(s) is (are) not equal to the output impedance(s) [14]. The gist of this definition is pictured in Figure 2.1 below, in which a 2-port device is considered. The transducer has at least two locations or ports at which it exchanges energy with the environment. The power at each port is defined by two variables, such as a current and a voltage for an electrical port or a velocity and a force for a mechanical port. The ratio analogous to the electrical impedance (voltage to current) is defined as the impedance. In a transducer with more than two ports, there would be multiple input ports and/or multiple output ports, but the port impedances would be different for each port.

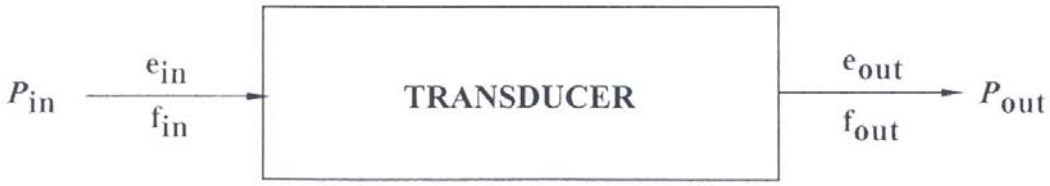

Fig. 2.1 Generic view of a transducer

Transducers may generally be divided into two classes [15]: sensors and actuators. Sensors and actuators are comprehensive classes of transducers, i.e., any transducer in operation is functioning at any given moment either as a sensor or as an actuator. Some transducers can operate as a sensor or as an actuator, but not as both simultaneously. Such transducers are said to be reversible. A typical example is a loudspeaker (actuator), which can be used to sense motions of the speaker diaphragm. Another example of a reversible

transducer is an accelerometer, which is designed to sense vibration, but can be used as a shaker.

Sensor is a device that detects or measures a physical quantity, and monitors a parameter of a system without disturbing that parameter. Actuator converts a signal (usually electrical) to some action, usually mechanical. It is a device, which impose a state on a system, hopefully independent of the load applied to them. In order to minimize the loading effect of sensor on the test system, the size and energy exchange of the sensor usually must be minimized. On the contrary, it is also impossible to achieve the ideal of a load-independent actuator, because there is always a load from the system under testing to the actuator. The desire to minimize the influence of this loading effect leads to large and high-power actuator. The discussions above make it clear that two major practical distinctions between sensors and actuators are the power level involved and the size required. These distinctions have made people think that it is difficult to build a transducer which functions well as both a sensor and an actuator at the same time.

However, taking advantages of the loading from the test system to the actuator, it is possible to “sense” the properties of the system from the input variables of the actuator so that the actuator functions both actuating and sensing simultaneously [16-21]. This chapter will concentrate on such transducers.

2.2 Concept of Impedance

Impedance is a characteristic property of any structures. Electrical impedance spectroscopy (EIS) has been recently applied in the medicine and biotechnology domain. Pseudo mechanical impedance characterizes the dynamic behavior of a structure under test and has been widely used to determine the dynamic response of systems and structural modal analysis [22-28]. The impedance method of analyzing the dynamic response of active material systems can be simply described: the interactions between actuators and structures are governed by the dynamic output characteristics of the actuators and the dynamic characteristics of the structure, i.e., the structural impedance [1, 2]. It is defined as the ratio of the exciting force at one point to the velocity at the same or another point of the same structure.

The impedance concept is widely used in the study of mechanical systems [1,2,7] [29, 30]. Impedances have a very important advantage in that they permit one to treat complex configurations relatively simply as elements of mechanical circuits. Such circuits are often very convenient, since they enable one to discern the important characteristics of a given system at a single glance. It is measured for purposes such as material characterization, structural design or health monitoring and thus, its improvements are a powerful design tool for function improvement and quality monitoring of structures under dynamic excitations [31].

Rossi et al. [32] has applied the impedance approach to study the dynamic response of one dimensional cylindrical ring structures. It is very convenient to apply the impedance method to study the structural dynamic response if the structural impedance of the ring is determined from the equation of motion of cylindrical structures.

In Gardonio's paper [30], the concept and evolution of impedance methods in structural dynamics is presented. The authors use these methods in most of their research work involving, for example, passive/active vibration control, structural acoustics problems, and rotor dynamics problems. They have found that there is only patchy treatment of the impedance mobility and approaches in many textbooks and in contemporary literature, and yet the approach is very powerful. An account of the conception and early development of mobility and impedance methods in structural dynamics is presented in that paper. A large number of papers and reports reviewed have indicated that the origin of the mechanical impedance concept was inspired by the work done by scientists at the end of 19^{th} century for electrical systems.

At present, there is still research in progress for characterization of impedance/mobility parameters of distributed flexible mechanical systems. In particular, much work is being carried out for the analysis of systems composed by one- or two-dimensional flexible systems (beams, plates and shells) connected along line or surface junctions[22-28].

2.3 Conventional Methods for Impedance Measurement

As described above, pseudo mechanical impedance, as one of frequency response functions, characterizes the dynamic behaviour of a mechanical system and its improvements are thus a powerful design tool for function improvement and quality monitoring of structures under dynamic excitations. An overview of relevant knowledge

and research about measurement of mechanical impedance, thus, will be presented in the following section.

2.3.1 Measurement using Conventional Transducers

To measure mechanical impedance of dynamic structure, normally a powerful excitation to actuate the test structure and an accurate measurement of the excitation force and the response velocity at the point of interest are demanded [33-36].

The excitation applied to the structure can be basically classified into two types: contact and non-contact. Contact excitation involves the connection of an exciter which remains attached to the structure throughout the test. Mechanical exciters, electromagnetic shakers and electrohydraulic shakers all belong to this category. Each of them has its advantages and disadvantages. Non-contact excitation uses devices which are either out of contact throughout the vibration or which are only in contact for a short time period. Hammer, a popular and relatively simple exciter to create vibrations, belongs to this category.

In addition to a powerful excitation mechanism, sensors for measuring the excitation force and the motion response are essential for mechanical impedance measurement. To be precise, the force transducer must be in series with the structure, between the parts of the structure on either side of the connection. For such measurements we usually use a so-called impedance head attached to an electro-dynamic exciter. Such an impedance head

incorporates two sensors: one for measuring the force, and the other for measuring the velocity (or acceleration). Figure 2.2 illustrates such a device system.

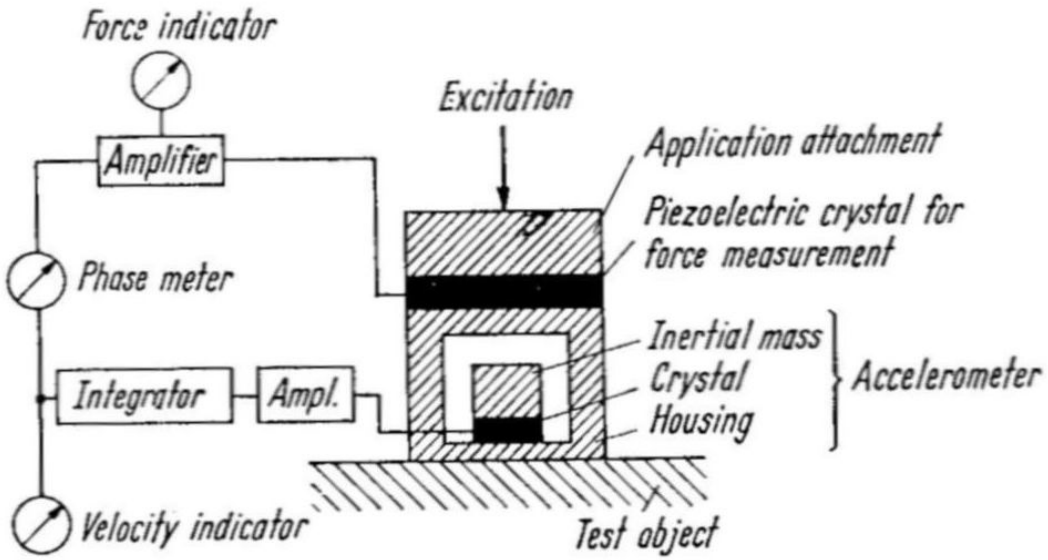

Fig. 2.2 Mechanical impedance measurement utilizing an impedance head [15]

The greatest problem associated with all impedance head measurements results from the effect of the apparatus on the quantity to be measured. Because the impedance head must be connected rigidly to the test object, it acts as part of the object. The connection between the test object and the impedance head is also of great importance. Great care must be taken to obtain a truly rigid connection and to ensure that only the desired components of motion are excited. Moreover, the size of the contact area also has an effect on the measurement. In principle, the contact area should be as small as possible, so that we may approach the “point-impedance” condition; however, needle-like impedance heads would have contact areas that are so small that they would sense only the test object’s local stiffness—which usually is of little interest.

Recently, there are many other developed devices available to measure the force and the motion. Nowadays, piezoelectric transducers are widely used for both types of measurement in the form of load cell, accelerometer and impedance head. Recently, lasers also become commonplace to provide a non-contact response transducer in the form of Laser Doppler Velocimeter (LDV) [4]. In the following, only one of the most widely used setup is addressed here as an illustration Figure 2.3. A common electromagnetic shaker is employed to excite the structure under testing; a load cell and an accelerometer are utilized to detect the excitation and the response. The load cell and the accelerometer can also be encapsulated into one housing, forming an impedance head. While, the working principles are basically the same.

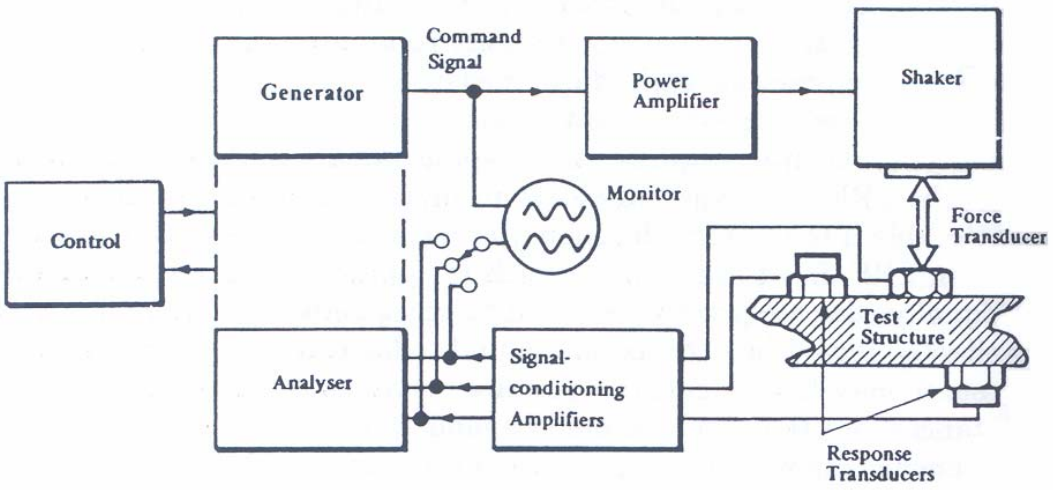

Fig. 2.3 General layout of FRF measurement system [4]

Shaker is utilized in this setup due to its easy availability. Its small size and high efficiency provides it with the capability to excite small structures at high frequencies [37-40]. One consideration concerning shaker is how to support or mount it on site. The general grounding requirement often poses inconvenience in experiments. In addition,

although it seems that shaker is capable of applying a force in one direction only, due to the fact that the motion of most practical structures is generally complex and multidirectional, an unwanted secondary form of excitation often exists. The usual solution is to attach the shaker to the structure via a driving rod or stinger which is assumed to be stiff in one direction while flexible in all other directions. However, if the stinger is too long or too flexible, big errors will be introduced into measurement. To supply strong enough vibrations, power amplifier is often necessary for a shaker.

Due to the working principles of force and response transducers showed in Figure 2.3, the heavier and larger of the transducers, the higher the sensitivity. However, the addition of even small transducers imposes unwanted loading effects to the structure, changing its dynamic properties. Such loading effects, including inertia loading and local stiffening, can't be completely compensated.

2.3.2 Measurement using Active Material

In the past two decades, many researches have been devoted to developing transducers using piezoelectric materials. Piezoelectric materials have many advantages that make them ideal for various actuators and sensors. They are capable of high resolution, zero friction, no wear and tear, achieving high resonant efficiency and fast response. They are also rugged, inexpensive, light-weight, space efficient, and easily shaped. Piezoelectric elements have been widely used as actuators and sensors in adaptive structures from beams and plates, to trusses and more complicated structures [31, 41-55]. Piezoelectric actuators are based on the inverse piezoelectric effect, through which the electrical energy

is converted into mechanical energy. For a piezoelectric actuator, typically the charge drawn on the electrodes in response to the driven voltage is ignored. On the other hand, piezoelectric sensors are based on the direct piezoelectric effect, through which mechanical energy is converted into electrical energy. For a piezoelectric sensor, the electrodes are essentially open-circuited or short-circuited to get a voltage or charge signal that can describe the measurand. The reversible transformational capability enables a piezoelectric element to be used as an actuator and a sensor simultaneously if both the drive voltage and the corresponding current are measured.

In 1994, an impedance method for dynamic analysis of active material systems has been developed by Liang, etc [22-26, 32, 56-62]. The impedance approach provides a straightforward approach to accurately determining the dynamic response of active material systems. In the impedance approach, the structural dynamic analysis and actuator electromechanical analysis are combined on the basis of matching structural and actuator impedance. To use the impedance model, one would only need the structural impedance at the actuator driving point (for single actuator cases), which may be calculated or measured without considering actuator-stiffening effect. On their work, variation of the mechanical impedance of the structure is detected by measuring the electrical impedance of PZT. A one-dimensional model governing the electro-mechanical coupling was successfully developed [6, 7]. The work proves the correctness of the concept.

In 1996, as part of the effort of making use of functional materials such as piezoelectric ceramics (PZT), C. A. Rogers and C. Liang [5] studied the electromechanical coupling of piezoelectric materials and structures. In their work, a pair of PZT patches were bonded

on or embedded permanently onto a structure. When the PZT patches were actuated out-of-phase, a pure bending moment excitation has been created along the edges of the PZT patches. In their work, a one-dimensional model governing the electromechanical coupling was developed. Their method provided a more accurate prediction of the force loading induced by the actuator than the static based model did. The novelty of their method is the combination of the electromechanical analysis of actuators and structural dynamic analysis of the host structure.

Later, Liang *et al.* extended the impedance modeling of the PZT patch actuator to multi-degree-of-freedom systems by addressing the dynamic modeling of an active beam. A pair of piezoelectric patches was collocated on both sides of the host cantilever beam. The equations of motion of the beam were first analytically developed and the corresponding solution was derived. The interaction between the host beam and the surface bonded piezoelectric actuators was then represented by pure line moments at the edges of the patches. Subsequently, the rotational impedance of the beam to line moments caused by the PZT patches was presented. Using similar procedure, Zhou *et al* [58] and Lalande [25, 26] applied the above approach to plate, shell and ring structures with surface bonded actuators.

In all the above papers by Liang and his team, it is important to note that to model the dynamic interaction between the surface-bounded PZT patch and the host structure, the impedance of the host structure has to be first determined by an analytical solution. In other words, this method relies on the closed-form analytical solutions of the structural impedance, which often needs a complex process to be determined. Therefore, in

applications, the method introduced is not only difficult to apply, but most significantly, calibrating the measurement system is inherently impossible due to the constitution of the measurement system.

2.3.3 Summary of the Conventional Methods

From the introduction above, we know there are a few methods/transducers for detection of mechanical impedance. The comparison of different measuring techniques are summarized and listed in Table 2.1.

Table 2.1 Comparison of conventional methods for mechanical impedance measurement

	Using conventional transducers	Using active material
Measurement system	Impedance head, shaker, load cell, accelerometer, conditioning amplifier, charge amplifier	Piezoelectric material patches are permanently bonded to the host structure
Inertia loading of the measurement system	The inertia loading from the conventional transducers are significant; Compensation of such loading is a complicated process.	Closed-form analytical solutions of the structural impedance are needed.
Difficulties	It's difficult to be practiced for miniature or micro systems because of the very limited space available to install actuators and sensors and the large loading effects introduced by these transducers.	It's difficult to apply for complex system. Calibrating the measurement system is inherently impossible due to the constitution of the measurement system.

As discussed above, existing methods and equipment are inconvenient and sometimes inaccurate in measuring mechanical impedance due to the large loading effects. In recent years, the trend of miniaturization in product design has introduced new problems in

measuring mechanical impedance [63]. The installation or accessing of the conventional transducers becomes very difficult or impossible due to the limited available space. Furthermore, the loading effects introduced by these transducers are often unsatisfactorily too big for any meaningful engineering measurement. Requirement for developing technique for impedance measurement is essential and imperative.

2.4 Simultaneous Sensing and Actuating (SSA) Method

Simultaneous sensing and actuating describes the technique of using a transducer to both actuate and sense concurrently. Compared to the traditional approach of using separate actuators and sensors, this technique can offer several advantages. A reduction in the number of sensing and actuation devices, and associated power, wiring and interfacing, immediately reduces cost and complexity. A self-sensed system can also offer increased robustness if an actuator can be used without sensors; it is generally noted that when a failure occurs in a sensor–actuator system, the fault is far more frequently due to sensor failure (or failure of related interfacing or wiring) than actuator failure.

Simultaneous sensing and actuating involves using a model of the actuator's behavior to estimate information about the actuator's state—e.g. position and/or force. Therefore it is a prerequisite that the actuator can be modeled. Simultaneous sensing and actuating is only possible if the actuator in question can act as both a sensor and actuator. That is to say that there must be some measurable parameter of the actuator that can provide sensing information. For example, electromechanical actuators convert electrical into mechanical power in order to drive a mechanical system attached to it. Because of internal electro-

mechanical interaction, the voltage and current at the input port of these actuators vary if the load driven by the transducer at the output port changes. Although actuators are in general designed large and powerful in order to keep the variations small and negligible, the variations of their input voltage and current still provide rich information about the load being driven. In order words, these actuators in principle are capable of doing sensing at the same time of actuating.

For decades, probing variations of the input current of induction motors for monitoring and diagnosis of motors and/or their driven mechanical systems have been under extensive study[64-66]. Rather than using delicate position sensors, the rotor position of brushless-dc and variable reluctance motors can be estimated by monitoring the motor voltage and current waveforms. No modifications are required of the motor itself. For instance, in Li's paper, on-line tool breakage detection of small diameter drills by monitoring the AC servo motor current is studied. In his work, a continuous wavelet transform was used to decompose the spindle AC servo motor current signal and the discrete wavelet transform was used to decompose the feed AC servo motor current signal in time–frequency domain. The tool breakage features were extracted from the decomposed signals. Experimental results show that the proposed monitoring system possessed an excellent on-line capability.

Another common industrial application of simultaneous sensing and actuating is electromagnetic levitation, which is often used to create non-contact "magnetic bearings"[67-70]. Simultaneous sensing and actuating is possible since the inductance of the electromagnetic coil varies measurably in relation to the size of the air gap between

the magnetic pole and suspended object. Using an alternating supply to the coil, it is possible to create a very simple, inherently stable magnetic levitation circuit.

Simultaneous sensing and actuating is also particularly suitable for devices where the addition of sensors is not feasible due to their size and mass. For example in audio loudspeakers, sensors would be impractical since their mass would significantly impede the dynamic response of the cone, and the cost would be prohibitive. Instead, the speaker's behavior can be modeled and predicted by mathematical equations. It has therefore been possible to self-sense the cone velocity [71] and sound pressure produced [72]. It is predicted that simultaneous sensing and actuating will become an important part of micro-miniature devices. A form of position simultaneous sensing and actuating has been demonstrated on a 3mmlinear actuator [73].

More and more studies have been carried out to the possibility and application of self-sensing actuator utilizing smart materials[16, 18, 40, 48]. In 1990s, Hagood and Anderson investigated the possibility of using a single piezoelectric patch as both structural actuator and sensor simultaneously [74-77]. In their method, a PZT patch actuator bonded to a one-dimensional cantilevered beam was used as a collocated strain rate sensor. The dynamic governing equations for a cantilevered beam with piezoelectric inclusions were derived based on Hamilton's principle and discretized in a Rayleigh-Ritz formulation. For the electro-elastic system, its actuator and sensor equations were described as Eqs. (2.1) and (2.2).

$$\left([M_s] + [M_p] \right)\{\ddot{r}\} + \left([K_s] + [K_p] \right)\{r\} - [\Theta]\{E\} = [B_f]\{F\} \qquad (2.1)$$

$$[\Theta]^T \{r\} + [C_p]\{E\} = [B_q]\{q\} \tag{2.2}$$

Simultaneous actuating and sensing was implemented by combining signals proportional to both the voltage applied to the piezoelectric and the charge drawn across its electrodes. The transfer function from the applied input voltage to the measured strain rate was then developed. For their method, some important points should be noted [42]: Firstly, the piezoelectric patch is sensitive to multiple components of strain, thus this method is only suitable for structures with simple geometries. It is difficult to be applied for two-dimensional plate or more complicated structures. Secondly, the signal is proportional to the average strain state over the extent of the piezoelectric patch. Finally, the PZT patch is permanently bonded to the beam and cannot be moved without destroying the beam or the PZT.

As mentioned above, simultaneous sensing and actuating methods have many advantages in mechanical impedance measurement when it compares to the conventional methods. In such approaches, however, the methods can only provide the trend of dynamic behaviors of structure of interest and is hardly to obtain a quantitative value. In many applications, they are mostly not used for measurement but for condition monitoring.

2.5 SSA Method Utilizing Transduction Matrix

2.5.1 SSA Transducers Based on Transduction Matrix

In the past decade, Ling and his teams put forward this SSA technique for mechanical impedance measurement [78-101]. In their works, a two-by-two matrix is built and utilized to describe the relationship between the input electrical variables and output mechanical variables. As it completely characterizes the forward actuating and backward sensing functions of the SSA transducer, it is termed a transduction matrix. Utilizing such transduction matrix, the mechanical impedance at the output port can be evaluated from the electrical impedance measured at the input port. Thus, using this technique, measurement of mechanical impedance is converted to measurement of electrical impedance, which is easily to achieve. Besides, the output potential value and flow value are also quantitatively determined. Since then, the sensing capability of a number of newly designed transducers as well as existing actuators such as motors, speakers, and shakers, has been investigated. In this section, several newly designed transducers using this technique will be introduced in detail. And applications of this technique in many fields will be presented in the next section. Details about how transduction matrix functions are introduced in Chapter 3.

2.5.1.1 Piezoceramic Inertial Actuator

In 1998, a Piezoceramic Inertial Actuator (PIA) was designed to measure mechanical impedance and monitor structural integrity without involving conventional sensors like accelerometers, load cells or impedance heads [9,10] [82, 83, 91, 94, 95]. The structure of the Piezoceramic Inertial Actuator (PIA) designed by Ling *et al.* is shown in Figure 2.4. The proof mass, the aluminum plate, the PZT patch, and other necessary frame works constitute a Piezoceramic Inertial Actuator.

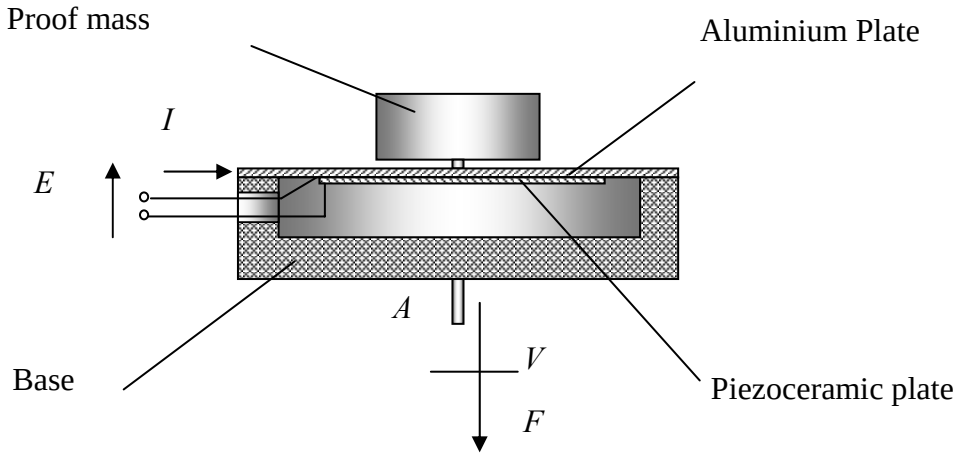

Fig. 2.4 Structure of a piezoceramic inertial actuator

When the actuator is attached to a host structure, there is an electromechanical interaction between the host structure and the actuator. In experiments, the actuator generated a reaction force to excite the test structure by accelerating an inertial mass. At the same time, the mechanical impedance of the structure was "senselessly" detected. Therefore, PIA functioned both actuating and sensing at the same time. A two-port model can model the actuator as shown in Figure 2.5, since the PIA is a linear dynamic transducer without internal energy generation or consumption.

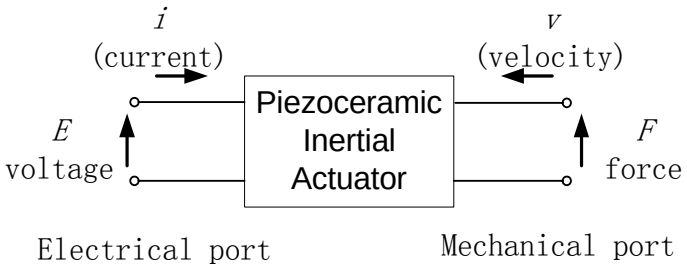

Fig. 2.5 Two-port model of PIA

The relationship between the input electrical voltage and current and the output mechanical force and velocity can be described by a transduction matrix,

$$\begin{Bmatrix} E \\ I \end{Bmatrix} = \begin{bmatrix} t_{11} & t_{12} \\ t_{21} & t_{22} \end{bmatrix} \begin{Bmatrix} F \\ V \end{Bmatrix} = [T] \begin{Bmatrix} F \\ V \end{Bmatrix} \tag{2.1}$$

[T] is named transduction matrix of the PIA and its four elements are complex transduction functions. In their research, they identify t_{11}, t_{12}, t_{21}, t_{22}, which are related with system parameters and frequency successful by experiment method. As we know that E and I are easy to measure compared with that of F and V. With known the E, I and the transfer matrix, F and V is easily calculated.

Figure 2.6 is schematic of measurement of mechanical impedance using PIA. In this experiment, the mechanical impedance of the beam at a point which is 1/6 of the beam span from the left end is first picked-up by an impedance head while a PIA servers as the exciter only at the same point [10]. Afterwards, the mechanical impedance at the same point is detected via the PIA as actuator and sensor simultaneously using above method. The measured and the “detected” mechanical impedance of the beam at the given location are compared and agreement is found between the two results. The validity of the above method “transduction matrix” and feasibility of PIA for mechanical impedance measurement are confirmed.

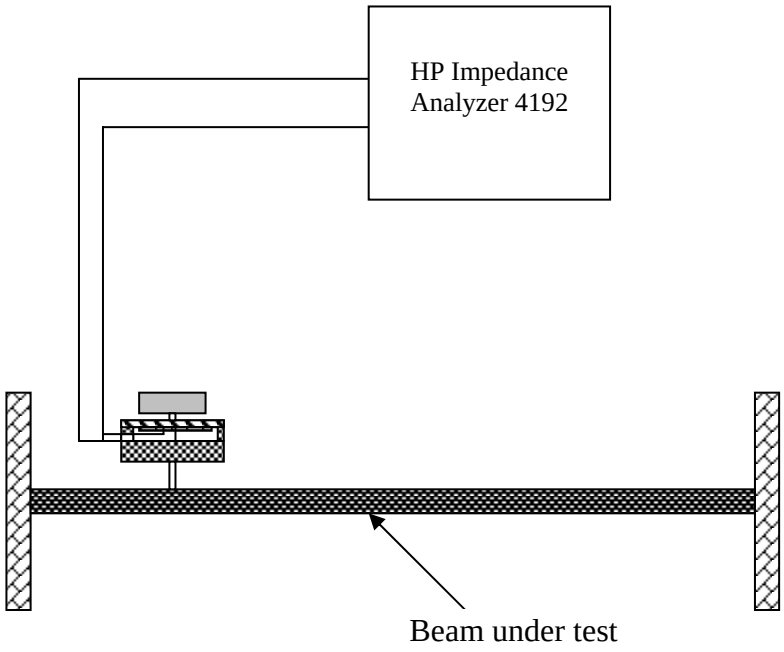

Fig. 2.6 Mechanical impedance detection by using a PIA

Furthermore, in 2001, the use of a PIA affixed to a structure as a collocated sensor cum actuator for monitoring structural integrity is also studied [9]. It's well understood that variations of the mechanical impedance directly indicates changes of structural properties, such as stiffness changes due to cracking, mass changes due to wearing, or changes of boundary conditions due to malfunctions of a coupling machine element. As revealed above, the input electrical impedance of a PIA attached to a structure is a sensitive function of the mechanical impedance of the structure at the attaching point. Therefore, any change of structural conditions due to problems of structural integrity, changes of supporting conditions, etc, can be detected by comparing the records of input electrical impedance of a PIA attached to a structure.

2.5.1.2 Electromagnetic Shaker

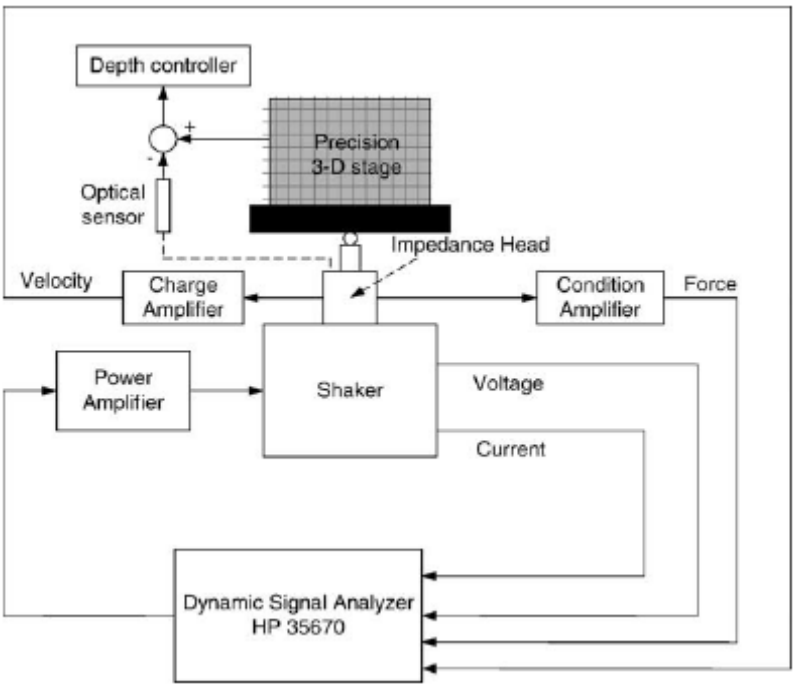

Fig. 2.7 Material characterization using a shaker as a sensor cum actuator

A study for utilizing electromagnetic shaker as SSA transducer is investigated by Yin and Ling in 2004 [8]. A small electromagnetic shaker together with an indenter fixed at its output end forms an electromechanical actuator which takes in ac electrical power and exerts dynamic indentation to the material specimen under testing as illustrated in Figure 2.7. When supplied with ac electrical power, a dynamic force was exerted to the specimen, indenting the ball to the specimen. At the same time, the input voltage and current of the shaker were measured, which contain information of the elastomer's vibration. A transduction matrix relating the input electrical voltage and current and the output force and velocity is calibrated experimentally. Since his transduction matrix neatly relates the mechanical impedance of the material with the electrical impedance measured at the input port of the actuator, the electromechanical transducer senses impedance simultaneously when actuating. Because no direct measurement of motion and force are required, this method posses advantages in testing miniature samples in situ and

development into a low cost handy tool for characterization of soft tissues, such as human skin is in progress.

Fig. 2.8 Portable shaker for characterizing mechanical property of human skin

Figure 2.8 shows the new designed portable shaker for testing mechanical property of human skin in vivo [88]. After characterizing the transduction matrix of shaker using a series masses, tests are done on three viscoelastic samples which are combined with two sets of silicon gels. Complex moduli and damping ratio of three samples are obtained which are with good coincidence with the results of DMA method. Furthermore, in her research, mechanical properties of human skin on different part of body have been measured on different subjects.

2.5.1.3 Bimorph Impedance Transducer

Since 2002, Hou and Ling designed a new Bimorph Impedance Transducer to accurately and conveniently measure both translational and rotational mechanical impedance [78]. The newly designed BIT contains two series bimorph cantilevers, as insulating layer and a rigid supporting block, as shown in Figure 2.9. The two bimorphs have identical

geometric and material characteristic and are symmetrically glued to the Glass Epoxide insulating layer, which effectively prevents the charge convection between the left and right bimorphs. The bottom of the insulating layer is tightly glued to the supporting block, which is made of Aluminum.

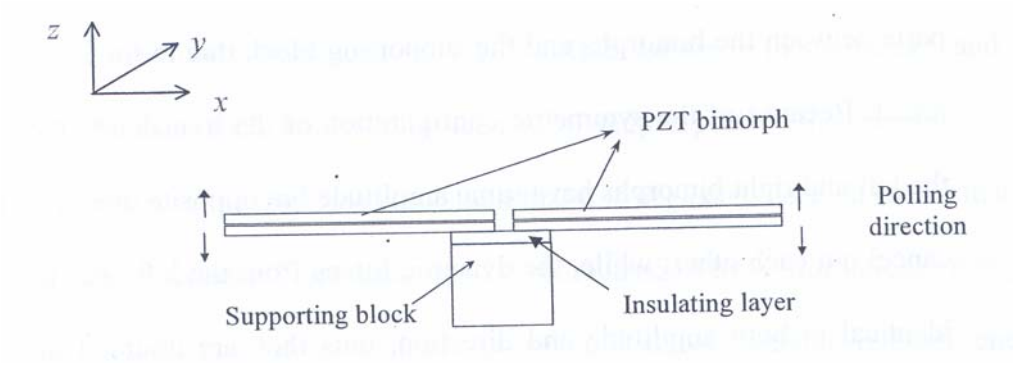

Fig. 2.9 Structure of bimorph impedance transducer

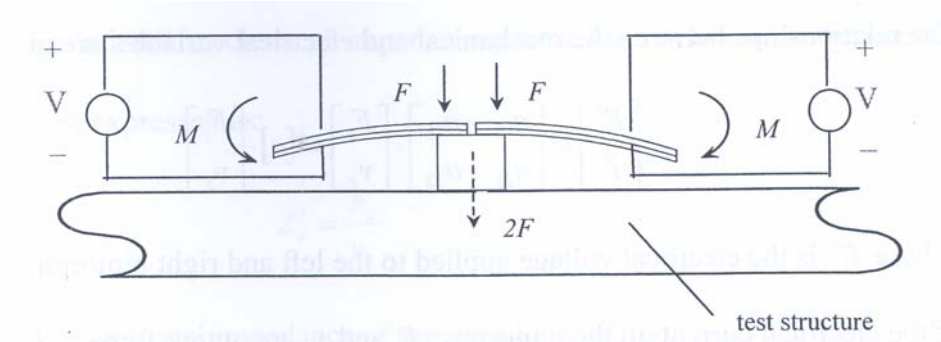

Fig. 2.10 Working principles of BIT for translational impedance measurement

As illustrated in Figure 2.10, if the left and right bimorphs are electrically connected in parallel, the ac electrical voltage supplied to the left and right bimorphs produces identical electrical fields. Hence the bimorphs bend upward or downward identically and

synchronously. Dynamic forces and moments are generated at the connecting parts between the bimorphs and the supporting block due to the inverse piezoelectric effect. Because of the symmetric configuration of the transducer, the moments from the left and right bimorphs have same amplitude but opposite direction, therefore they cancel out each other; while, the dynamic forces from the left and right bimorphs are identical in both amplitude and direction, thus they are doubled in magnitude and exerted to the tested structure through the supporting block. In this process, the BIT functions actuation.

At the same time of actuating, the response of the structure affects the motion of the transducer by introducing additional deformation to the piezoelectric bimorphs. The electrical impedance of the BIT changes due to direct piezoelectric effect. Therefore the information on flexural vibrations of the structure is embedded into the input electrical impedance of the transducer. It is possible to evaluate the translational impedance at the excitation point through measuring the input electrical impedance of the transducer. In this way, the transducer may perform sensing simultaneously.

In their works, the transducer functions actuating and sensing simultaneously during measurement, which the measurement of translational/rotational impedance is simply performed by measuring the input electrical impedance of BIT. After calibration of transduction matrix, BIT is utilized to numerically measure translational/rotational impedance of structures ranging from one-dimensional beam, two-dimensional plate, to rigid block. And measuring results are agreed with analytical results by ANSYS. Furthermore, experiments are also successfully carried out to further examine the validity

of BIT in translational and rotational impedance measurement. Finally, this transducer is utilized for characterizing linear viscoelastomers and magnetorheological elastomer.

2.5.2 Other Applications

Besides the transducers introduced above, this technique has been used in the fields of monitoring structural integrity, material characterization, monitoring wire bonding, measuring drilling torque, monitoring electrical discharge machining process and diagnosing welding process.

In 2001, Xie and Ling designed a piezo-driven cantilever for material characterization [95]. The device consisted of a metal cantilever beam and a piezoelectric patch bonded to the surface of the cantilever, as shown in Figure 2.11. An indenter affixed to the free tip of the cantilever served as the output point. It was a spherical ball controlled by a linear motor to indent the material at various depths and set the material specimens such as aluminum and polytene into vibrations. It was concluded that through measurement of electrical impedance of the PZT patch, the variations of material properties were correctly detected with good sensitivity. It was also qualitatively found that higher elastic modulus of the specimen and bigger indentation depth corresponded to greater shift in resonant frequencies of the electrical impedance. As an indentation method basically, this technique did not require specimen preparation as needed in tensile test. This sensorless testing also eliminated the needs of high-resolution force and displacement sensors usually needed in conventional tensile test.

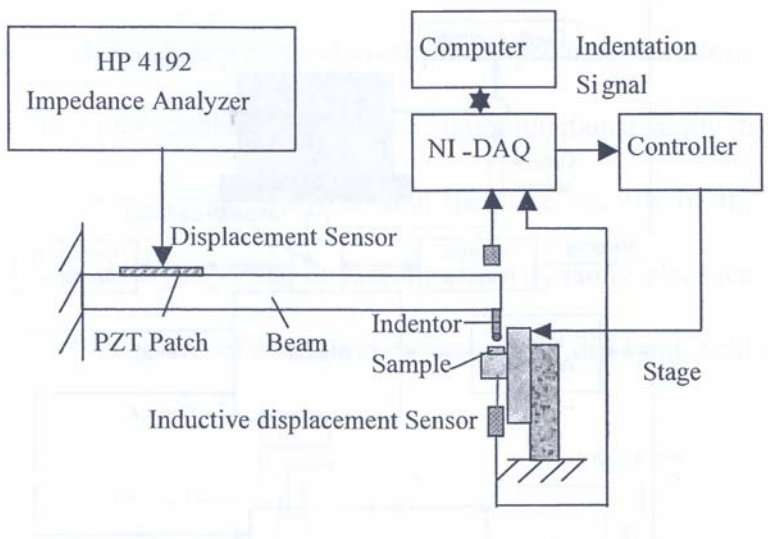

Fig. 2.11 Material characterization using a piezo-driven cantilever

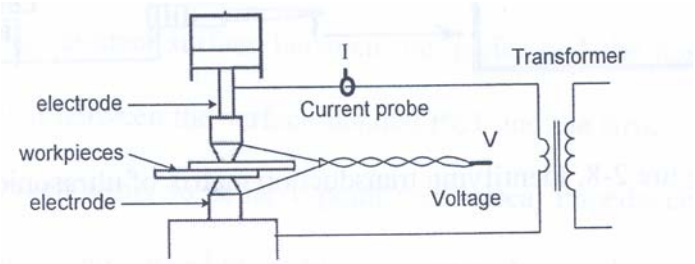

Fig. 2.12 A spot welding system

Due to its benefits and convenience, the simultaneous sensing and actuating (SSA) technique was utilized to monitor and characterize manufacturing processes. Ling and Wan applied this technique in monitoring the quality of resistance spot welding [96]. They developed a novel method to measure the variation of the input electrical impedance of a welding process through measuring the input current and voltage signals (Figure 2.12). The obtained real and imaginary parts of electrical impedance were found to represent the variation of the real electrical resistance and inductance along time in a welding process. Experimental studies proved that the time records of the resistance differ from what was

widely reported in literature as "dynamic electrical resistance", and faithfully reflect the phase of a welding process under different welding conditions.

When using SSA technique to study the mechanism of ultrasonic wire bonding process, the PZT-driven actuating mechanism of a wire bonder was viewed as an SSA device. A 2 x 2 transduction matrix was developed to correlate the electrical input variables (voltage & current) of the PZT driver to the mechanical output variables (force & linear velocity) at the tip of the capillary [97, 98]. The identification procedure was illustrated in Figure 2.13. After the transduction matrix was identified, the force and velocity at the tip of the capillary was obtained from the input voltage and current of the PZT driver. Consequently, mechanical impedance of the bonding interface where the bonding process occurs was in-situ detected derived in real time. Since this mechanical impedance was directly related with the variation of bonding mechanism, it was used to indicate the time varying material property in the bonding interface.

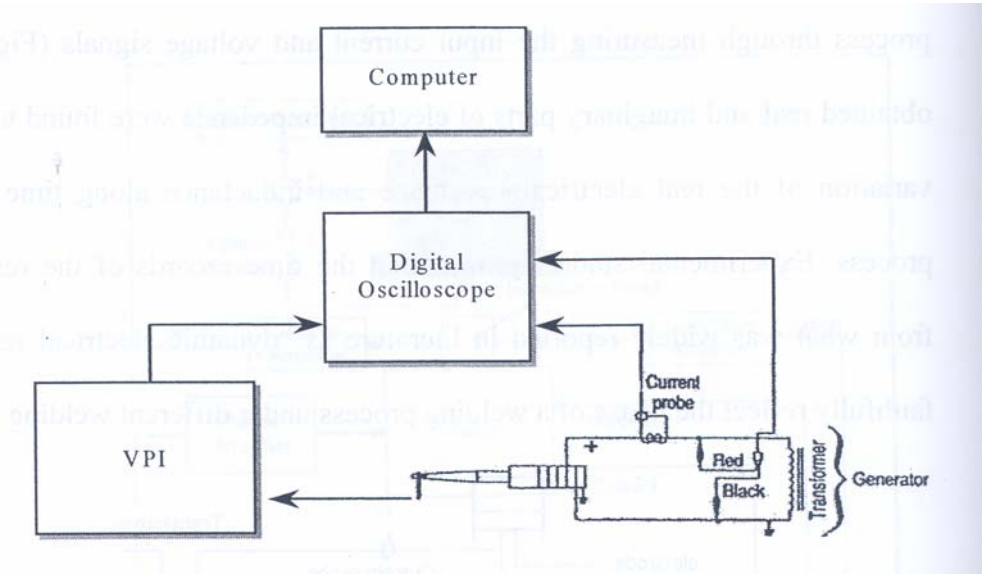

Fig. 2.13 Identifying transduction matrix of ultrasonic wire bonder

SSA technique was also applied to ultrasonic welding of thermoplastics, micro-drilling, measuring drilling torque and monitoring electrical discharge machining process, of which preliminary results could be found in some published papers.

In summary, it is concluded that SSA technique provides a neat and convenient way for FRF measurement. However, performances including sensing and actuating capability of the SSA transducers are not discussed in their works. In order to further explore the performances of proposed transducers, in the following chapters, a PZT driven actuating cantilever for sensing simultaneously is select for investigation because of the convenience of making it in miniature or micro dimensions. Since cantilever is the simplest flexural mechanism, building a PZT bonded cantilever with precise dimensions in mini scale or micro scale is technically feasible either through ultra-precision engineering means or via photolithograph based micro system technology.

CHAPTER 3

DYNAMICS OF A PZT-COATED CANTILEVER

The knowledge of transducers for mechanical impedance measurement presented in last chapter reveals that simultaneous sensing and actuating transducers have great advantages in this dynamic measurement. Also the possibility of PZT-coated cantilever utilized as such transducer for dynamic measurement has been preliminary investigated. In this chapter, the proposed simultaneous sensing and actuating (SSA) technique using transduction matrix will be discussed firstly and dynamics of PZT-coated cantilever will be studied in detail [104]. In the study, the cantilever is viewed as an electromechanical system with an electrical input port and a mechanical output port. Among the input electrical voltage and current and the output mechanical force and motion at the output port, four frequency response functions exist and together form a two-by-two matrix. This matrix is termed a transduction matrix as it completely characterizes the forward actuating and backward sensing functions of the cantilever transducer. To derive the four components of the transduction matrix, the coupled equations governing the piezoelectromechanical behavior of the cantilever will be solved in close form. It will then be proved that the determinant of the matrix is in general unity, as it should be for linear and reciprocal dynamic systems without internal energy generation and consumption. To

explore the potential of the proposed transducer, the transduction matrix obtained will be utilized in a numerical experiment where the mechanical impedance at the tip of a test cantilever beam is simultaneously measured while it is excited by a PZT-coated cantilever.

3.1 General Equations for Electro-Elastic System

For coupled electromechanical systems, the generalized form of Hamilton's principle can be written as

$$\int_{t_1}^{t_2} \left[\delta\left(T - U + W_e - W_m\right) + \delta W\right] dt = 0 \tag{3.1}$$

where

$$T = \int_{V_s} \frac{1}{2} \rho_s \dot{u}^T \dot{u} dV + \int_{V_p} \frac{1}{2} \rho_p \dot{u}^T \dot{u} dV \tag{3.2}$$

$$U = \int_{V_s} \frac{1}{2} S^T T dV + \int_{V_p} \frac{1}{2} S^T T dV \tag{3.3}$$

$$W_e = \int_{V_p} \frac{1}{2} E^T D dV \tag{3.4}$$

are the kinetic, strain and electrical energy, and the magnetic energy, W_m, is zero. The virtual work due to discrete applied point forces and charges is

$$\delta W = \sum_{i=1}^{nf} \delta u(x_i) \cdot f(x_i) - \sum_{j=1}^{nq} \delta \phi_j q_j \tag{3.5}$$

In equations (3.2-3.5), D(x) is a vector of electrical displacement, E(x) is a vector of electric field, S(x) is a vector of material strain, T(x) is a vector of material stresses, $\phi(x)$ is a scalar electrical potential, $u(x_i)$ is a vector of mechanical displacements, $f(x_i)$ is a vector of applied forces at x_i, and q_j is an applied charge at node j. The linear constitutive relations of the piezoelectric are

$$\begin{bmatrix} D \\ T \end{bmatrix} = \begin{bmatrix} \varepsilon^S & e \\ -e_t & c^E \end{bmatrix} \begin{bmatrix} E \\ S \end{bmatrix} \tag{3.6}$$

where the subscript *t* denotes a transpose of a material property matrix. The piezoelectric constants *e* and clamped dielectric coefficients ε^S can be expressed in terms of the more commonly used *d* matrix, the short circuit elastic stiffness matrix c^E, and the free dielectric coefficients ε^T:

$$e = dc^E, \qquad \varepsilon^S = \varepsilon^T - dc^E d_t \tag{3.7}$$

For the non-piezoelectric structure, $T = c_s S$ and

$$S = L_u u(x), \qquad E = L_\phi \phi(x) = -\nabla \cdot \phi(x) \tag{3.8}$$

where L_u is a differential operator for the particular elasticity problem and L_ϕ is a negative gradient operator.

Using a Rayleigh-Ritz formulation, the displacement and potential functions are expressed in terms of generalized co-ordinates as

$$u(x,t) = \Psi_r(x)r(t) = \left[\Psi_{r_1}(x)\cdots\Psi_{r_n}(x)\right]\begin{bmatrix} r_1(t) \\ \vdots \\ r_n(t) \end{bmatrix} \tag{3.9}$$

$$\phi(x,t) = \Psi_v(x)v(t) = \left[\Psi_{v_1}(x)\cdots\Psi_{v_m}(x)\right]\begin{bmatrix} v_1(t) \\ \vdots \\ v_m(t) \end{bmatrix} \tag{3.10}$$

where r_i is the generalized mechanical co-ordinate, v_i is the generalized electrical coordinate and Ψ is the mode shape function of the system. The strain and field terms may be expressed as basis functions multiplying the generalized co-ordinates,

$$S(x,t) = N_r(x)r(t) \quad \text{and} \quad E(x,t) = N_v(x)v(t) \tag{3.11}$$

where

$$N_r(x) = L_u\Psi_r(x), \qquad N_v(x) = L_\phi\Psi_v(x) \tag{3.12}$$

The equations of motion of the piezoelectric coupled electro-mechanical system can be derived by substituting Eqs. (3.2—3.5), (3.6) and (3.8) into Eq. (3.1), resulting in two matrix equations. These will be called the sensor and actuator equations of the electroelastic system and are the basis for a straightforward analysis of the simultaneous sensor/actuator problem.

$$\left(\left[M_s\right]+\left[M_p\right]\right)\{\ddot{r}\}+\left(\left[K_s\right]+\left[K_p\right]\right)\{r\}-\left[\Theta\right]\{E\}=\left[B_f\right]\{F\} \tag{3.13}$$

$$\left[\Theta\right]^T\{r\}+\left[C_p\right]\{E\}=\left[B_q\right]\{q\} \tag{3.14}$$

The mass matrices for the structure and the piezoelectric are defined by integrals over the volumes of the structure and piezoelectric respectively

$$M_s = \int_{Vs} \Psi_r^T \rho_s \Psi_r dV \tag{3.15}$$

$$M_p = \int_{Vp} \Psi_r^T \rho_p \Psi_r dV \tag{3.16}$$

where ρ represents density and the stiffness matrices (dropping the explicit spatial dependence of the integrands) are defined by

$$K_s = \int_{Vs} N_r^T c_s N_r dV \tag{3.17}$$

$$K_p = \int_{Vp} N_r^T c^E N_r dV \tag{3.18}$$

The piezoelectric capacitance matrix, C_p, and the electro-mechanical coupling matrix, Θ, are defined by

$$C_p = \int_{V_p} N_v^T \varepsilon^S N_v dV \tag{3.19}$$

$$\Theta = \int_{V_p} N_v^T e_t N_v dV \tag{3.20}$$

and finally the forcing matrices are defined by

$$B_f = \begin{bmatrix} \Psi_{r_1}^T(x_{f_1}) & \cdots & \Psi_{r_1}^T(x_{f_k}) \\ \vdots & \ddots & \vdots \\ \Psi_{r_n}^T(x_{f_1}) & \cdots & \Psi_{r_n}^T(x_{f_k}) \end{bmatrix} \tag{3.21}$$

$$B_q = \begin{bmatrix} \Psi_{v_1}^T(x_{q_1}) & \cdots & \Psi_{v_1}^T(x_{q_k}) \\ \vdots & \ddots & \vdots \\ \Psi_{v_m}^T(x_{f_1}) & \cdots & \Psi_{v_m}^T(x_{q_k}) \end{bmatrix} \tag{3.22}$$

For the standard case where an electrical coordinate is associated with the voltage on each piezoelectric electrode, $B_q = I$. Although a Rayleigh-Ritz form has been considered here, a finite-element based approach is not substantially different.

Equations (3.13) and (3.14) represent the general equations for an elastic body with piezoelectric material and arbitrary electrode arrangement and piezoelectric geometry. The actuator equations (3.13) are those typically used to model voltage driven piezoelectric actuators. Since the voltage is commanded across the piezoelectric the capacitance and other dynamics are ignored. The sensor equations (3.14) are typically used to find the voltage appearing across the piezoelectric when the structure is deformed. If there is no leakage and the electrodes are open circuited, then q is zero and the voltage appearing on the electrodes for a prescribed mechanical deflection is given by the sensor equation.

3.2 Actuator and Sensor Equations of a PZT-Coated Cantilever

In this section the general equations derived in the previous sections for the piezoelctrically coupled electro-mechanical systems will be applied to the simple cantilevered. Figures 3.1 and 3.2 detail the cantilever actuator under study. At an appropriate location, on one side of the cantilever a patch of PZT is bonded. Supplied with electrical power in z direction, the PZT patch expands and contracts in x-y plan due to inverse piezoelectric effect and in turn creates bending vibration of the beam. This PZT-

coated cantilever is utilized as an electromechanical actuator and viewed as a two-port system in which the electrical supply is the input port and the free end is the output port in the proposed method. When carrying out experiments, similarly to in conventional applications of shakers, a stinger should be utilized to link the output port of the transducer with the test object in order to ensure a single direction of exerted forces.

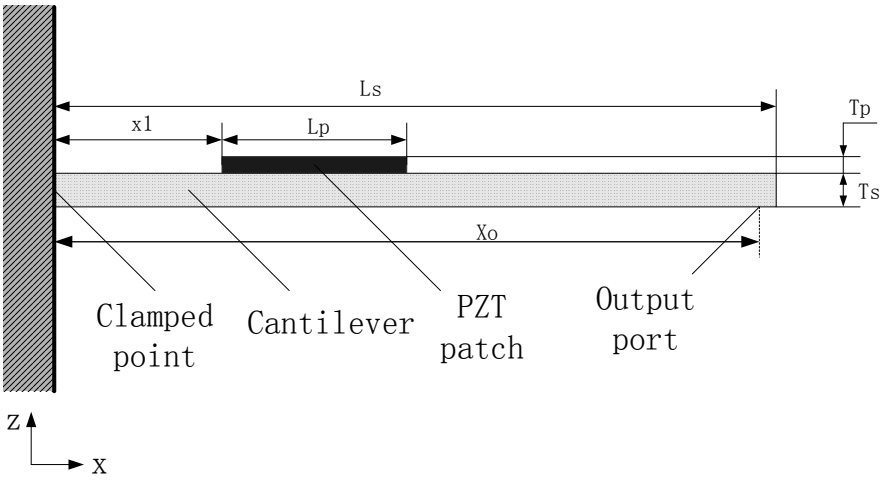

Fig. 3.1 Front view of PZT-coated cantilever

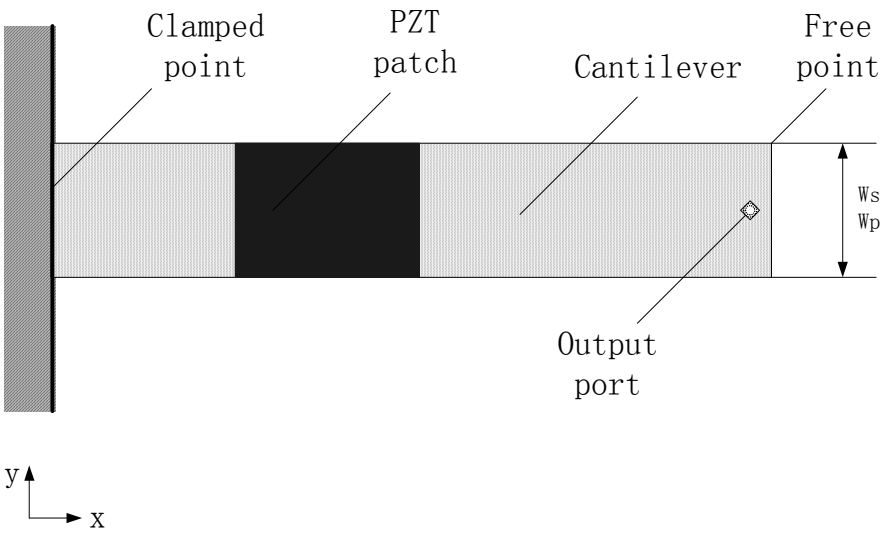

Fig. 3.2 Top view of PZT-coated cantilever

During actuating, the load to the actuator due to the test object affects the motion of the cantilever which causes further deformation to the PZT patch in addition to the original one. Due to direct piezoelectric effect, the voltage and current measured at the input port therefore contain both the electrical supply and response, and reflect the existence and properties of the object under testing.

At this stage, assumptions must be made regarding the differential operators to use in the formulation. The assumptions of a Bernoulli-Euler beam are made; and in addition, in order to increase the accuracy of the strain model within the piezoceramics, the condition that there is no stress through the thickness direction of the beam or the piezoceramics is enforced. The displacement operator can be modified within the beam and piezoceramic to enforce this stress free condition.

$$S = L_u u = \begin{bmatrix} 0 & 0 & -y\dfrac{\partial^2}{\partial x^2} \\ 0 & 0 & vy\dfrac{\partial^2}{\partial x^2} \\ 0 & 0 & 0 \\ 0 & 0 & 0 \\ 0 & 0 & 0 \\ 0 & 0 & 0 \end{bmatrix} \begin{bmatrix} u_1 \\ u_2 \\ u_3 \end{bmatrix} \tag{3.23}$$

where v is the Poisson's ratio of the structure or piezoceramic. It is assumed that the electric field is constant through the piezoceramic thickness, so the potential operator becomes

$$E = L_\phi \phi = \begin{bmatrix} 0 \\ 0 \\ -\dfrac{\partial}{\partial z} \end{bmatrix} \phi \tag{3.24}$$

At this point the designer must decide upon the shapes of the assumed displacement field and electrical potential. For the displacement field the first n cantilever beam exact mode shapes are used. The exact modes are adequate since the mass and stiffness distributions are close to being uniform. The displacement vector is then represented by

$$u = \begin{bmatrix} \psi_{r_1} & \cdots & \psi_{r_n} \end{bmatrix} \begin{bmatrix} r_1 \\ \vdots \\ r_n \end{bmatrix} = \Psi_r \cdot r \tag{3.25}$$

Similarly, the potential field within the piezoceramic can be represented in terms of the voltages.

$$\phi = \begin{bmatrix} \Psi_{v_1} \end{bmatrix} v_1 = \Psi_v \cdot v \tag{3.26}$$

This shape gives constant electric field in the first piezoceramic. The constant field assumption is good because the piezoceramics have uniform thickness, t_p, which is assumed thin enough to prevent significant fringe effects.

Substituting these matrices into Eqs. (3.15-3.22), the mass, stiffness, coupling and capacitance matrices for the system can be found. The mass, stiffness, coupling and capacitance matrices for the PZT-coated cantilever system can be found, which are given

in terms of integrals over the length of the cantilever [102]. The equations for these matrices are shown below:

$$M_s = \int_0^L A_s \Psi_r^T \rho_s \Psi_r \partial x \tag{3.27}$$

$$M_{pi} = \int_{a_{i1}}^{a_{i2}} A_{pi} \Psi_r^T \rho_{pi} \Psi_r \partial x \tag{3.28}$$

$$K_s = \int_0^L I_s (\Psi_r'')^T \hat{c}_s (\Psi_r'') \partial x \tag{3.29}$$

$$K_{pi} = \int_{a_{i1}}^{a_{i2}} I_{pi} (\Psi_r'')^T \hat{c}_{pi} (\Psi_r'') \partial x \tag{3.30}$$

$$\Theta_i = \int_{a_{i1}}^{a_{i2}} \frac{S_{pi}}{t_{pi}} (\Psi_r'')^T \hat{e}_{pi} \partial x \tag{3.31}$$

$$C_{pi} = \int_{a_{i1}}^{a_{i2}} \frac{A_{pi}}{t_{pi}^2} \hat{\varepsilon}_{pi} \partial x \tag{3.32}$$

where ρ represents density, i is the piezoelectric index, and a_{i1} and a_{i2} are the endpoints of the ith piezoelectric. The remaining terms are defined by

$$\hat{c}_s = \begin{bmatrix} -1 & \nu_s & 0 & 0 & 0 & 0 \end{bmatrix} c_s \begin{bmatrix} -1 \\ \nu_s \\ 0 \\ 0 \\ 0 \\ 0 \end{bmatrix} \tag{3.33}$$

$$\hat{c}_{pi} = \begin{bmatrix} -1 & \nu_{pi} & 0 & 0 & 0 & 0 \end{bmatrix} c_{pi}^E \begin{bmatrix} -1 \\ \nu_{pi} \\ 0 \\ 0 \\ 0 \\ 0 \end{bmatrix} \tag{3.34}$$

$$\hat{e}_{pi} = \begin{bmatrix} 0 \\ 0 \\ 1 \end{bmatrix} \begin{bmatrix} -1 & \nu_{pi} & 0 & 0 & 0 & 0 \end{bmatrix} c_{pi}^{E} d_{ti} \begin{bmatrix} 0 \\ 0 \\ -1 \end{bmatrix} \tag{3.35}$$

$$\hat{\varepsilon}_{pi} = \begin{bmatrix} 0 & 0 & -1 \end{bmatrix} \varepsilon_{pi}^{s} \begin{bmatrix} 0 \\ 0 \\ -1 \end{bmatrix} \tag{3.36}$$

where the superscript $()^{E}$ represents that the values are measured at constant electrical field, and the superscript $()^{s}$ represents that the values are measured at constant strain. For a beam with PZT on a single side, A_{pi}, S_{pi} and I_{pi} are defined by

$$A_{pi} = w_b \int_{t_b}^{t_b + t_{pi}} \partial y \tag{3.37}$$

$$S_{pi} = w_b \int_{\frac{t_b - t_{pi}}{2}}^{\frac{t_b + t_{pi}}{2}} y \partial y \tag{3.38}$$

$$I_{pi} = w_b \int_{\frac{t_b - t_{pi}}{2}}^{\frac{t_b + t_{pi}}{2}} y^2 \partial y \tag{3.39}$$

Therefore, the actuator and sensor equations for PZT cantilever can be derived from Eqs. (3.13) and (3.14), i.e.

$$\left([M_s] + [M_p] \right) \{\ddot{r}\} + \left([K_s] + [K_p] \right) \{r\} - [\Theta] \{E\} = [B_f] \{F\} \tag{3.40}$$

$$[\Theta]^T \{r\} + [C_p] \{E\} = [B_q] \{q\} \tag{3.41}$$

where vector $\{r\}$ represents the generalized displacement coordinates of the assumed modes, vector $\{F\}$ is external point forces, the vectors $\{q\}$ and $\{E\}$ represent the charge and potential on the piezoelectric electrodes, $[M_s]$, $[M_p]$, $[K_s]$ and $[K_p]$ are the mass and

stiffness matrices for the structure and piezoelectric patch, $[C_p]$ is the piezoelectric capacitance matrix, $[\Theta]$ is the electromechanical coupling matrix, and $[B_f]$ and $[B_q]$ are the forcing matrices. Obviously all the matrices characterizing the system are functions of the assumed modes $\psi_n(x)$ used in the Rayleigh-Ritz method as well as the physical properties such as density, Young's modulus, piezoelectric coefficients, etc.

Generally, sensing with piezoelectric materials can be done in two different ways. In the standard case, the voltage at the piezoelectric electrodes is measured by a high impedance amplifier, which allows no current flow. The electrodes are essentially open circuited and thus the applied charge is zero, ($\{q\}=\{0\}$). Another sensing approach uses a charge amplifier with low impedance. In this case, the electrodes are essentially shorted and thus the applied voltage is zero, ($\{E\}=\{0\}$). In the case of simultaneous sensing and actuating, however, the piezoelectric material performs both actuating and sensing functions simultaneously. Therefore, the voltage is specified and nonzero, and the charge applied to the electrodes is no longer zero as well. Additionally, as the case we studied has single value voltage throughout the piezoelectric electrode, $[B_q]=[\backslash I_\backslash]$. And the force vector reduces to scalar, $[B_f]$ can be shown as

$$B_f = \begin{bmatrix} 0 & \cdots & 0 & \Psi_{r_1}(x_f) \\ \vdots & \ddots & \vdots & \vdots \\ \vdots & & 0 & \vdots \\ 0 & \cdots & 0 & \Psi_{r_n}(x_f) \end{bmatrix} \tag{3.42}$$

The electrical circuit shown in Figure 3.3 helps us to understand the physical significance of the terms in the above equations. The piezoelectric material behaves like a transformer, converting mechanical energy to electrical and vice versa. By examining the electrical side of the piezoelectric transformer, the terms in equations can be interpreted one by one, physically. The inherent piezoelectric capacitance is parallel to the piezoelectric transformer. Any applied current is therefore split between the current flowing into the capacitor, called i_{elec}, and that flowing into the piezoelectric transformer, called i_{mech}. In simultaneous sensing and actuating, the electrical current at the input port is referred to as i_{tot} and thus satisfies

$$\underbrace{[\Theta]^T\{\dot{r}\}}_{i_{mech}} + \underbrace{[C_p]\{\dot{E}\}}_{i_{elec}} = \underbrace{\{i\}}_{i_{tot}} \tag{3.43}$$

which is Eq. (3.41) after taking the derivative with respect to time.

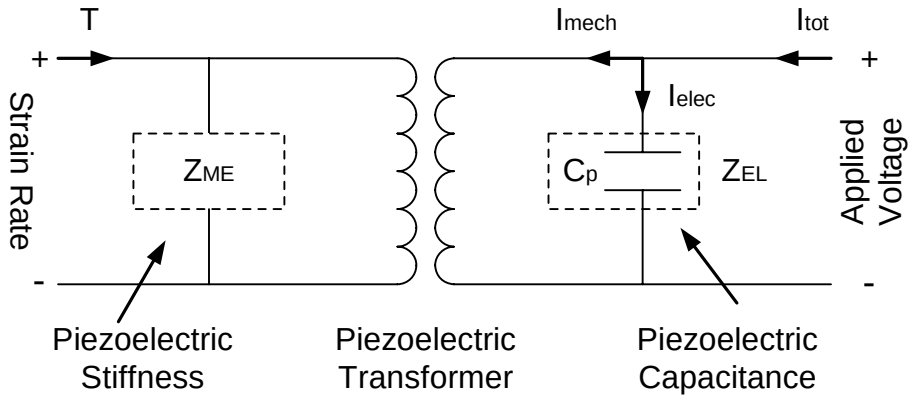

Fig. 3.3 Electrical circuit analogy of the piezoelectric transducer

3.3 Transduction Matrix of a PZT-Coated Cantilever

Since there is only a single PZT patch bonded to the cantilever, the vectors $\{q\}$, $\{i\}$ and $\{E\}$, and the capacitance matrix $[C_p]$ can be reduced to scalars. The vector $\{F\}$ also reduces to a scalar because only the force in z direction is considered. As a result, the actuator and sensor equations are simplified:

$$[M]\{\ddot{r}\}+[K]\{r\}=[\Theta]E+[B_f]F \tag{3.44}$$

$$i=[\Theta]^T\{\dot{r}\}+C_p\dot{E} \tag{3.45}$$

where $[M]=[M_s]+[M_p]$ and $[K]=[K_s]+[K_p]$. By solving the associated eigenvalue problem of Eq. (3.44) together with boundary conditions at the clamped and free end of the cantilever, the natural frequencies ω_n and the normalized eigenvectors $[\Phi]$ for the system are obtained. Using modal expansion,

$$\{r\}=[\Phi]\{\eta\} \tag{3.46}$$

the governing equation are decoupled. Solving them gives

$$\{\eta\}=\begin{bmatrix}\ddots & & 0\\ & \dfrac{1}{\omega_n^2-\omega^2} & \\ 0 & & \ddots\end{bmatrix}[\Phi]^T([\Theta]E+[B_f]F) \tag{3.47}$$

As regards the lightly damped structures, the modal damping ratio can be introduced without affecting the generality; the above equation is thus modified to

$$\{\eta\}=\begin{bmatrix}\ddots & & 0\\ & \dfrac{1}{\omega_n^2+2j\xi_n\omega_n\omega-\omega^2} & \\ 0 & & \ddots\end{bmatrix}[\Phi]^T([\Theta]E+[B_f]F) \tag{3.48}$$

Substituting the above equation into Eq. (3.46), the generalized coordinate $\{r\}$ is obtained as

$$\{r\} = [\Phi]\{\eta\} = [\mathrm{H}]E + [P]F \tag{3.49}$$

where

$$[H] = [\Phi]\begin{bmatrix} \ddots & & 0 \\ & \dfrac{1}{\omega_n^2 + 2j\xi_n\omega_n\omega - \omega^2} & \\ 0 & & \ddots \end{bmatrix}[\Phi]^T[\Theta], \text{ and}$$

$$[P] = [\Phi]\begin{bmatrix} \ddots & & 0 \\ & \dfrac{1}{\omega_n^2 + 2j\xi_n\omega_n\omega - \omega^2} & \\ 0 & & \ddots \end{bmatrix}[\Phi]^T[B_f].$$

The solutions of the actuator and sensor equations shown in Eq. (3.49) and (3.45) are then utilized to derive the four elements of the transduction matrix. Since the excitation voltage is harmonic, the velocity distribution along the cantilever is

$$v(x,t) = [\Psi]\{\dot{r}\} = [\Psi][\mathrm{H}]E \cdot j\omega + [\Psi][P]F \cdot j\omega \tag{3.50}$$

and the current appearing at the input port is

$$i = [\Theta]^T[H]E \cdot j\omega + [\Theta]^T[P]F \cdot j\omega + j\omega \cdot C_p E \tag{3.51}$$

Since the above-described transducer is linear and reciprocal, the FRFs (frequency response functions) among the voltage and current at the input port and the force and velocity at the output port together form a two by two matrix (shown in Figure 3.4),

$$\begin{Bmatrix} E \\ i \end{Bmatrix} = \begin{bmatrix} t_{11} & t_{12} \\ t_{21} & t_{22} \end{bmatrix}\begin{Bmatrix} F \\ v \end{Bmatrix} = [T]\begin{Bmatrix} F \\ v \end{Bmatrix} \tag{3.52}$$

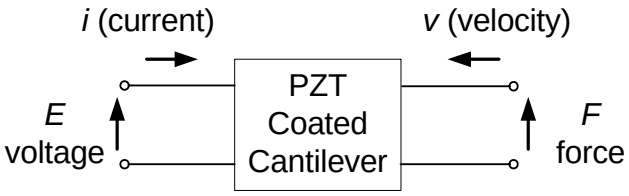

Fig. 3.4 Four-pole model of the PZT-coated cantilever

Since this matrix properly characterizes the forward actuating and the backward sensing function of an electromechanical transducer, it is called a transduction matrix. From Eq. (3.52), it is obvious that the matrix elements could be determined by imposing conditions at the output port of the transducer as follows:

$t_{11} = \frac{E}{F}\Big|_{v=0}$ Transfer function of voltage to force if the output point is clamped;

$t_{21} = \frac{i}{F}\Big|_{v=0}$ Transfer function of current to force if the output point is clamped;

$t_{12} = \frac{E}{v}\Big|_{F=0}$ Transfer function of voltage to velocity if the output point is free;

$t_{22} = \frac{i}{v}\Big|_{F=0}$ Transfer function of current to velocity if the output point is free.

Rearranging Eq. (3.50) and (3.51) builds up the transduction matrix,

$$\begin{bmatrix} E \\ i \end{bmatrix} = \begin{bmatrix} t_{11} & t_{12} \\ t_{21} & t_{22} \end{bmatrix} \begin{bmatrix} F' \\ v \end{bmatrix} = \begin{bmatrix} t_{11} & t_{12} \\ t_{21} & t_{22} \end{bmatrix} \begin{bmatrix} -F \\ v \end{bmatrix} \tag{3.53}$$

Note that *F'* by definition refers to the force generated by the cantilever at its tip and to the object being excited. It is opposite in direction to the force *F* applied to the cantilever having been used in the course of the derivation. The four FRFs of the transduction matrix are finally obtained as (Publication 1):

$$t_{11} = \frac{E}{F'}\Big|_{v=0} = \frac{[\Psi][\mathrm{P}]}{[\Psi][H]} \tag{3.54}$$

$$t_{12} = \frac{E}{v}\Big|_{F'=0} = \frac{1}{[\Psi][H]\cdot j\omega} \tag{3.55}$$

$$t_{21} = \frac{i}{F'}\Big|_{v=0} = ([\Theta]^T[H]\cdot j\omega + C_p\cdot j\omega)\cdot\frac{[\Psi][\mathrm{P}]}{[\Psi][H]} - [\Theta]^T[P]\cdot j\omega \tag{3.56}$$

$$t_{22} = \frac{i}{v}\Big|_{F'=0} = \frac{[\Theta]^T[H] + C_p}{[\Psi][H]} \tag{3.57}$$

Considering Figure 3.4 and Equation (3.52), if the energy flows from left to right in the figure, i.e., the device functions as an actuator, the determinant of matrix *T*, denoted by det(*T*) is required to be as small as possible. Thus, the desired force and velocity can be achieved while the required electrical energy is very small. Small electrical input can result in enough mechanical impedance response.

On the other hand, if the energy flows in an inverse direction, i.e., the device functions as a sensor, det(*T*) is desired to be as large as possible. Therefore, very small responses, no matter force or velocity, or their small variation can result in obvious change of the electrical variables.

The above transducer is a linear system and its transduction functions obey the reciprocity theorem. From the definitions of the four transfer functions, we can get the transduction matrix, which can describe the system in the round. The determinant of the transduction matrix should be unity according the reciprocity theorem [103] (Appendix A), i.e.

$$|T| = t_{11} \cdot t_{22} - t_{12} \cdot t_{21} = 1 \tag{3.58}$$

If the input electrical impedance is made known, the output mechanical impedance can be calculated on the basis of Eq. (3.52):

$$Z_M = \frac{F}{v} = \frac{t_{22} Z_e - t_{12}}{t_{11} - t_{21} Z_e} \tag{3.59}$$

where $Z_e = \dfrac{E}{i}$ is the electrical impedance of the input port;

$Z_M = \dfrac{F}{v}$ is the mechanical impedance of the output port.

3.4 Simultaneous Sensing and Actuating by a PZT Cantilever

In order to confirm the derivation in the above, in the following the determinant of the transduction matrix will be first proved to be unity for a transducer cantilever. Moreover, to validate the proposed method, a numerical experiment will be conducted in which the transducer is employed to “measure” the point mechanical impedance at the tip of a cantilever beam structure through numerical simulation. The results from the numerical experiment will be compared with the same impedance calculated from its corresponding finite element model.

The transducer cantilever consists of an aluminum cantilever beam of 90mm in length, 12mm in width and 1.0mm in thickness. The PZT patch bonded to its top surface is 20mm long, 12mm wide and 0.2mm thick. This PZT patch is 5mm from the root of the beam (x_p = 5mm) and the output port in the two-port model is designated at a point close to the free end of the cantilever (x_o/L=0.965). The configuration of the transducer cantilever is shown in Figure 3.1 and 3.2 and some geometry and material parameters of aluminum and the PZT are listed in Table 3.1 and 3.2. The numerical experiment performed to identify the transduction matrix *[T]* was carried out by finite element simulation via ANSYS using a proportional damping ratio of 0.005. Solid 5 and Solid 45 elements, both with eight nodes, were selected to model the PZT and aluminum components of the transducer cantilever respectively.

Table 3.1 Material properties of cantilever transducer components

Component	Cantilever	Symbol	PZT patch	Symbol
Material	Aluminum		Piezoceramic	
Density (kg/m^3)	2690	ρ_s	7800	ρ_p
Young's Modulus ($\times 10^9\ N/m^2$)	70.3	E_s		
Poisson's Ratio	0.34	υ_s	0.3	υ_p
Length(mm)	90	L_s	20	L_p
Width(mm)	12	W_s	12	W_p
Thickness(mm)	1.0	T_s	0.2	T_p
Position(mm)			5	x_1

Table 3.2 Material properties of utilized piezoelectric material

Category	Unit	Symbol	PZT (Fuji c9)
Density	(kg/m^3)	ρ_p	7800
Poisson's Ratio		υ_p	0.3
Elastic Modulus	$(\times 10^9\ N/m^2)$	c_{11}^E	64
		c_{33}^E	60
		c_{55}^E	27
Piezoelectric Constants	$(\times 10^{-12}\ m/V)$	d_{31}	-300
		d_{33}	600
		d_{15}	550
Relative Dielectric Constants		$\varepsilon_{11}^T/\varepsilon_0$	4700
		$\varepsilon_{33}^T/\varepsilon_0$	6300

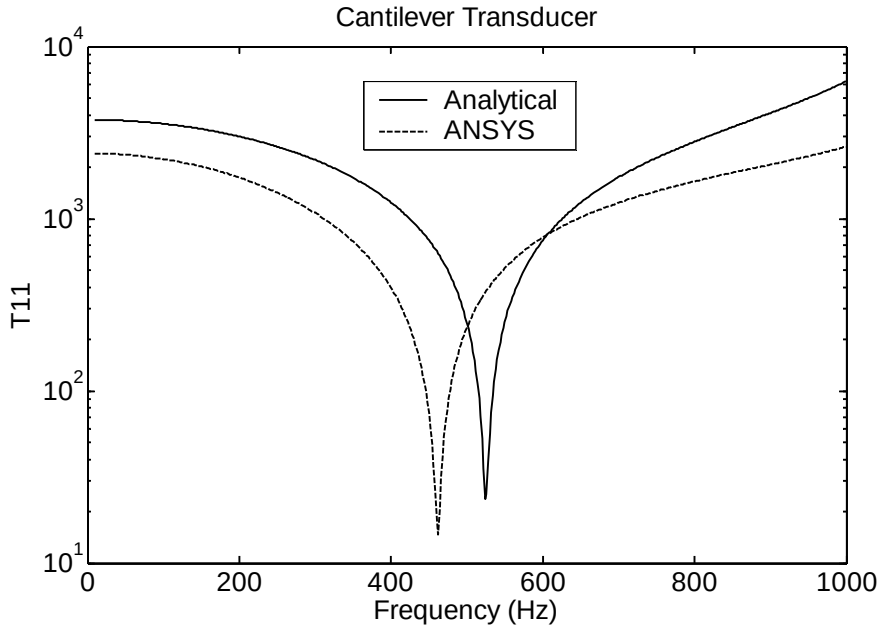

Fig. 3.5 Transduction element t_{11}

Figures 3.5-3.8 show the transduction matrix evaluated using Eqs. (3.54-3.57) and identified by the above finite element simulation. It is seen that, although in general they match well, some assumptions made in the analysis and the numerical errors in the finite element simulation cause small discrepancies, particularly near higher order resonance

frequencies. When the method is implemented in future, attention should be paid to these errors in the transduction matrix if evaluated by numerical simulations.

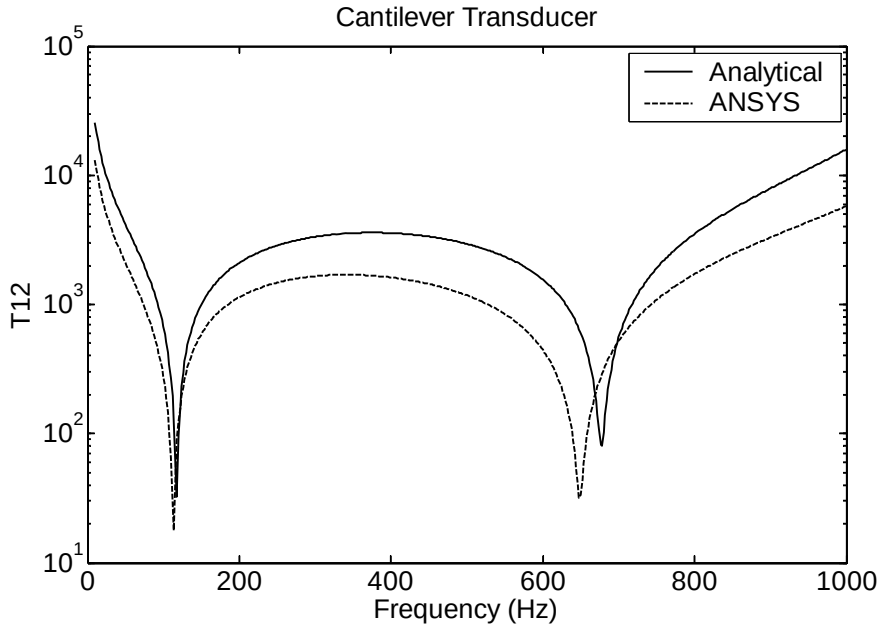

Fig. 3.6 Transduction element t_{12}

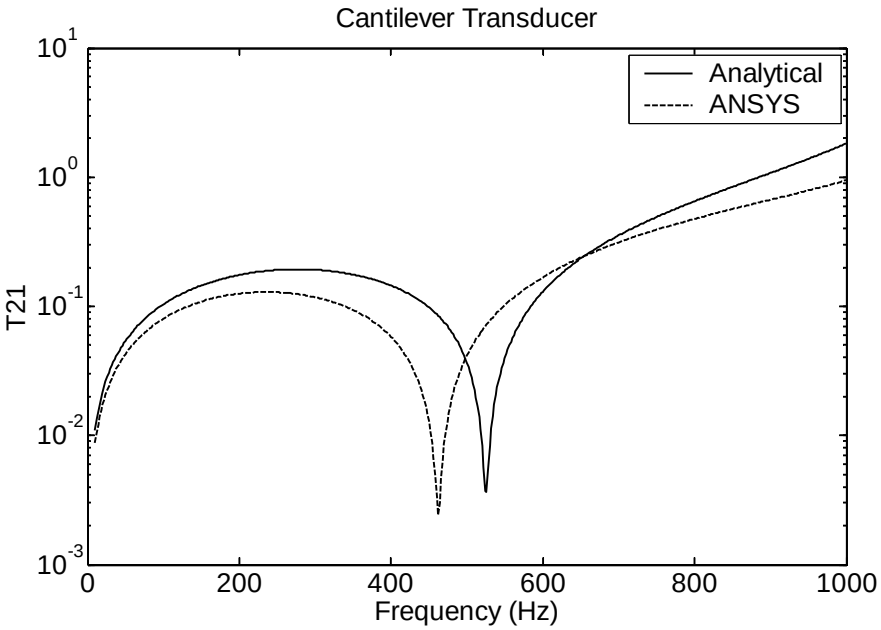

Fig. 3.7 Transduction element t_{21}

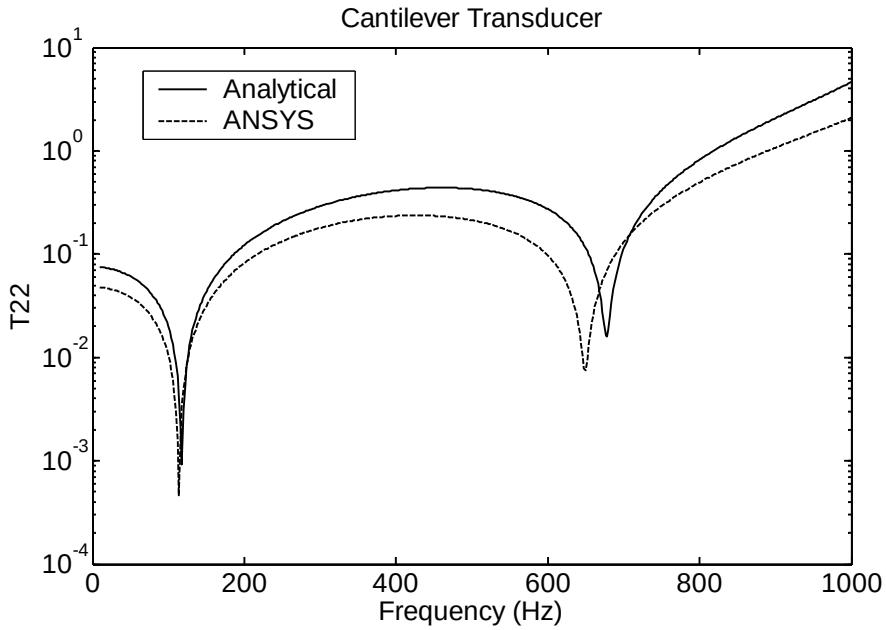

Fig. 3.8 Transduction element t_{22}

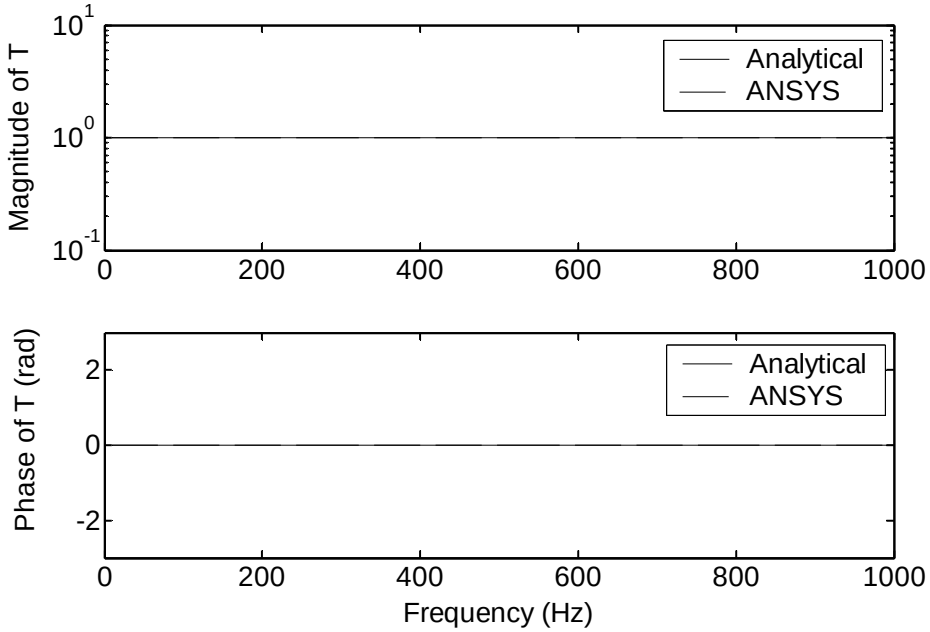

Fig. 3.9 Determinant of matrix [*T*]

Figure 3.9 presents the determinant of the transduction matrix obtained from both the derived analytical solutions and finite element results. At the frequency of interest, the results are unity in magnitude and zero in phase, which matches expectation and reflects the reciprocity property of the PZT-coated cantilever. This reciprocity actually is the basis of the capability of simultaneous sensing and actuating.

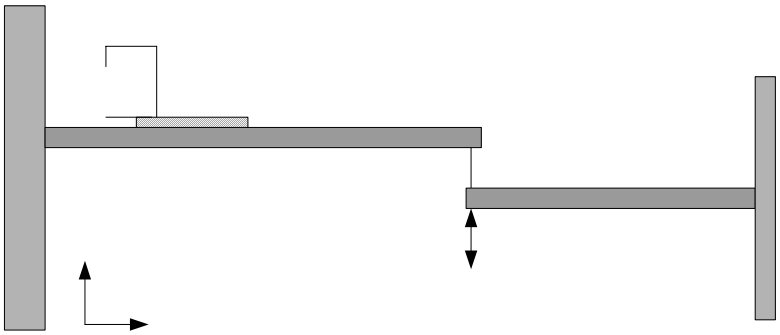

Fig. 3.10 Schematic of measurement system

The PZT-coated cantilever, after "calibration" as in the above, was then exploited as a sensing cum actuating transducer to detect the point mechanical impedance of a test beam structure near its tip as shown in Figure 3.10. The test beam is also a cantilever, which is 60mm long, 8mm wide and 0.5mm thick. A stinger normally used in vibration test to connect a shaker and test object is included in the testing set-up. In the experiment, voltage is supplied to the piezoelectric patch in order to excite the test beam structure. The input electrical impedance of the cantilever transducer is then detected and used together with the four FRFs in Eq. (3.59) to calculate the mechanical impedance at the excitation point. A finite element model of the test beam, in which Solid 45 and Combin 14 elements were selected to model the test beam and connection spring respectively, was also built

using ANSYS to calculate the point mechanical impedance at the same location. Figures 3.11 and 3.12 show the model. The enlarged view is shown in Figure 3.13.

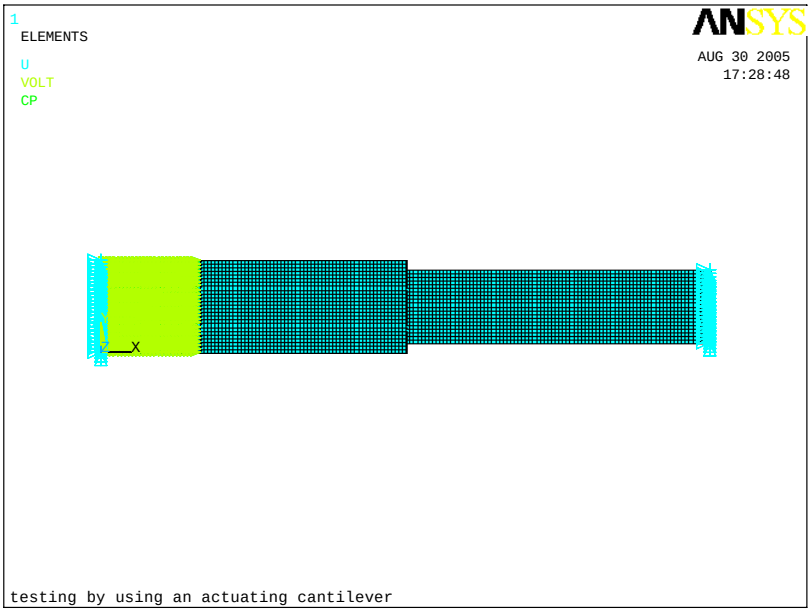

Fig. 3.11 ANSYS model of measurement system (top view)

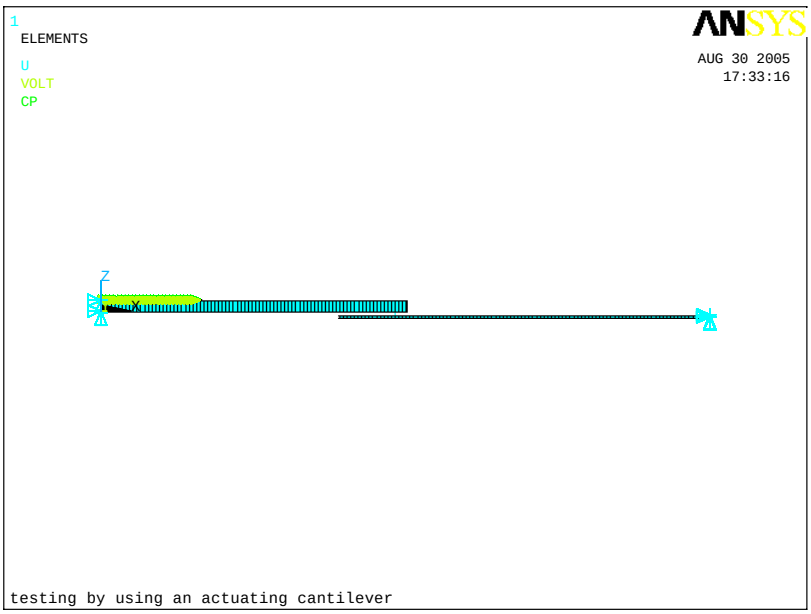

Fig. 3.12 ANSYS model of measurement system (front view)

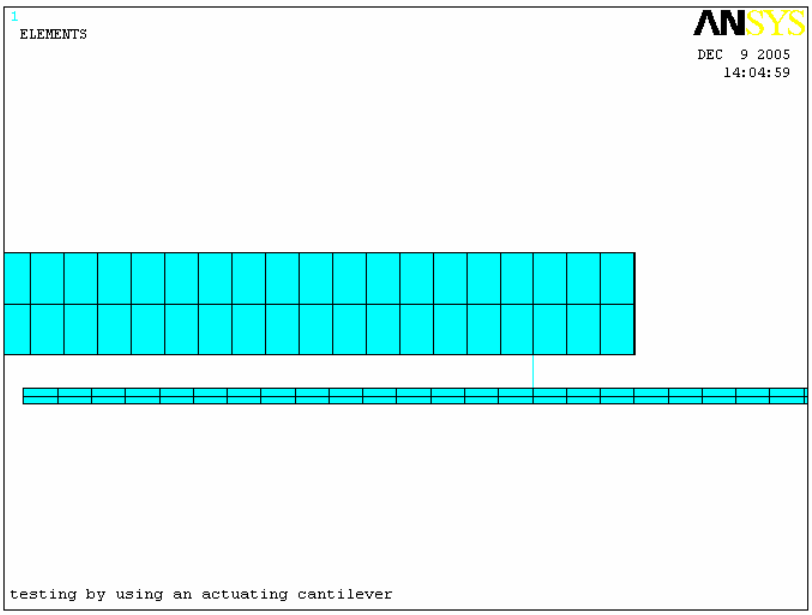

Fig. 3.13 ANSYS model of measurement system (enlarged view)

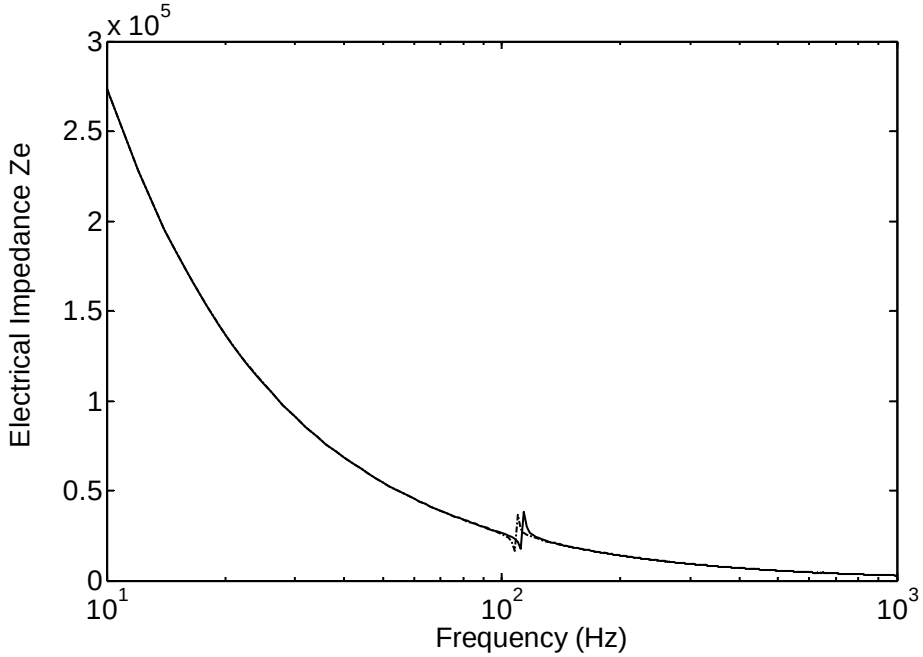

Fig. 3.14 “Measured” (solid) and “detected” (dash) input electrical impedance

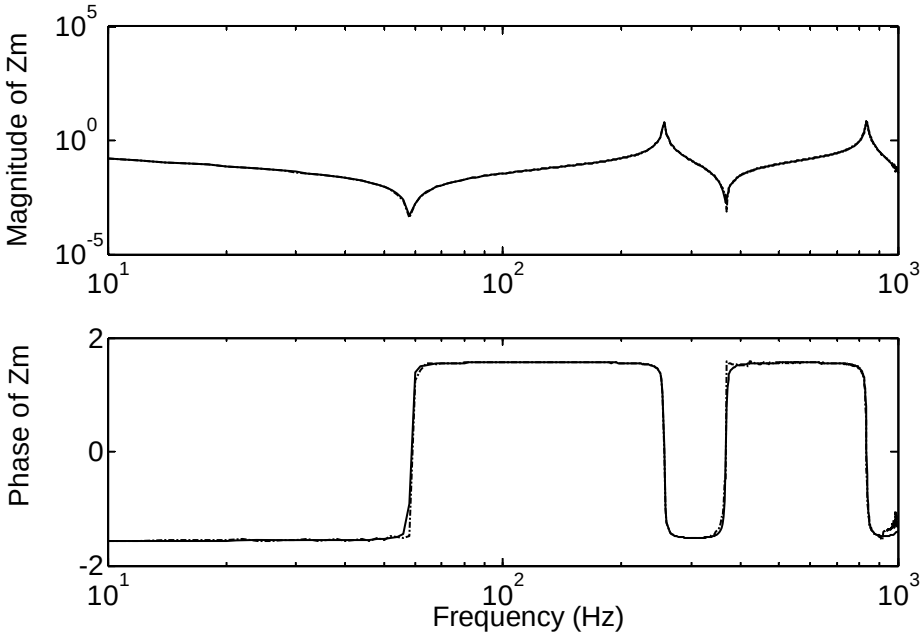

Fig. 3.15 A comparison of Z_m of sample between real (dash) and "detected" (solid) results

The mechanical impedance of the sample beam at free end is first detected by using harmonic analysis of ANSYS. Afterwards, the mechanical impedance at the same point is detected via the SSA device, in which the stinger is modeled as a spring. The input voltage equals to 1, and then the input current will be determined. Then the electrical input impedance of the PZT-coated beam attached on the beam is "measured" and shown in Figure 3.14.

Followed the mechanical impedance at the excitation point was calculated according to Eq. (3.59) from the "measured" electrical impedance. The real and the "detected" mechanical impedance of the beam at the given location are compared in Figure 3.15. The solid line is the real result obtained by using harmonic analysis of ANSYS and the dash line is the "detected" result calculated by the proposed technique. In Figure 3.15, the two

sets of results match well and no significant discrepancies are seen in the frequency range of interest.

3.5 Concerns in Experimental Identification of Transduction Matrix

In experiments, direct identification of these transduction elements is impractical. For calibrating t_{11} and t_{21} described in Eq. (3.52), which should be identified under clamped condition, output force is required to be measured. However, it is very difficult to let the output port really clamped. For calibrating t_{12} and t_{22}, measurement of linear velocity also poses difficulty in experiments. Basically there are two ways to measure velocity: contact measurement using an accelerometer and non-contact measurement employing a Laser Doppler Velocimeter. In the first way considerable loading error will be introduced; the second way is also inconvenient due to synchronization between LDV and impedance analyzer used to measure the input electrical variables.

To overcome the above experimental difficulties, an alternative calibration method is developed to characterize the transducer. Rewrite Eq. (3.59), the input electrical impedance Z_e and the mechanical impedance Z_m measured at the output port can be correlated as

$$Z_m = \frac{t_{22}Z_e - t_{12}}{t_{11} - t_{21}Z_e} = Z_{mo}\frac{Z_e - Z_{ef}}{Z_e - Z_{ec}} \tag{3.60}$$

where Z_m is the mechanical impedance of the structure under testing; Z_e is the corresponding electrical input impedance of the transducer loaded by the structure under testing; Z_{mo} is the mechanical impedance of the transducer when it is electrically open-circuited, i.e. $Z_{mo} = \frac{F}{v}\Big|_{i=0} = -\frac{t_{22}}{t_{21}}$; Z_{ec} and Z_{ef} are the electrical impedance of the transducer when it is mechanical clamped and free respectively, i.e. $Z_{ec} = \frac{E}{i}\Big|_{v=0} = \frac{t_{11}}{t_{21}}$, and $Z_{ef} = \frac{E}{i}\Big|_{F=0} = \frac{t_{12}}{t_{22}}$. Mechanical impedance, thus, can be calculated from the corresponding electrical input impedance of the actuator, when impedances Z_{mo} , Z_{ec} and Z_{ef} , the intrinsic attributes of the cantilever transducer, are fully known.

Impedances Z_{mo} , Z_{ec} and Z_{ef} are essentially frequency response functions of the transducer, in principle, they can be made known by calibrating the device in advance under various mechanical boundary conditions and electrical terminal conditions. Among the 3 impedances, Z_{ef} can be easily calibrated by letting the output port free mechanically while Z_{mo} and Z_{ec} are much more difficult to calibrate. This is because mechanical clamp conditions and electrical open-circuit conditions are difficult to be realized in a laboratory. In some cases, it remains a big problem for high frequency force measurement.

To overcome these problems, a method is put forward to indirectly identify Z_{mo} and Z_{ec} from a set of the measured Z_{ef} and Z_e of the actuator when various known masses are applied to its output port.

We can rewrite Eq. (3.60) as following:

$$aZ_{mo} + bZ_{ec} = c \tag{3.61}$$

where $a = \dfrac{Z_e - Z_{ef}}{Z_M}$; $b = 1$; $c = Z_e$.

For a given mass as a load of transducer under calibration, a, c can be measured and calculated. We can build a group of simultaneous equations as following based on a set of Z_e and Z_M obtained by adding various masses to the mechanical port of the transducer.

$$\begin{bmatrix} a_1 & b_1 \\ a_2 & b_2 \\ \cdots & \cdots \\ a_n & b_n \end{bmatrix} \cdot \begin{bmatrix} Z_{mo} \\ Z_{ec} \end{bmatrix} = \begin{bmatrix} c_1 \\ c_2 \\ \cdots \\ c_n \end{bmatrix} \tag{3.62}$$

where $a_k = \dfrac{Z_e^k - Z_{ef}}{Z_M^k}$; $b_k = 1$; $c_k = Z_e^k$; $k = 1,2,\cdots,n$. n is the number of experiment times of adding masses to the mechanical port of the transducer.

Z_{mo} and Z_{ec}, therefore, can be identified by solving these over-determined simultaneous equations. The least square solution of the above mentioned equations can be derived as following:

$$Z = [A^T A]^{-1} A^T C \tag{3.63}$$

where

$$Z = \begin{bmatrix} Z_{mo} \\ Z_{ec} \end{bmatrix};$$

$$A = \begin{bmatrix} a_1 & b_1 \\ a_2 & b_2 \\ \cdots & \cdots \\ a_m & b_m \end{bmatrix};$$

$$C = \begin{bmatrix} c_1 \\ c_2 \\ \cdots \\ c_m \end{bmatrix}.$$

3.6 Summary

In this chapter, a method of making use of PZT-coated cantilevers as both vibration exciters and sensors simultaneously to measure the point mechanical impedance of structures is proposed and investigated numerically. Supplied with voltage, the cantilever vibrates and exerts forces to test structure connected to its tip. Due to the load from the test structure, the PZT patch of the cantilever undergoes variations of input electrical impedance. Probing the input electrical impedance quantitatively detects the mechanical impedance imposed at the output port of the cantilever transducer provided its transduction matrix is known.

A transduction matrix is defined to characterize the forward actuating and backward sensing capability of an electro-mechanical transducer. It is a two by two matrix consisting of four frequency response functions between the input electrical voltage and current and the output force and velocity of the transducer. The four components can be evaluated analytically, numerically or experimentally following different boundary conditions. After it is made available, the mechanical impedance at the output port of an electromechanical transducer can be evaluated from the electrical impedance actually measured at the input port through it using Eq. (3.59). In this study, in order to be more generally useful for future studies, our evaluations were made in closed form by solving the governing equations of the PZT-coated cantilever. After it had been made available, the matrix was exploited in a numerical experiment for measuring the mechanical impedance of a simple beam structure. Comparison of the point mechanical impedance obtained by finite element simulation and by the proposed method shows that the proposed method works as designed.

One major obstacle to using an actuator as a sensor simultaneously for dynamic measurement is the loading effect caused by transducer. Sensors are conventionally made small and desired to cause little or negligible loading effect and thus minimize the deviation of the measurand from its real value. In simultaneous sensing and actuating, the transducer by no means satisfies this requirement due to the actuator role it plays. As a result, simultaneous sensing and actuating has traditionally been employed more for condition monitoring, where detecting the trend of a system “signature” over time fulfills the monitoring purpose [104]. To measure a dynamic quantity precisely, the loading effect from the transducer has to be properly removed. As demonstrated in [77], solving coupled

governing equations removes the loading effect naturally and can be used in some simpler cases. The introduction of a transduction matrix offers an effective and convenient way to remove the loading effect quantitatively and makes simultaneous sensing and actuating available for accurate dynamic measurements [94].

The method presented was originally proposed to overcome difficulties in dynamic measurement of miniature structures. In such cases, not only does the loading effect caused by vibration exciter create unacceptable errors, the space available for proper installation of force and motion sensors is also very limited. The proposed method avoids both difficulties and offers a feasible alternative for dynamic testing of structures in mini-scale or even micro-scale. As for the realization of the cantilever transducer, whether by ultra-precision machinery or lithography-based micro system technology, fabricating a PZT bonded tiny cantilever is problem-free in the state of arts [105]. Through building such a transducer either integrated with or separate from the test object, the dynamic properties of a test structure could be identified by measuring its mechanical impedance as numerically demonstrated in the above. Further study has been in progress to address a number of problems in implementing the method. One of the major concerns is how to decide the dimensions and system parameters of the transducer which provide the optimal compromise between the sensing and actuating capability. A transducer cantilever which supplies more power for excitation is usually less sensitive to the load imposed at its tip. Such problem will be studied in the following chapter.

CHAPTER 4

OPTIMIZATION FOR BEST SSA

In the last chapter, a method, making use of a PZT-coated cantilever as both a vibration exciter and sensor simultaneously to measure mechanical impedance of structures, was proposed and investigated numerically. The presented method was originally proposed to overcome the difficulties existing in the dynamic measurement of miniature structures and to offer a feasible alternative for dynamic testing of structures in mini-scale or even micro-scale. Further study, in this chapter, will focus on an optimisation to decide the dimensions and system parameters of the transducer which provides the optimal compromise between the sensing and actuating capability. For this purpose, performance indices of a cantilever transducer, which is used as a sensor, include sensitivity and an effective dynamic frequency range, and factors indicating or influencing actuating capability, such as energy efficiency and output force. These should be investigated firstly. On the basis of the above investigation, an optimization will be done by utilizing these performance indices to balance its sensing and actuating capability to improve the capability of the cantilever transducer. Besides these, a comparison of performances between the new and original cantilever transducer will then be done by numerical simulation and the validity of optimization strategy will thus be numerically examined.

Since the cantilever transducer functions as an actuator for sensing simultaneously, performance indices indicating actuating and sensing capabilities are highlighted in this section. In this study, a spring-mass-damper (SMD) system is selected as a load driven by the cantilever transducer. As shown in Figure 4.1, for the convenience, the dimensions and material properties of the cantilever transducer is the same as those described in Section 3.4 (Table 3.1 and 3.2). Thus, values of the transduction matrix [*T*] are also the same as those derived in Section 3.4 (Figures 3.5-3.8). Material properties of the spring-mass-damper system are listed in Table 4.1. The characteristics of the cantilever transducer as a sensor will be presented firstly. This will be followed by an introduction of the actuator characteristics including energy efficiency and output force.

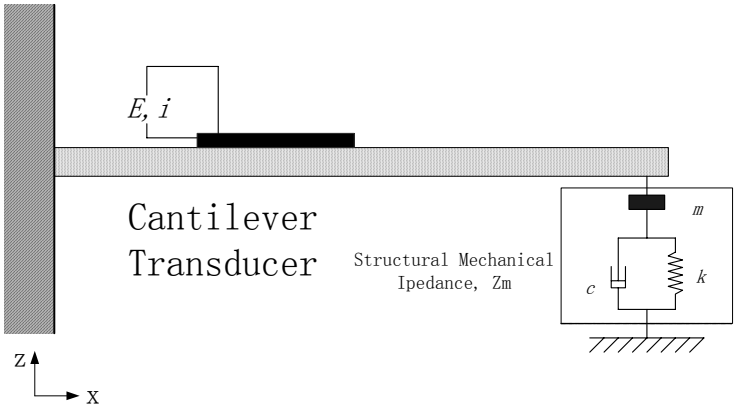

Fig. 4.1 Cantilever transducer driven spring-mass-damper system

Table 4.1 Parameters of a spring-mass-damper (SMD) system

Component	Mark	SMD system
Mass	m	$100mg$
Damping ratio	ζ	0.01
Natural frequency	f_n	$50Hz$

4.1 Performance Indices of Measuring Impedance using Cantilever Transducer

The most interesting index is the sensitivity of the cantilever transducer towards detecting mechanical impedance and effective dynamic frequency ranges.

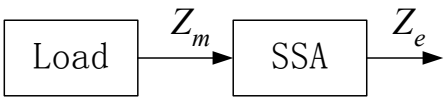

Fig. 4.2 Model of SSA transducer used as a sensor

For the sensor shown in Figure 4.2, the input variable is the mechanical impedance of the dynamic system and output variable is the electrical impedance. According to the definition of sensitivity, the sensitivity of the SSA cantilever transducer, therefore, can be expressed as follows:

$$K = \frac{\partial Z_e}{\partial Z_m} = \frac{t_{11}t_{22} - t_{12}t_{21}}{(t_{21}Z_m + t_{22})^2} = \frac{1}{(t_{21}Z_m + t_{22})^2} \tag{4.1}$$

Figure 4.3 shows the numerical results of the cantilever transducer's sensitivity evaluated by using Eq. (4.1). It is observed that the sensitivity is not constant but a function of frequency. However, in the low frequency range before the first natural frequency, it can be regarded as constant. We regard this range as an effective dynamic frequency range for sensing, and therefore the cantilever transducer is feasible for sensing in this range. In our study, both sensitivity and effective dynamic frequency range are utilized as performance indices indicating the sensing capability of the cantilever transducer.

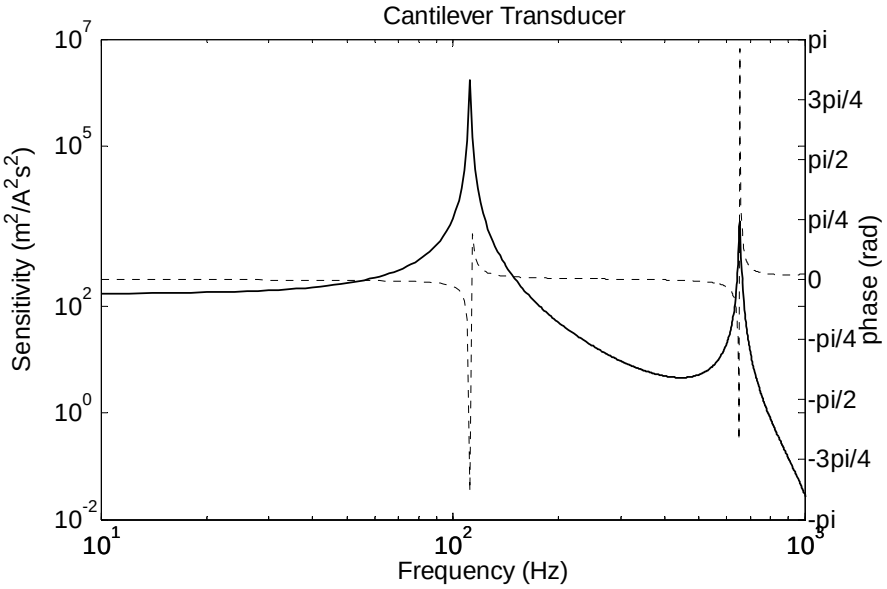

Fig. 4.3 Sensitivity of PZT-coated cantilever

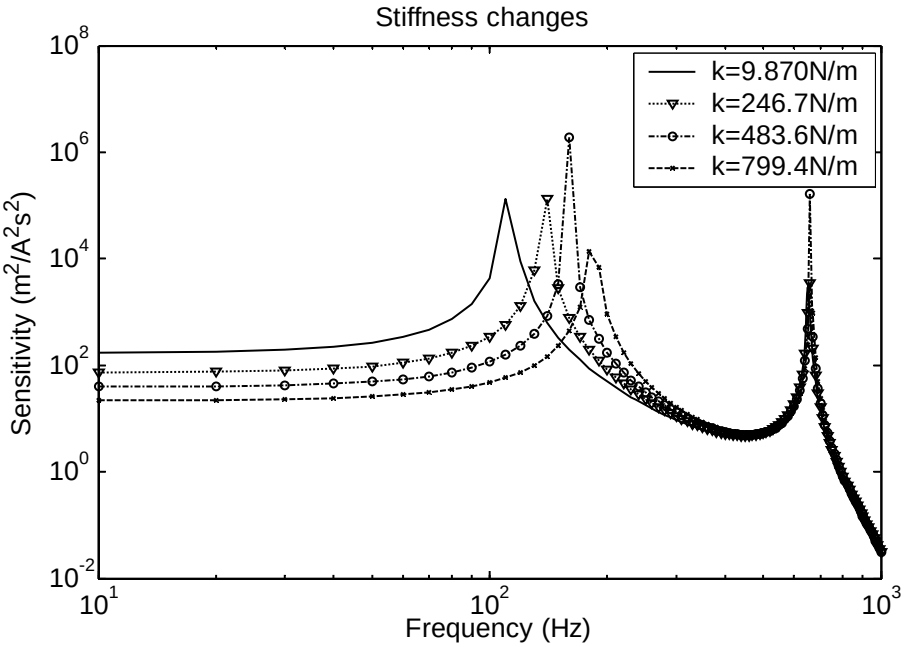

Fig. 4.4 Influence of stiffness on the cantilever transducer's sensitivity

Influences of stiffness, mass and damping factors on the sensitivity of the cantilever transducer are also investigated and the numerical results are shown in Figures 4.4-4.6. From Figure 4.4, it is found that if the stiffness increases, the effective frequency range will increase, while the sensitivity of the cantilever transducer will decrease conversely. It

is also seen from Figure 4.5 that the effective frequency range is affected by the mass factor while the sensitivity of the cantilever transducer is almost the same in the frequency range of interest. Besides, if the structural damping is considered, the damping factor doesn't affect the sensitivity and effective frequency ranges, as illuminated in Figure 4.6.

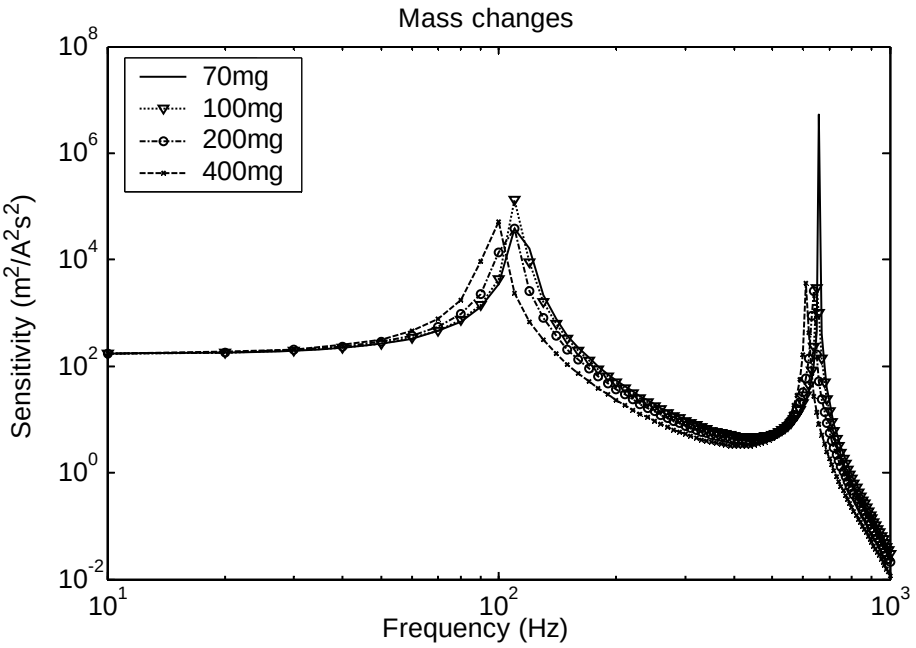

Fig. 4.5 Influence of mass on the cantilever transducer's sensitivity

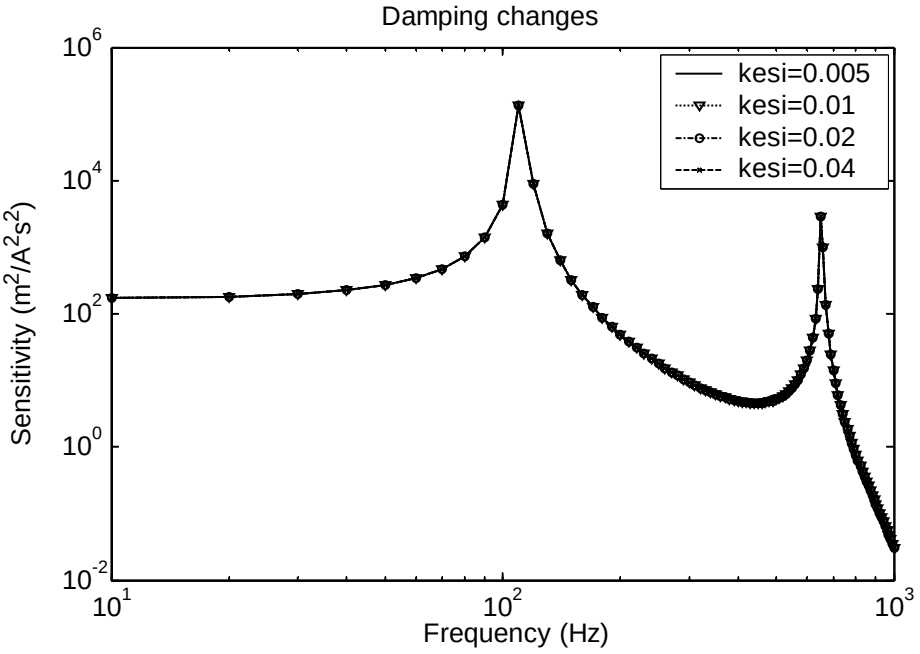

Fig. 4.6 Influence of damping on the cantilever transducer's sensitivity

4.2 Performance Indices of Exerting Forces using Cantilever Transducer

Another area of interest is the energy efficiency of the cantilever transducer, which represents actuator effectiveness to excite the system. Another important actuator index is the output force when the actuator drives the load.

4.2.1 Energy Efficiency

Energy efficiency describes the capability of the actuator to transfer the supplied electrical energy into structural mechanical energy (kinetic or potential energy of the mechanical system). It is similar to the electric power factor used in the theory of electricity, which is defined as the ratio of total dissipative electrical power to apparent electrical power for an electrical network. The following is a brief introduction of the energy efficiency.

The model for an actuator is shown in the Figure 4.7. The input is an apparent power, W_A, and transfers into dissipative power, W_D, and reactive power, W_R. Where the reactive power remains and flows within the system and the dissipative power is the power transformed into other energy forms.

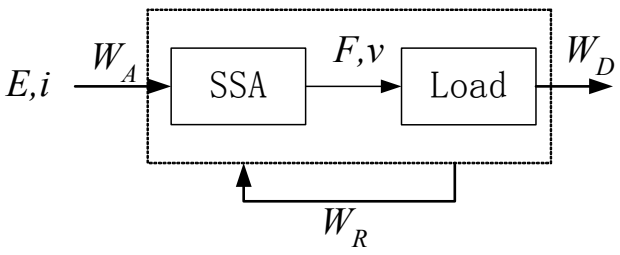

Fig. 4.7 Model of the cantilever transducer used as an actuator

If a voltage, $E = v\sin(\omega \cdot t)$, is applied, the current measured in the circuit will be $I = i\sin(\omega \cdot t + \phi)$. The voltage and current are related by the admittance, $Y = \mathrm{Re}(Y) + i\,\mathrm{Im}(Y)$, of the load. Then the apparent power, W_A, dissipative power, W_D, and reactive power, W_R, can be calculated in the following equations:

$$W_A = I_e V_e = \frac{v^2}{2}|Y| \tag{4.2}$$

$$W_D = W_A \cos\phi = \frac{v^2}{2}\mathrm{Re}(Y) \tag{4.3}$$

$$W_R = W_A \sin\phi = \frac{v^2}{2}\mathrm{Im}(Y) \tag{4.4}$$

Where I_e and V_e are the RMS current and voltage, respectively.

In order to maintain a constant voltage supply for the actuator at various frequencies, the power requirement, i.e., the minimum power rating of the voltage source, should be no less than the following value over the frequency of interest:

$$W_{rating} = \frac{v^2}{2}\max(|Y|) \tag{4.5}$$

The real admittance includes two parts: part one is from the damping of the mechanical systems and the other is from the internal loss of the actuator. The power consumption due to the damping of the mechanical system, or dissipative mechanical power, is associated with the structural vibration. The power due to the internal loss of the actuators is dissipated in terms of heat generated within the actuators, which is an essential quantity in

the thermal stress analysis of the system. The energy efficiency of the actuator in driving the system, therefore, should be defined as:

$$\psi = \frac{\text{Dissipative Mechanical Power}}{\text{Supplied Electric Power}} = \frac{\text{Re}(Y)}{|Y|} \tag{4.6}$$

where Y is the coupled electromechanical admittance resulting from the mechanical loss of the mechanical system and is expressed in the equation shown below.

$$Y = \frac{i}{E} = \frac{1}{Z_e} = \frac{t_{21}Z_m + t_{22}}{t_{11}Z_m + t_{12}} = \frac{1}{Z_{ec}} \cdot \frac{Z_m + \frac{t_{22}}{t_{21}}}{Z_m + Z_A} \tag{4.7}$$

where Z_{ec} is the electrical impedance of the cantilever transducer when it is mechanically clamped, i.e. $Z_{ec} = \frac{E}{I}\Big|_{v=0} = \frac{t_{11}}{t_{21}}$; Z_A is the mechanical impedance of the cantilever transducer at the output port when it is electrically short-circuited, which is calculated using $Z_A = \frac{F'}{v} = -\frac{F}{v}\Big|_{E=0} = \frac{t_{12}}{t_{11}}$.

The energy efficiency defined considers only the mechanical dissipative power as a result of structural damping, which may only be predicted theoretically. Additionally, it represents the percentage of the electrical energy transferred into mechanical energy and dissipated within the structure as a result of the structural damping, acoustic radiation, friction, etc, according to the definition of structural loss factor:

$$\eta = \frac{U_{MD}}{2\pi U_M} \tag{4.8}$$

where U_{MD} is the dissipative mechanical energy and U_M is the total mechanical energy or total kinetic and potential energy. A larger dissipated power, therefore, indicates larger

vibration energy (or a larger response). Higher energy efficiency means that more electrical power has been transferred into mechanical power, resulting in larger structural response and higher energy dissipative mechanical power. Therefore, the energy efficiency can be used to represent actuator effectiveness or control authority.

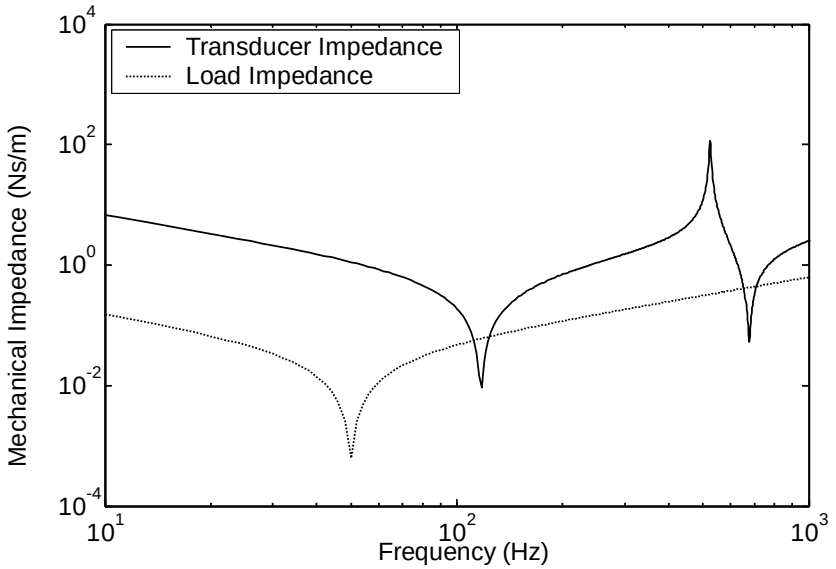

Fig. 4.8 Mechanical impedance of the cantilever transducer and spring-mass-damper system

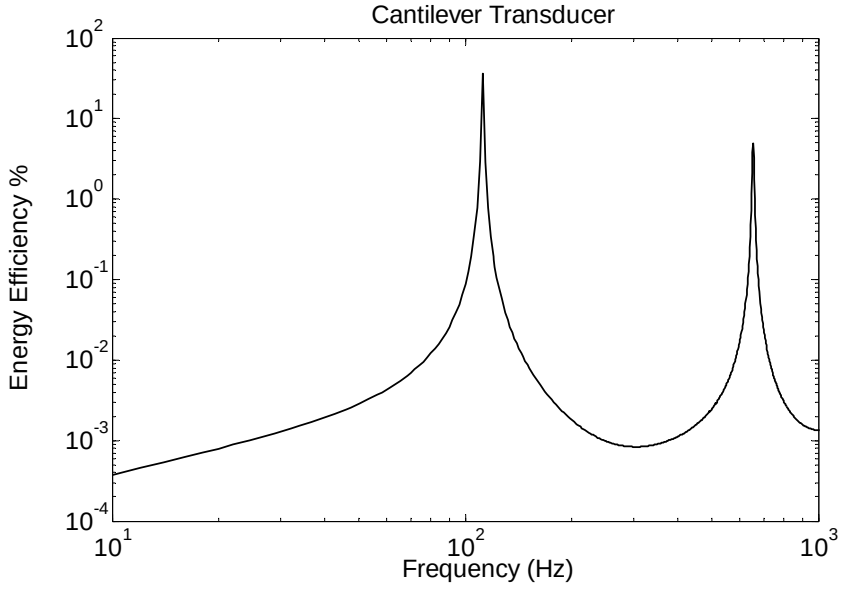

Fig. 4.9 Energy efficiency of the cantilever transducer

Figure 4.8 shows the impedance matching of the cantilever transducer and spring-mass-damper system. The transducer impedance, Z_A, is the mechanical impedance of the cantilever transducer at the output port when it is electrically short-circuited, which is calculated using $Z_A = \frac{F'}{v} = -\frac{F}{v}\Big|_{E=0} = \frac{t_{12}}{t_{11}}$ and shown as the solid line. Note that F by definition refers to the force generated by the cantilever at its tip and to the object being excited. It is opposite in direction to the force F', which is applied to the cantilever having been used in the course of the derivation. The mechanical impedance of the spring-mass-damper system at the testing point can be calculated using Eq. (4.9) and shown as the dashed line.

$$Z_m = \frac{F}{v} = c + mj\omega - jk/\omega = 2\zeta m\omega_n + mj\omega - jm\omega_n^2/\omega \tag{4.9}$$

Figure 4.9 shows the energy efficiency of the cantilever transducer based on Eq. (4.6). It is concluded that the actuator becomes the most efficient when the actuator impedance matches the structural impedance as illustrated in Figures 4.8 and 4.9. For a continuous system, there are many peaks corresponding to the natural vibration mode of the system. The height of a peak indicates the effectiveness of the actuator to excite that mode. Therefore, the energy efficiency can be used in the optimal design of actuator configuration and location, and can be used as a performance index of the actuating capability of the cantilever transducer. It is necessary to state that the impedance matching between the actuator and its load means that both impedances are complex conjugate.

4.2.2 Output Force

Another important actuator index of interest is the output force when the actuator drives the load. The output characteristics of an excitation device, such as a shaker, are usually expressed in terms of its free stroke and dynamic blocking force [6]. If a PZT actuator is driving a mechanical system, the output force and displacement of the PZT actuator are related. For actuators, we control the transducer input by specifying the input voltage E [14]. From the four-pole model of the cantilever transducer, the following equation can be obtained.

$$E = t_{11}F + t_{12}v \tag{4.10}$$

If the mechanical impedance of the mechanical system is Z_m, it means that $v = F / Z_m$. The interactive force can be obtained as;

$$F = \frac{Z_m}{Z_m + Z_A} \cdot \frac{E}{t_{11}} = \frac{Z_m}{Z_m + Z_A} F_b \tag{4.11}$$

where Z_A is the mechanical impedance of the cantilever transducer at the output port when it is electrically short-circuited, i.e. $Z_A = \frac{t_{12}}{t_{11}}$. F_b is the dynamic blocking force by assuming an infinite mechanical impedance, which is $\frac{E}{t_{11}}$. Thus, the characteristic of the output force is determined by the impedance matching and the dynamic blocking force.

From Eq. (4.11), if the impedance of the mechanical system is at its lowest, which corresponds to its resonance, the force provided by the actuator is at its lowest. If the structural impedance, $Z_{m,}$ matches the actuator impedance, Z_A, the actuator provides the maximum force and power. In the previous section, it was also concluded that when the actuator impedance matches the structural impedance, the actuator becomes more efficient, which has higher energy efficiency. An important remaining factor, which also influences the characteristic of output force, is the dynamic blocking force, F_b. This performance

measure is just the force at the actuator output when the output is prevented from moving, which is assumed as an infinite mechanical impedance, when a drive signal is applied [52]. It is commonly described in terms of output force per input voltage.

Figure 4.10 shows the numerical results of output force when the selected cantilever transducer is clamped. It is found that the output force is very low and an improvement of the cantilever transducer for a higher output force is essential.

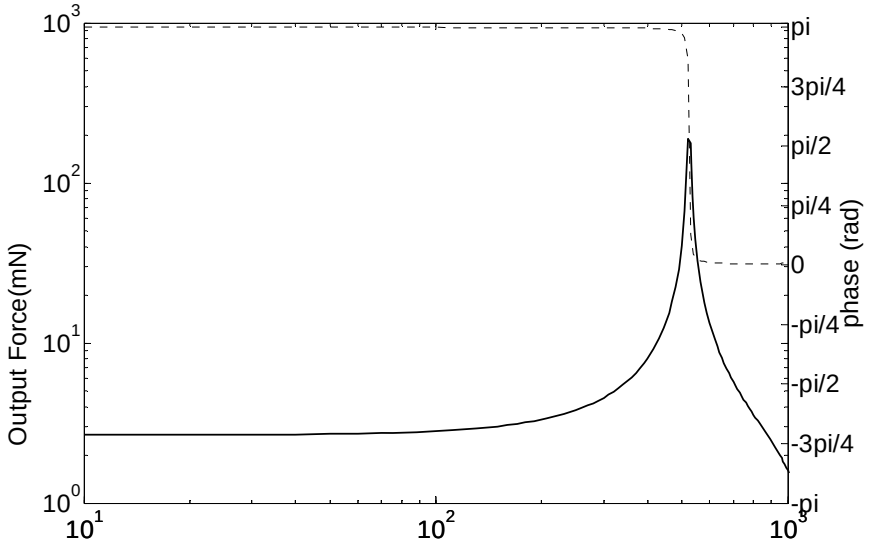

Fig. 4.10 Output force of the cantilever transducer

On the basis of the performance investigation mentioned above, in the following section, an optimization strategy is employed to improve the performances of the cantilever transducer. After that, a comparison of performances between the optimal and original cantilever transducer by numerical simulation will be presented to validate the optimization strategy.

4.3 Optimization Strategy

On the basis of the above investigation, the optimization strategy is then created and carried out to achieve the best performances of the cantilever transducer for simultaneous sensing and actuating. In the optimization process, the optimization algorithm used will be introduced firstly in the following section.

4.3.1 Design Optimization and Algorithm

Designing is a complex human process that has resisted comprehensive description and understanding [107]. The design process can be described in many ways, but we can see immediately that there are certain elements in the process that any description must contain: recognition of need, an act of creation, and a selection of alternatives. Traditionally, the selection of the "best" alternative is the phase of design optimisation. Informally, design optimisation involves [108-111]:

- The selection of a set of variables to describe the design alternatives;
- The selection of an objective (criterion), expressed in terms of the design variables, which we seek to minimize or maximize;
- The determination of a set of constraints, expressed in terms of the design variables, which must be satisfied by any acceptable design;
- The determination of a set of values for the design variables, which minimize (or maximize) the objective, while satisfying all the constraints.

Philosophically, optimization formalizes what humans (and designers) have always done. Operationally, it can be used in design, in any situation where analysis is used and is therefore subjected to the same limitations.

The following will introduce the optimal algorithm compendiously, which is used to design the cantilever transducer. There are many different classes of algorithms, for example, distinguishing from scale of design variable, it has medium-scale (standard) and large-scale algorithms. Here the algorithms, which are used for our case, are list below [112-118].

- Standard algorithms
  - Quasi-Newton Implementation
  - SQP Implementation
- Large-Scale algorithms

These algorithms are presented in detail in Appendix B.

4.3.2 Objective Functions

As described in previous sections, we know that the actuating capability of the cantilever transducer is very weak. The objective function of the optimization for the cantilever transducer design, therefore, is mainly to improve the output force of the cantilever transducer, while the other capabilities, including effective dynamic frequency range, sensitivity and energy efficiency, are also considered in terms of constraints shown in Eq. (4.12).

$$\min : f(x) = -\overline{F} \tag{4.12a}$$

where $\overline{F}$ is the mean value of output force in the effective dynamic frequency range.

$$\begin{cases} c_1(x): \text{first natural frequency}: f_1 > f^* \\ c_2(x): \text{sensitivity}: \mathrm{K} > k^* \\ c_3(x): \text{energy efficiency}: \psi > \psi^* \end{cases} \tag{4.12b}$$

It's known from the performance investigation that the cantilever transducer has low output force, high sensitivity, a low effective frequency range and low energy efficiency. Hence, in the optimization, the main objective function is to greatly increase the output force under the condition of relative sensitivity ($k^* = 1$), effective frequency range ($f^* = 400$) and energy efficiency ($\psi^* = 40\%$). Actually, other strategies, such as improving the energy efficiency, the sensitivity, output power or free stroke as the objectives, have also been selected to try to achieve the best performances. However, the results are less effective than the current strategy.

4.3.3 Design Variables

In the optimization, a set of variables is selected to describe the designed cantilever transducer. Seven design variables are chosen (See Figures 3.1 and 3.2):

- Length of aluminium beam L_s;
- Length of PZT patch L_p;
- Width of cantilever beam W_s;

- Width of PZT patch W_p;
- Thickness of cantilever beam T_s;
- Thickness of PZT patch T_p;
- Position of PZT patch x_1.

The remainder of the parameters listed in Table 3.1 and 3.2 are considered as constant parameters in the optimization. Width of beam and PZT patch, thickness of beam and PZT are assumed to be independent of *x*. It is seen from Eq. 3.37 to Eq. 3.39 that I_p, A_p and S_p are also independent of *x*. Another assumption is given that the width of cantilever beam W_s is the same as the width of PZT patch W_p, which is signed as W in general.

4.3.4 Constraints

After the objective functions are determined and expressed in terms of design variables, a set of constraints should be considered for the optimal process in the following step. Constraints are very important in design optimisation and an active constraint represents a design requirement that has direct influence on the optimization process. There are two kinds of boundary constraints—lower boundary and upper boundary.

- Lower boundary constraints

For the reason of construction, the equations for these constraints are shown below.

$g_1 : x_1 \geq 0$;

$g_2 : L_p \geq 0.1L_s$;

$g_3 : W_s \geq 0.01L_s$;

$g_4 : T_s \geq 0.01L_s$;

$g_5 : T_p / T_s \geq 0.01$.

- Upper boundary constraints

From Figs. 3.1 and 3.2, it is known that the length of the PZT patch must be less than the length of the cantilever beam and the upper boundary of the position of PZT patch x_1 is also determined for the constructional reason. As a beam, the ratio of width or thickness to the length of beam must be less than 0.2. Hence, the upper boundary conditions are determined and expressed in the following equations.

$g_6 : x_1 \leq 0.6L_s$;

$g_7 : L_p \leq L_s$;

$g_8 : W_s \leq 0.2L_s$;

$g_9 : T_s \leq 0.2L_s$;

$g_{10} : T_p / T_s \leq 1$;

$g_{11} : L_p + x_1 \leq L_s$.

4.4 Numerical Validation

After the strategy has been created, an optimization will be carried out to decide the dimensions and system parameters of the transducer. Firstly, a sensitivity analysis of modal models, which describe the rates of change of the modal parameters with the design variable in the spatial model, will be introduced. It is utilized in the optimization to calculate the gradient values of the objective functions or constraints. Secondly, the dimensions and parameters of the cantilever transducer are obtained through the optimization and finally, the performance of the optimized cantilever transducer will be studied and then compare to that of the original cantilever transducer to validate the optimization strategy.

4.4.1 Modal Sensitivity

It has been known that differential equations of motion for an undamped n-degree-of-freedom system can be written in the matrix form shown in Eq.(4.13) [119]:

$$[M]\{\ddot{r}\}+[K]\{r\}=\{F\} \tag{4.13}$$

Using a modal model to solve this problem, by converting the system matrices [M] and [K] (the spatial model) to the two eigenmatrices $\left[\overline{\omega}_r^2\right]$ and $[\Phi]$, we can change Eq. (4.13) into Eq. (4.14):

$$\{r\}=[\Phi]\{\eta\} \tag{4.14}$$

where we can obtain the natural frequencies ω_n and the normalized eigenvectors $[\Phi]$ for the system, by which, we can derive the following diagonalization for $[M]$ and $[K]$ as

$$[\Phi]^T[M][\Phi] = [I] \tag{4.15}$$

$$[\Phi]^T[K][\Phi] = [\omega_n^2] \tag{4.16}$$

We can now differentiate the equation of motion shown in Eq. (4.13) with respect to an arbitrary variable, p, that might be an individual mass or stiffness in the original model, m_i or k_j, or which might be an individual element in the spatial model matrices, m_{ij} or k_{ij}.

$$([K]-\omega_r^2[M])\frac{\partial\{\phi\}_r}{\partial p}+\left(\frac{\partial[K]}{\partial p}-\omega_r^2\frac{\partial[M]}{\partial p}-\frac{\partial\omega_r^2}{\partial p}[M]\right)\{\phi\}_r=\{0\} \tag{4.17}$$

Next, we can premultiply this expression by $\{\phi\}_r^T$:

$$\{\phi\}_r^T([K]-\omega_r^2[M])\frac{\partial\{\phi\}_r}{\partial p}+\{\phi\}_r^T\left(\frac{\partial[K]}{\partial p}-\omega_r^2\frac{\partial[M]}{\partial p}-\frac{\partial\omega_r^2}{\partial p}[M]\right)\{\phi\}_r=0$$

or

$$\{0\}+\{\phi\}_r^T\left(\frac{\partial[K]}{\partial p}-\omega_r^2\frac{\partial[M]}{\partial p}\right)\{\phi\}_r-\frac{\partial\omega_r^2}{\partial p}=0$$

and so[120, 121]

$$\frac{\partial\omega_r}{\partial p}=\frac{1}{2\omega_r}\{\phi\}_r^T\left(\frac{\partial[K]}{\partial p}-\omega_r^2\frac{\partial[M]}{\partial p}\right)\{\phi\}_r \tag{4.18}$$

A similar, although somewhat lengthier, analysis can be made for the eigenvector sensitivity terms, as follows. We can use the previous equation (4.17) together with the fact that the eigenvector sensitivity term can always be expressed as a linear combination of the original eigenvectors:

$$\left([K]-\omega_r^2[M]\right)\sum_{j=1}^{N}\gamma_{rj}\{\phi\}_j+\left(\frac{\partial[K]}{\partial p}-\omega_r^2\frac{\partial[M]}{\partial p}-\frac{\partial\omega_r^2}{\partial p}[M]\right)\{\phi\}_r=\{0\}$$

This time, we shall premultiply the equation by $\{\phi\}_s^T$ and exploit the various orthogonality properties, which apply to form:

$$\{\phi\}_s^T\left([K]-\omega_r^2[M]\right)\sum_{j=1}^{N}\gamma_{rj}\{\phi\}_j+\{\phi\}_s^T\left(\frac{\partial[K]}{\partial p}-\omega_r^2\frac{\partial[M]}{\partial p}-\frac{\partial\omega_r^2}{\partial p}[M]\right)\{\phi\}_r=0$$

so

$$\left(\omega_s^2-\omega_r^2\right)\gamma_{rs}+\{\phi\}_s^T\left(\frac{\partial[K]}{\partial p}-\omega_r^2\frac{\partial[M]}{\partial p}\right)\{\phi\}_r=0$$

hence γ_{rs} and thence[120, 121]

$$\frac{\partial\{\phi\}_r}{\partial p}=\sum_{\substack{s=1\\ s\neq r}}^{N}-\left(\frac{\{\phi\}_s^T\left(\frac{\partial[K]}{\partial p}-\omega_r^2\frac{\partial[M]}{\partial p}\right)\{\phi\}_r}{\left(\omega_s^2-\omega_r^2\right)}\right)\{\phi\}_s \tag{4.19}$$

In Chapter 3, actuator and sensor equations of the cantilever transducer have been derived, which are expressed as Eqs. (4.20) and (4.21).

$$[M]\{\ddot{r}\}+[K]\{r\}=[\Theta]E+[B_f]F \tag{4.20}$$

$$i=[\Theta]^T\{\dot{r}\}+C_p\dot{E} \tag{4.21}$$

where,

$$[M]=[M_s]+[M_p] \tag{4.22}$$

$$[K]=[K_s]+[K_p] \tag{4.23}$$

where $[M_s]$ and $[M_p]$ are mass matrices for the cantilever and piezoelectric patch shown in Eq. (3.27) and (3.28) respectively; $[K_s]$ and $[K_p]$ are stiffness matrices for the cantilever and the piezoelectric patch shown in Eq. (3.29) and (3.30) respectively.

From the Eqs. (4.22), (3.27), (3.28), the sensitivity analysis of modal models are expressed as:

$$\frac{\partial M}{\partial L_p} = A_p \Psi_r{}^T \rho_p \Psi_r \Big|_{x=x_2} \tag{4.24}$$

$$\frac{\partial M}{\partial W} = \frac{\partial A_s}{\partial W} \rho_s \Gamma_s + \frac{\partial A_p}{\partial W} \rho_p \Gamma_p \tag{4.25}$$

$$\frac{\partial M}{\partial T_s} = \frac{\partial A_s}{\partial T_s} \rho_s \Gamma_s \tag{4.26}$$

$$\frac{\partial M}{\partial T_p} = \frac{\partial A_p}{\partial T_p} \rho_p \Gamma_p \tag{4.27}$$

$$\frac{\partial M}{\partial x_1} = A_p \Psi_r{}^T \rho_p \Psi_r \Big|_{x=x_1}^{x=x_2} \tag{4.28}$$

where,

$$x_2 = x_1 + L_p \tag{4.29}$$

$$\Gamma_s = \int_0^L \Psi_r{}^T \Psi_r dx \tag{4.30}$$

$$\Gamma_p = \int_{x_1}^{x_2} \Psi_r{}^T \Psi_r dx \tag{4.31}$$

The following equations are derived from Eq. (4.23), (3.29) and (3.30).

$$\frac{\partial K}{\partial L_p} = I_p (\Psi_r'')^T \hat{c}_p (\Psi_r'')\Big|_{x=x_2} \tag{4.32}$$

$$\frac{\partial K}{\partial W} = \frac{\partial I_s}{\partial W}\hat{c}_s \Lambda_s + \frac{\partial I_p}{\partial W}\hat{c}_p \Lambda_p \tag{4.33}$$

$$\frac{\partial K}{\partial T_s} = \frac{\partial I_s}{\partial T_s}\hat{c}_s \Lambda_s + \frac{\partial I_p}{\partial T_s}\hat{c}_p \Lambda_p \tag{4.34}$$

$$\frac{\partial K}{\partial T_p} = \frac{\partial I_p}{\partial T_p}\hat{c}_p \Lambda_p \tag{4.35}$$

$$\frac{\partial K}{\partial x_1} = I_p (\Psi_r'')^T \hat{c}_p (\Psi_r'')\Big|_{\substack{x=x_2 \\ x=x_1}} \tag{4.36}$$

where,

$$\Lambda_s = \int_0^L (\Psi_r'')^T (\Psi_r'') dx \tag{4.37}$$

$$\Lambda_p = \int_{x_1}^{x_2} (\Psi_r'')^T (\Psi_r'') dx \tag{4.38}$$

4.4.2 Optimal Results

In order to design a proper cantilever transducer, which can most efficiently sense and actuate the SMD system, the proposed optimization strategy is utilized, in which $k^* = 1$, $f^* = 400$ and $\psi^* = 40\%$. Finally, the optimal parameters of the new cantilever transducer have been obtained using the software program (MATLAB software, See Appendix B) and dimensions of the cantilever transducer are listed in Table 4.2.

Table 4.2 Dimensions of the cantilever transducer

Design Variables	Symbol	Original	New
Length of beam	L_s	L'	L
Width of beam	W_s	0.133 L'	0.092L
Thickness of beam	T_s	0.011 L'	0.092L
Length of PZT	L_p	0.222 L'	0.965L
Width of PZT	W_p	0.133 L'	0.092L
Thickness of PZT	T_p	0.002 L'	0.043L
Position of PZT	x_1	0.056 L'	0

Mark: *L'=90mm*; *L=190mm*

4.4.3 Performance of the Optimized Cantilever Transducer

Using the dimensions derived, the transduction matrix of the new cantilever transducer can be calculated from Eq. 3.54 to Eq. 3.57. The numerical results are shown in the Figures 4.11—4.14, in which the solid line represents the new cantilever transducer and the dashed line is the original transducer.

From Figure 4.15, it is seen that the determinant of the new transduction matrix is unity and the phase is near to zero. The reciprocity of the transducer system mentioned in Chapter 3 also exists in the transduction functions.

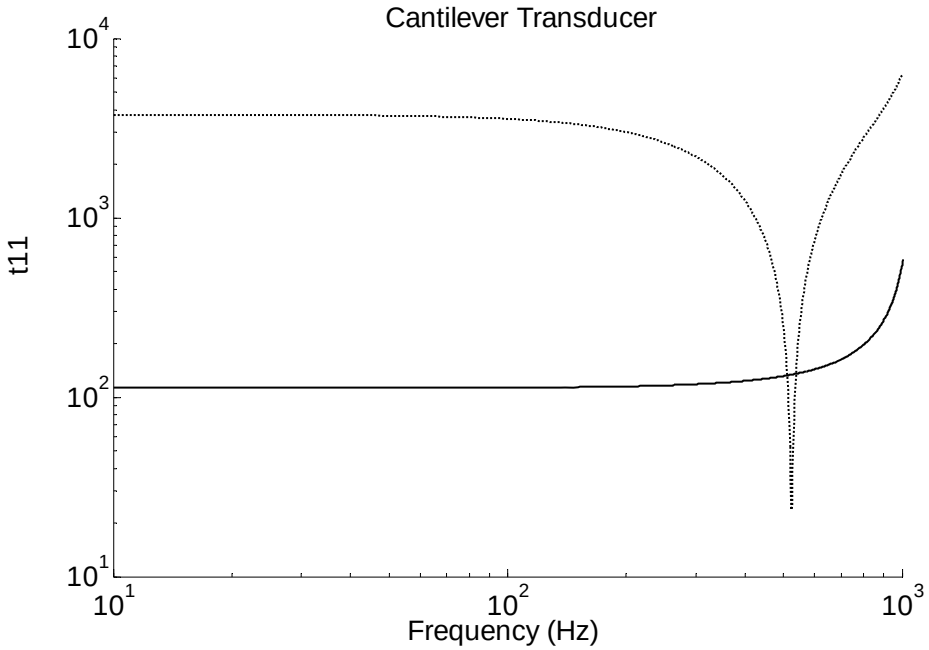

Fig. 4.11 Numerical results of the transduction element t_{11}

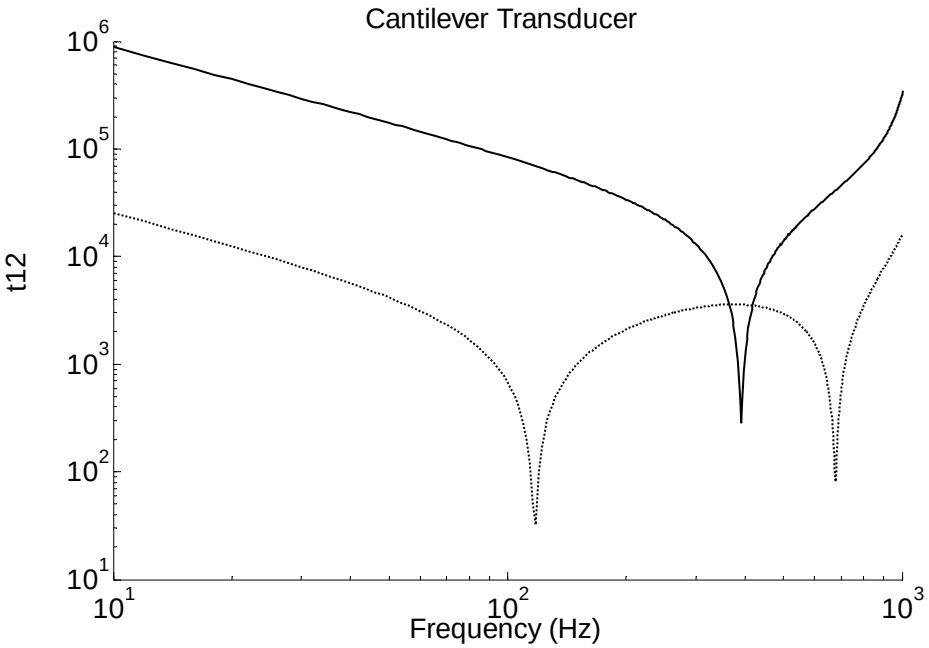

Fig. 4.12 Numerical results of the transduction element t_{12}

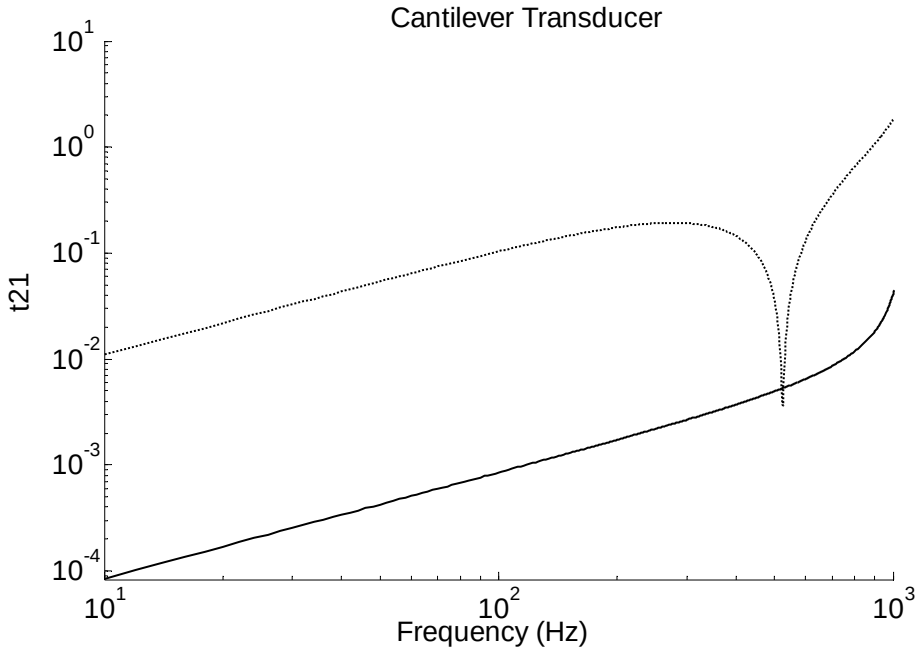

Fig. 4.13 Numerical results of the transduction element t_{21}

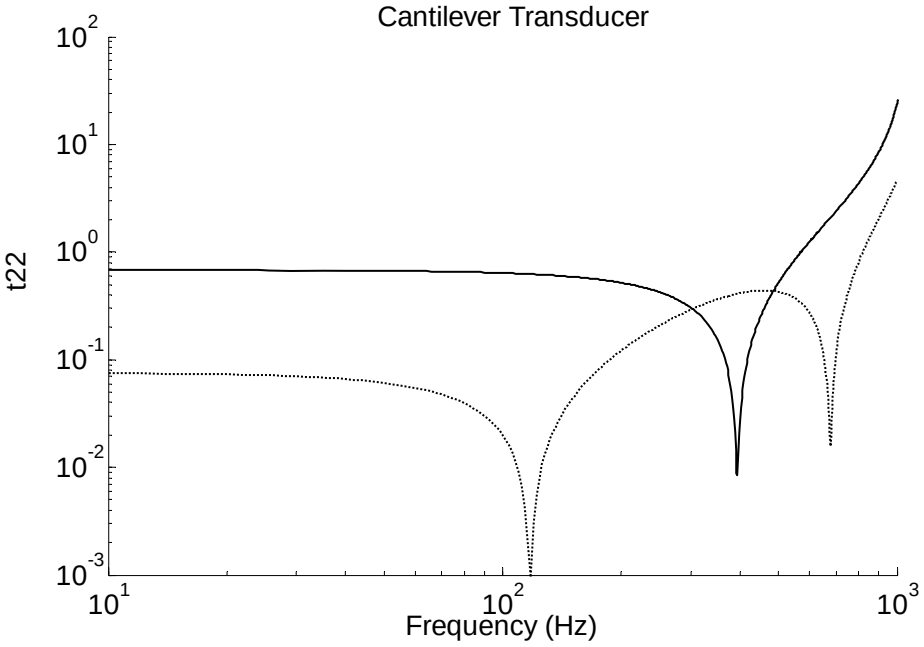

Fig. 4.14 Numerical results of the transduction element t_{22}

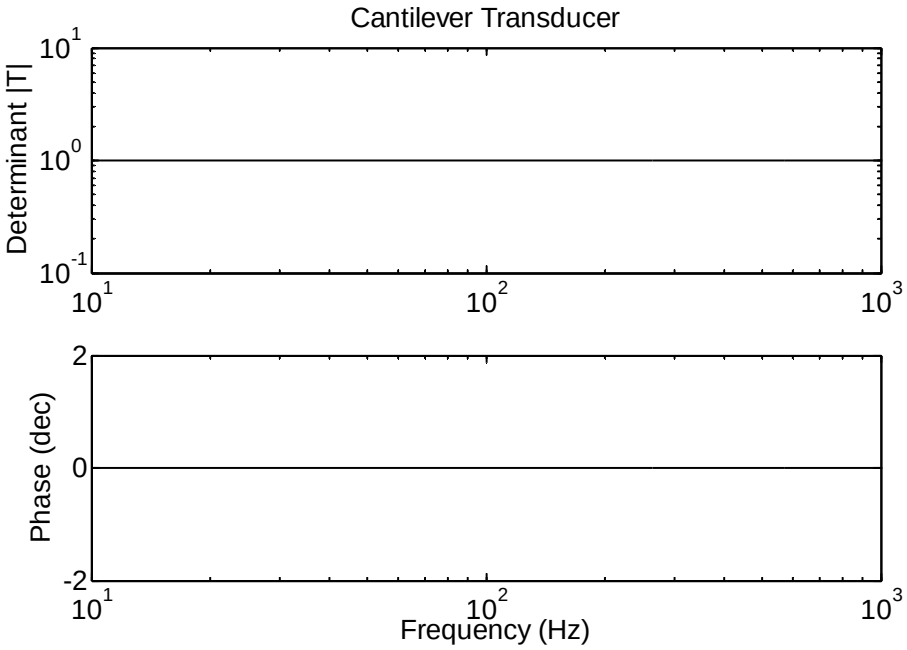

Fig. 4.15 Determinant of the new transduction matrix [*T*]

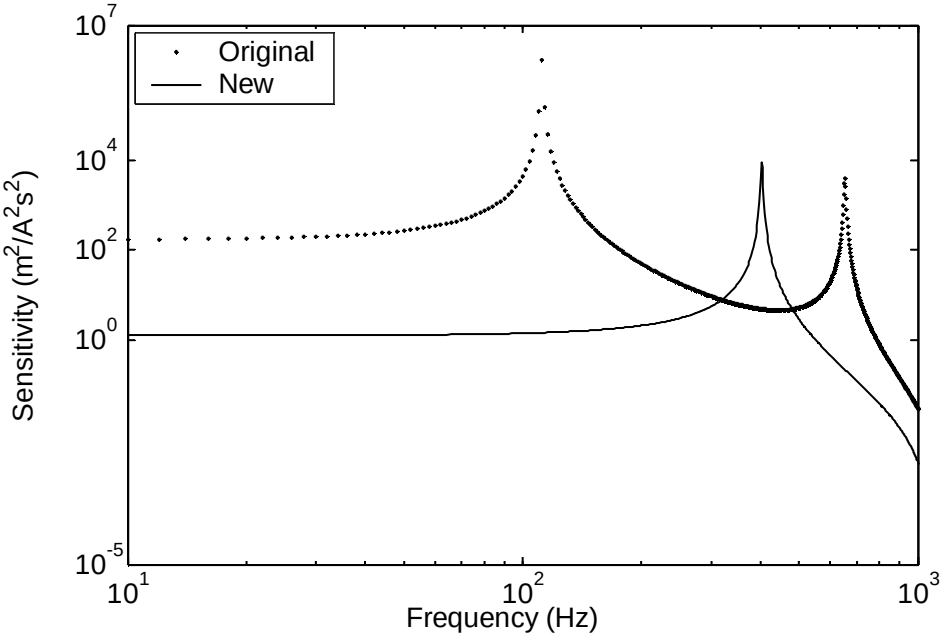

Fig. 4.16 A comparison result of sensitivity

between the origin (dot) and the new cantilever transducer (solid)

The performances of the new cantilever transducer are also studied and a comparison between the original and the new cantilever transducer has been done. Figure 4.16 shows the comparison results of the sensitivity between the original (dot line) and the new cantilever transducer (solid line). The effective frequency range of the new cantilever transducer greatly increases while the sensitivity reduces as illustrated in Figure 4.16. As we know, the sensitivity of the original transducer is very high, which is not necessary. After the optimization, the sensitivity of the new transducer greatly reduces but it is also more than 1. Hence, the new cantilever transducer is also effective in sensing the spring-mass-damper system.

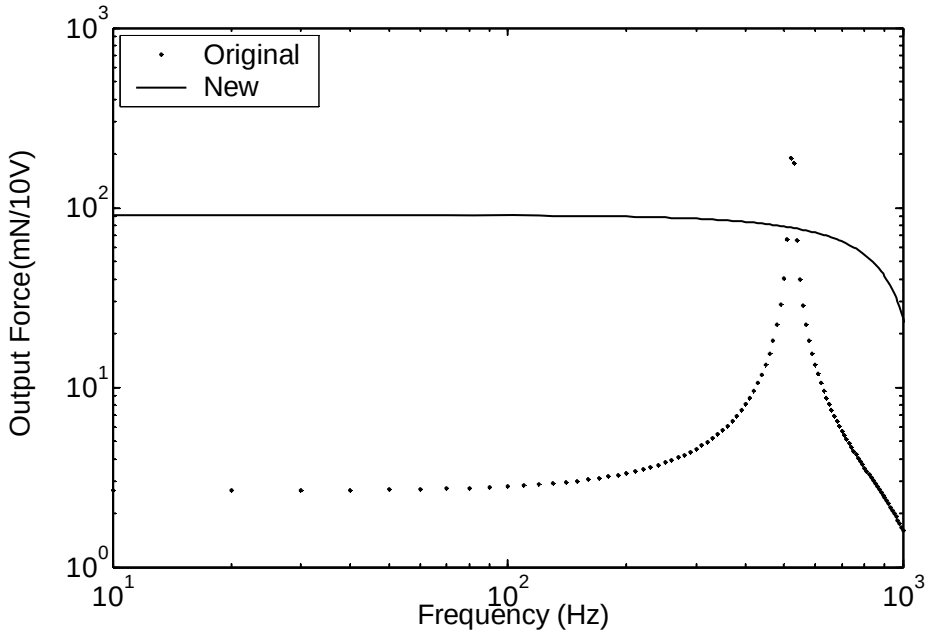

Fig. 4.17 A comparison result of output force

between the origin (dot) and the new cantilever transducer (solid)

A comparison result of the output force between the original and the new cantilever transducer is also shown in Figure 4.17. It is observed that the force at the output port of the new transducer is much higher and more stable than the original one. It means that the actuating capability of the new transducer has increased greatly. Thus, from Figures 4.16

and 4.17, it is concluded that the sensing and actuating capability of the new cantilever transducer has been balanced. From the above numerical simulation, it is demonstrated that the performances of the new cantilever transducer are better than those of the original transducer and that the optimization strategy is feasible to design a cantilever transducer for the best simultaneous sensing and actuating.

4.5 Summary

Since the PZT coated cantilevers can serve as a vibration exciter and a sensor simultaneously to measure point mechanical impedance of structures, their performances including sensing and actuating capabilities, such as sensitivity, effective operating frequency range, energy efficiency and output force, have been analyzed and studied numerically. From the numerical investigation, it is concluded that the sensitivity of the cantilever transducer is affected by the mechanical impedance of the load of interest and the transducer can be used in the low frequency range before the first natural frequency. It's also known that the sensitivity and effective dynamic frequency range are affected by stiffness and mass. If the stiffness increases, the effective dynamic frequency range will increase, while the sensitivity will conversely decrease. When the mass increases, the effective dynamic frequency range will decrease, while the sensitivity remains almost the same. If the structural damping is considered, the damping factor doesn't affect the sensitivity and dynamic frequency range.

In this chapter, the energy efficiency of the cantilever transducer which drives a SMD system has also been studied and numerical results show that energy efficiency is an important performance index for designing our cantilever transducer. Energy efficiency reveals the energy conversion between the electrical power and mechanical power and represents actuator effectiveness to excite the system and energy efficiency. It is well known that the actuator becomes most efficient when the actuator impedance matches the structural impedance. The resonance of the electro-mechanical system occurs when the actuator impedance and structural impedance are matching. Since the transducer impedance Z_A is an intrinsic attribute and can be influenced by parameters of the cantilever, such as length, width and thickness of PZT patch and the cantilever beam. The cantilever transducer can be designed as an optimal actuator to excite a system of interest, when the impedance Z_A matches the structural impedance of system.

Since output force is another important index of the actuating capability of the transducer. The equation for numerical calculation of the output force is derived and the numerical simulation is also done. From the numerical results, it's known that the original PZT coated cantilever is not an effective actuator to drive the load, though its sensitivity is very high. Therefore, optimal design of the cantilever transducer for SSA is necessary.

Based on this investigation and numerical results, an optimization strategy is employed to design the cantilever transducer for best simultaneous sensing and actuating. The objective function of the optimization is to improve the output force of the cantilever transducer and the other capabilities, including effective dynamic frequency range,

sensitivity and energy efficiency. These were also considered in terms of constraints. By comparing performances of the new cantilever with those of the original cantilever, it can be seen that the effective frequency range greatly increases and sensitivity is also enough to sense the load. More importantly, the actuating capability of the transducer is strongly emphasized. It is proved by numerical simulation that the new cantilever is a good actuator with balanced sensing capabilities and the optimization strategy is successful in designing the cantilever transducer for simultaneous sensing and actuating.

CHAPTER 5

EXPERIMENTAL INVESTIGATION

In the last chapter, the performances of a PZT-coated cantilever serving as a vibration exciter and a sensor simultaneously have been thoroughly studied. Besides, an optimization strategy has been created and carried out to achieve the best performances of the cantilever transducer for simultaneous sensing and actuating. Through the numerical simulations, it has been demonstrated that the performances of the new cantilever transducer are better than those of the original transducer and the optimization strategy is feasible to design a cantilever transducer for best SSA. To verify the validity of the proposed optimization, in Chapter 5, a cantilever transducer will be designed by the proposed optimization strategy and then utilized in the experiments for the mechanical impedance measurement.

5.1 An Optimized PZT-Coated Cantilever

In this experiment, a PZT patch has been provided in a specified dimension (L_p, W_p, T_p are given) and material (Fuji-C91), thus, a new optimisation has been conducted using the same strategy except the design variables. The design variables in this optimisation are the

length and thickness of the cantilever beam and the position of the bonded PZT patch onto the cantilever beam. Finally, the dimensions of the optimized cantilever transducer are listed in Table 5.1. The material properties of the cantilever beam and PZT patch are listed in Table 5.2. Since, in practice, it is difficult to paste the PZT patch on the clamped end of cantilever beam, the distance from the PZT patch to the clamped end is 1.71*mm*.

Table 5.1 Dimensions of a PZT-coated cantilever

Component	Length (*mm*)	Width (*mm*)	Thickness (*mm*)	Position (*mm*)
Cantilever	88.0	25.0	3.0	
PZT (given)	25.0	25.0	0.202	0

Table 5.2 Material properties of a PZT-coated cantilever

Category	Unit	Cantilever (Al)	PZT (Fuji C-91)
Density	(kg/m^3)	2690	7800
Poisson's Ratio		0.34	0.38
Elastic Modulus	$(\times 10^9\ N/m^2)$	70.23	$c_{11}^E = 59$ $c_{33}^E = 54$ $c_{55}^E = 24$
Piezoelectric Constants	$(\times 10^{-12}\ m/V)$		$d_{31} = -330$ $d_{33} = 640$ $d_{15} = 820$
Relative Dielectric Constants			$\varepsilon_{11}^T / \varepsilon_0 = 4400$ $\varepsilon_{33}^T / \varepsilon_0 = 5500$

As mentioned in the Chapter 3, once the transduction matrix of the cantilever transducer is completely calibrated, the mechanical impedance can be detected by measuring the input electrical impedance using the following equation.

$$Z_m = \frac{t_{22}Z_e - t_{12}}{t_{11} - t_{21}Z_e} = Z_{mo}\frac{Z_e - Z_{ef}}{Z_e - Z_{ec}} \tag{5.1}$$

where Z_m is the mechanical impedance of the structure under testing; Z_e is the corresponding electrical input impedance of the transducer loaded by the structure under testing; Z_{mo} is the mechanical impedance of the transducer when it is electrically open-circuited, i.e. $Z_{mo} = \frac{F}{v}\Big|_{i=0} = -\frac{t_{22}}{t_{21}}$; Z_{ec} and Z_{ef} are the electrical impedance of the transducer when it is mechanical clamped and free respectively, i.e. $Z_{ec} = \frac{E}{i}\Big|_{v=0} = \frac{t_{11}}{t_{21}}$, and $Z_{ef} = \frac{E}{i}\Big|_{F=0} = \frac{t_{12}}{t_{22}}$.

In the experiment, the cantilever transducer will be calibrated firstly before the measurement. After the calibration, case studies utilizing rigid block and beam structure as a sample of cantilever transducer will be carried out in the following sections.

5.2 Calibration of the Cantilever Transducer

As mentioned in Section 3.5, in experiments, direct identification of these transduction elements is impractical. This is because mechanical clamp conditions and electrical open-circuit conditions are difficult to be realized in a laboratory. An alternative way to identify the transduction properties of the cantilever transducer is introduced in Section 3.5. In the experiment, three impedances Z_{mo} , Z_{ec} and Z_{ef} are essentially frequency response

functions of the transducer. In principle, they can be made known by calibrating the device in advance under various mechanical boundary conditions and electrical terminal conditions. Among these impedances, Z_{ef} can be easily calibrated by letting the output port free mechanically. While Z_{mo} and Z_{ec} will be indirectly identified from a set of the measured Z_{ef} and Z_e of the actuator when various known masses are applied to its output port. The calibration method is described in Section 3.5 in detail and will not be repeated. The equations used in the calibration are listed below.

$$Z = [A^T A]^{-1} A^T C \tag{5.2}$$

where

$$Z = \begin{bmatrix} Z_{mo} \\ Z_{ec} \end{bmatrix} \tag{5.3a}$$

$$A = \begin{bmatrix} a_1 & b_1 \\ a_2 & b_2 \\ \cdots & \cdots \\ a_m & b_m \end{bmatrix} \tag{5.3b}$$

$$C = \begin{bmatrix} c_1 \\ c_2 \\ \cdots \\ c_m \end{bmatrix} \tag{5.3c}$$

where

$$a_k = \frac{Z_e^k - Z_{ef}}{Z_M^k} \tag{5.4a}$$

$$b_k = 1 \tag{5.4b}$$

$$c_k = Z_e^k \tag{5.4c}$$

where $k = 1,2,\cdots,n$. n is the number of times of adding masses to the mechanical port of the transducer.

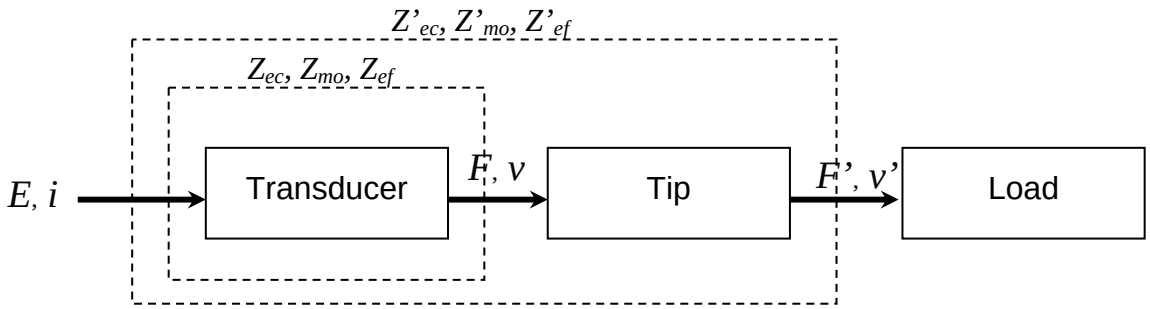

Fig. 5.1 A schematic of the cantilever transducer with tip

In this experiment, in order to test an object, a tip has to be fixed at the end of the cantilever. The load will be driven by the cantilever transducer through the tip. The schematic of the system is shown in Figure 5.1. The transduction functions of the cantilever transducer will be calibrated using Eq. (5.2) by adding different masses. For the cantilever transducer, the following equation can be derived from Eq. (5.1).

$$Z_M + Z_M\big|_{tip} = Z_{mo}\frac{Z_e - Z_{ef}}{Z_e - Z_{ec}} \tag{5.5}$$

For the whole system including the cantilever and the tip shown in Figure 5.1, from Eq. (5.1), the following equation can be obtained.

$$Z_M = Z'_{mo}\frac{Z_e - Z'_{ef}}{Z_e - Z'_{ec}} \tag{5.6}$$

where Z'_{mo}, Z'_{ef} and Z'_{ec} are the transduction function of the whole system including the cantilever transducer and the tip. In these impedances, Z'_{ef} can be measured directly,

which is the input electrical impedance when no load is on the whole system. The other two impedances will be calculated when Z_{mo} , Z_{ec} and Z_{ef} are calibrated using the following method. Firstly, the mechanical impedance of the tip will be measured by solving Eq. (5.5) and (5.6) if no load is added on the system, where $Z_m=0$. The equation is shown in Eq. (5.7).

$$Z_m\Big|_{tip} = Z_{mo} \cdot \frac{Z'_{ef} - Z_{ef}}{Z'_{ef} - Z_{ec}} \tag{5.7}$$

Secondly, when the system is under an electrically open-circuited condition, the input electrical impedance turns to infinite, then,

$$Z'_{mo} = Z_{mo} - Z_m\Big|_{tip} \tag{5.8}$$

Also, when the system is under a mechanical clamped condition, Z'_{ec} is derived.

$$Z'_{ec} = Z_{ec} \tag{5.9}$$

5.2.1 Experimental Setup

Figure 5.2 shows the experimental setup of the cantilever transducer without the tip for the calibration. Dimensions of the cantilever components have been listed in Table 5.1 and the material properties of the cantilever beam and PZT patch are listed in Table 5.2.

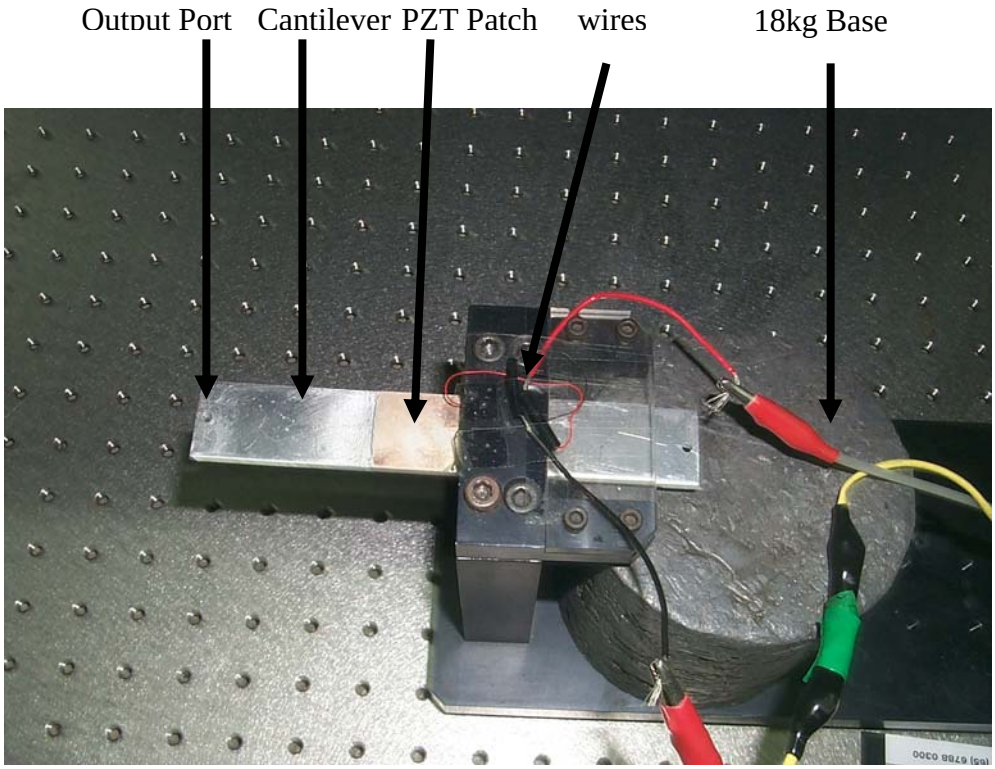

Fig. 5.2 A picture of the cantilever transducer without tip

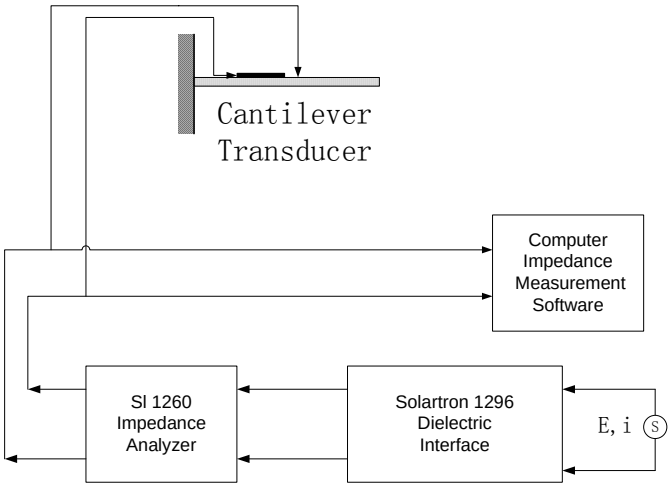

Fig. 5.3 A schematic of the calibration system

The schematic view of the calibration system is shown in Figure 5.3, where the signal of voltage is generated from SI 1260 Impedance Analyzer as shown in Figure 5.4. The current is also measured by this impedance analyzer. After that, both voltage and current signals are analyzed in the computer impedance measurement software. Finally, the input electrical impedance is obtained. In this experiment, the input voltage is set to be 3 Volts and the working frequency range is set from 1*Hz* to 1000*Hz* with an interval of 1*Hz*.

Fig. 5.4 A picture of SI 1260 and Solartron 1296

As mentioned above, in order to calibrate Z_{ec} and Z_{mo} of the cantilever transducer, several masses are needed for the calibration. The picture of selected masses is shown in Figure 5.5 and the mass is listed in Table 5.3.

Fig. 5.5 A picture of selected masses

Table 5.3 Selected masses for the calibration

Mass (*mg*)	A	B	C	D
1 (Fe)	358.5	948.7	1654.6	2019.8
2 (Al)	250.0	537.6	1068.3	1366.1
3 (Al)	413.0	738.4	1460.8	1853.3
4 (Fe)	899.24	1654.3	2362.4	

5.2.2 Measurement of Z_{ef}

To measure frequency response function Z_{ef}, the cantilever transducer works under free condition, as illustrated in Figure 5.2. An excitation voltage with an amplitude of 3 Volt is applied to the cantilever transducer by SI 1260 Impedance Analyzer. At the same time, the input electrical impedance Z_{ef} is measured. From the definition of Z_{ef}, which is $Z_{ef} = \frac{E}{i}\Big|_{F=0} = \frac{t_{12}}{t_{22}}$ and Eq. (3.54—3.57), numerical results of Z_{ef} are also obtained.

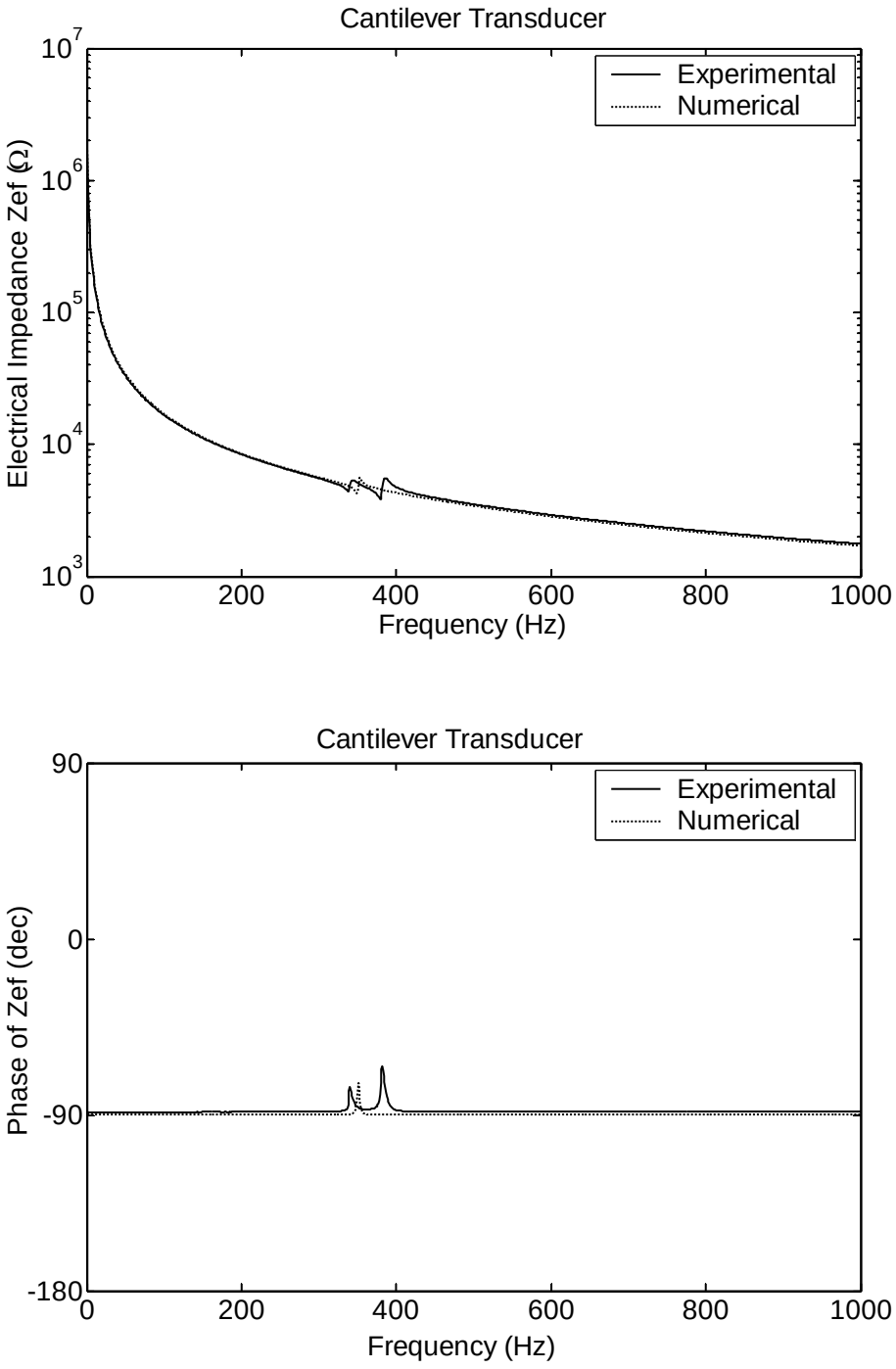

Fig. 5.6 Comparison of Z_{ef} between numerical (dash) and experimental (solid) results

In the Figure 5.6, the amplitude and phase characteristics of the experimentally determined Z_{ef} are compared with the numerical results. Although the peak values and resonant frequency are a little different for the two methods due to damping, in general, close agreement in both amplitude and phase is found. However, in the experimental results, an extra resonant frequency is found in the figure due to the bending in Y direction.

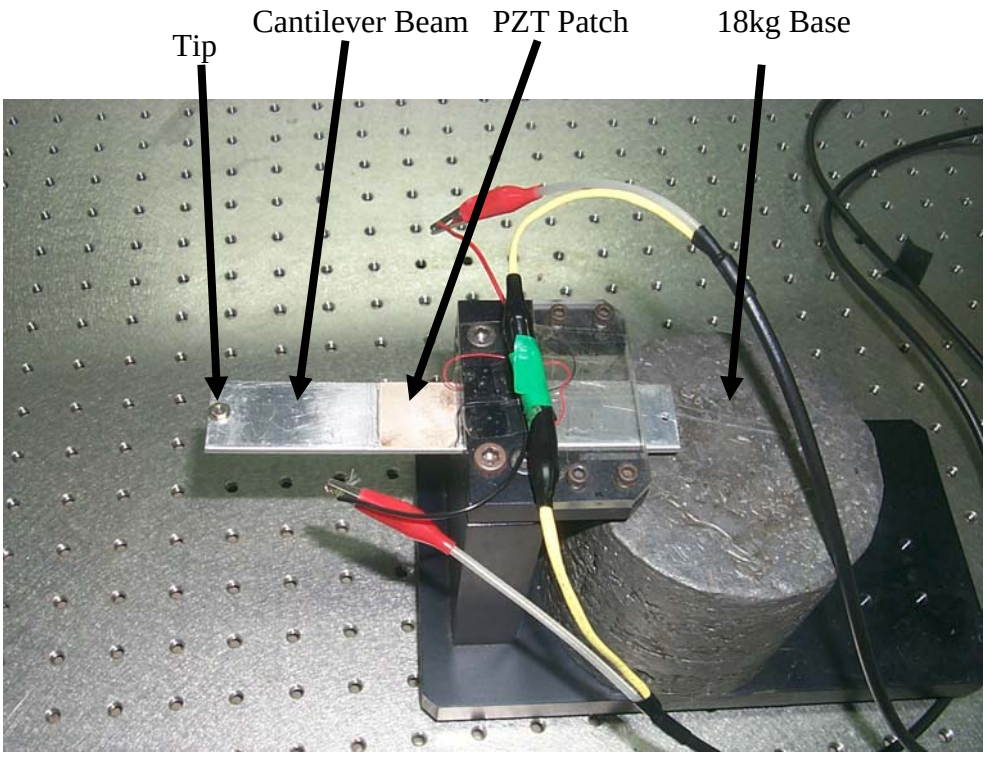

Fig. 5.7 Picture of cantilever transducer with tip

Fig. 5.8 Components of tip

After that, experimental results Z_{eft} of the cantilever transducer with tip are also obtained. The picture of the system and the tip are shown in Figure 5.7 and 5.8 respectively. The tip consists of an indenter, screw and washer, with a total mass of 1574.29*mg*. Figure 5.9 shows the experimental results of Z_{eft}, in which the solid line is the magnitude and the dashed line is the phase. It is noted that the tip is regarded as a mass without stiffness in the experiment, while the washer, which introduces the stiffness, may brings some discrepancies, especially in the high frequency range.

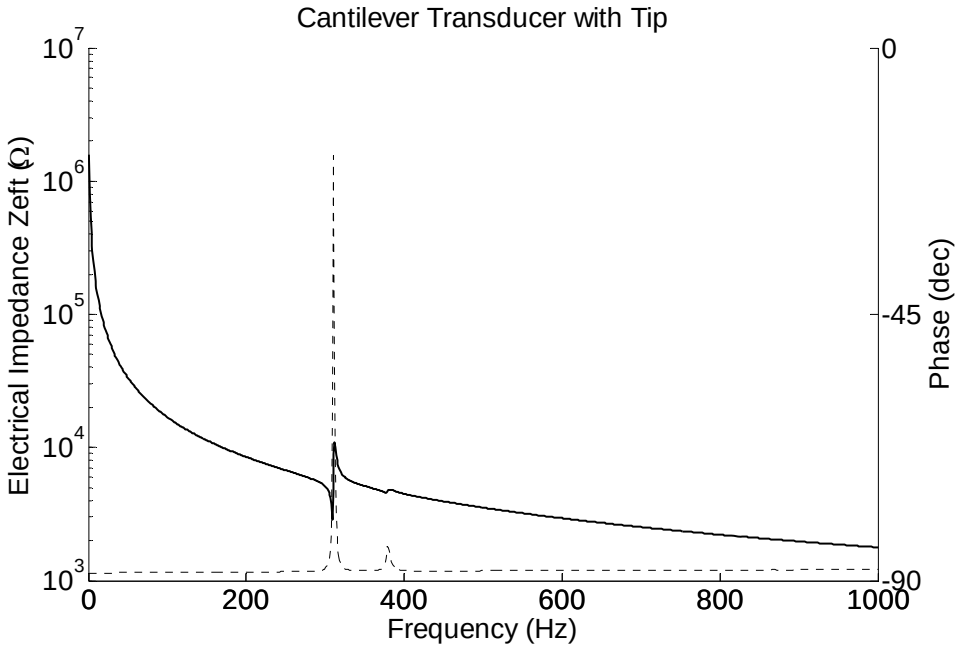

Fig. 5.9 Experimental results of Z_{eft}

5.2.3 Experimental Evaluation of Z_{ec} and Z_{mo}

As we know, Z_{mo} is the mechanical impedance of the transducer when it is electrically open-circuited, i.e. $Z_{mo} = \frac{F}{v}\Big|_{i=0} = -\frac{t_{22}}{t_{21}}$. Z_{ec} is the electrical impedance of the transducer

when it is mechanical clamped, i.e. $Z_{ec} = \frac{E}{i}\Big|_{v=0} = \frac{t_{11}}{t_{21}}$. Z_{mo} and Z_{ec} are much more difficult to calibrate because mechanical clamp conditions and electrical open-circuit conditions are difficult to establish in a laboratory. To overcome these problems, several masses are selected as loads applied to the output port of the cantilever transducer. After the electrical impedance responses under different loads are measured, Z_{mo} and Z_{ec} can be evaluated by solving Eq. (5.2). In the calibration, selected masses are listed in Table 5.3. The experimental setup is depicted in Figure 5.10. A calibration mass is glued to the output port of the cantilever transducer by double-sided glue. After AC voltage with the same amplitude and phase is supplied to the cantilever transducer, the electrical impedance Z_e^m is measured by the SI Impedance Analyzer.

Fifteen calibration masses are utilized to experimentally determine Z_{ec} and Z_{mo}. For each mass, testing illustrated in Figure 5.10 is carried out. The measured electrical impedance corresponding to each different calibration masses is overlay vs. frequency in Figure 5.11. Due to having many curves measured and the difficulty in showing them in one figure, in Figure 5.11, only 5 curves are random selected and shown. The enlarged figure around resonance is depicted in Figure 5.12. In the figure, from the left to the right, each curve represents the electrical impedance response when the cantilever transducer is loaded with a different mass. It is found that Z_e^m directly reflects the properties of the mechanical load attached to the transducer. The greater the calibration mass, the lower the resonance. In the experimental results, the extra resonant frequency is also found in the figure due to the bending in Y direction.

From the measured electrical impedance Z_e^m, calibration functions Z_{mo} and Z_{ec} are easily calculated using Eq. (5.2). These experimentally determined Z_{mo} and Z_{ec} are compared with the numerical results in Figures 5.13 and 5.14. It is observed that Z_{mo} and Z_{ec}, which are determined via two calibration ways, are comparable. This validates the practicability of the present calibration method. The discrepancy is more outstanding in low frequency ranges, which suits the fact that high accuracy exists in the operating frequency range of the cantilever transducer. The difference between the experimental and numerical results is also due to the fact that the numerical studies are based on ideal conditions; while, in experiments, the fabrication of the cantilever transducer and calibration masses is not absolutely ideal. Nevertheless, the confirmation of theoretical predictions by the experimental results is quite clear.

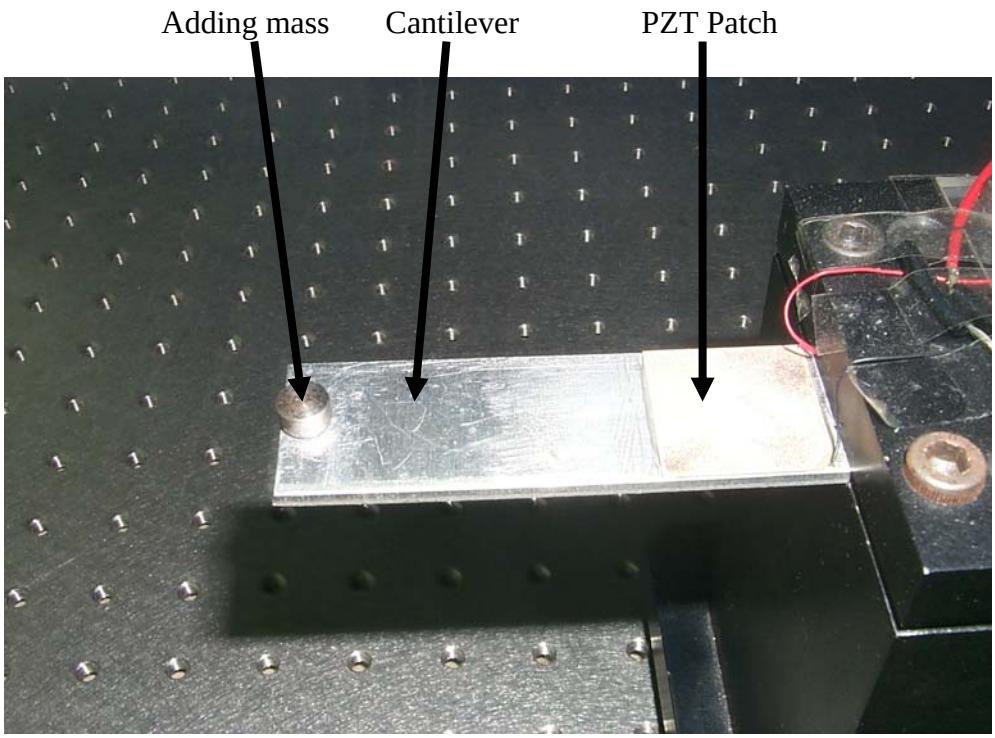

Fig. 5.10 Picture of setup for evaluation of Z_{ec} and Z_{mo}

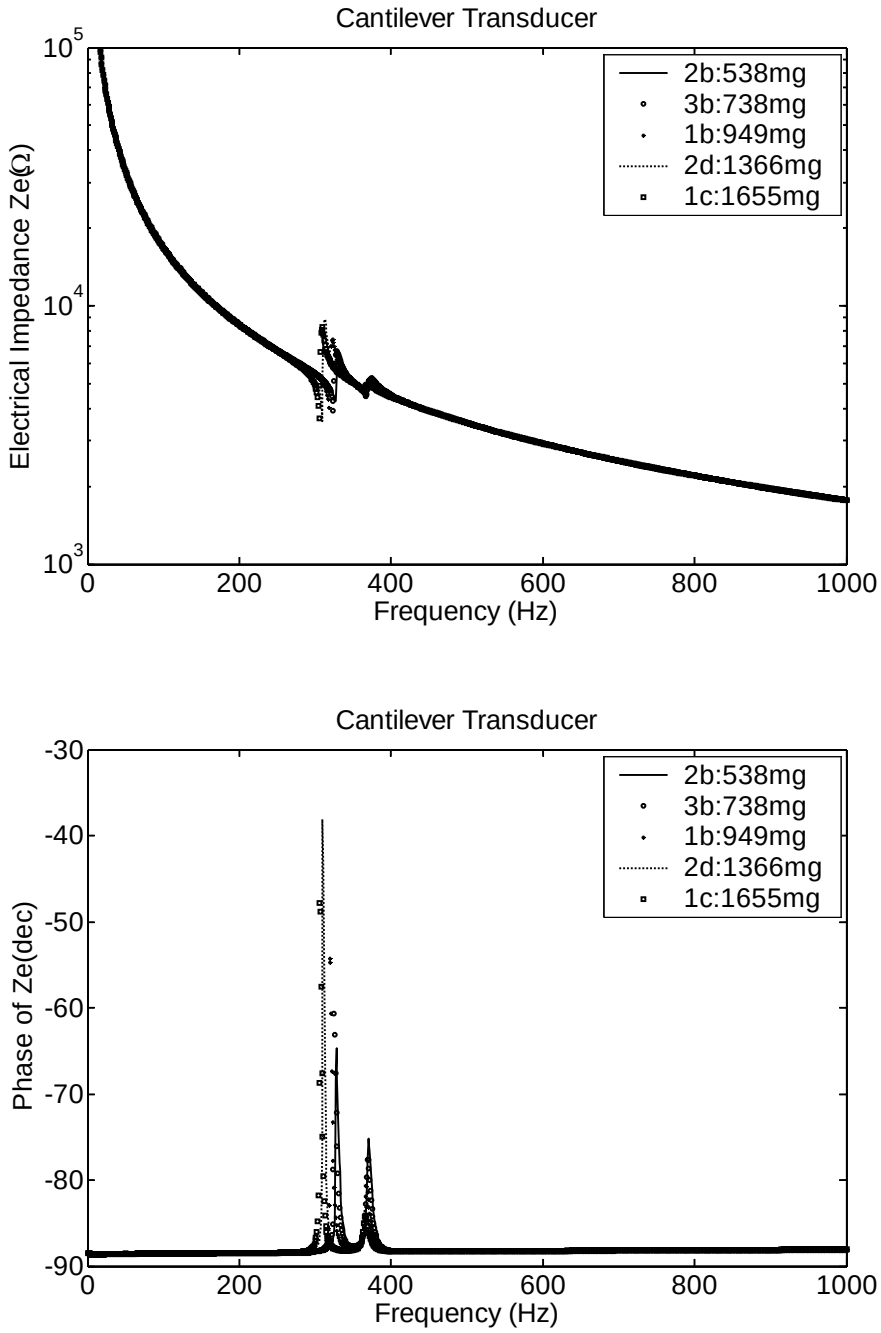

Fig. 5.11 Electrical impedance corresponding to different additional masses

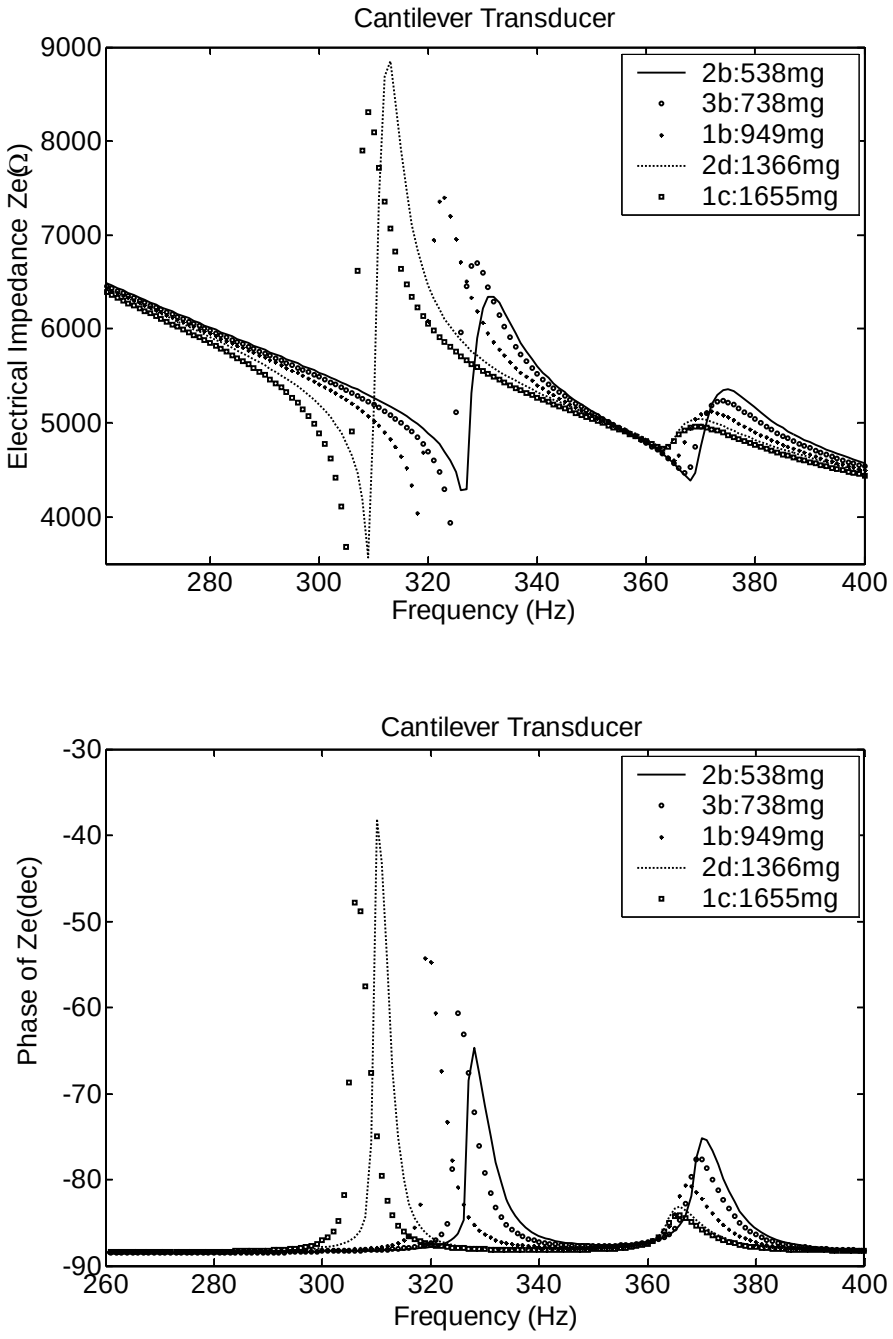

Fig. 5.12 Electrical impedance responses around resonance

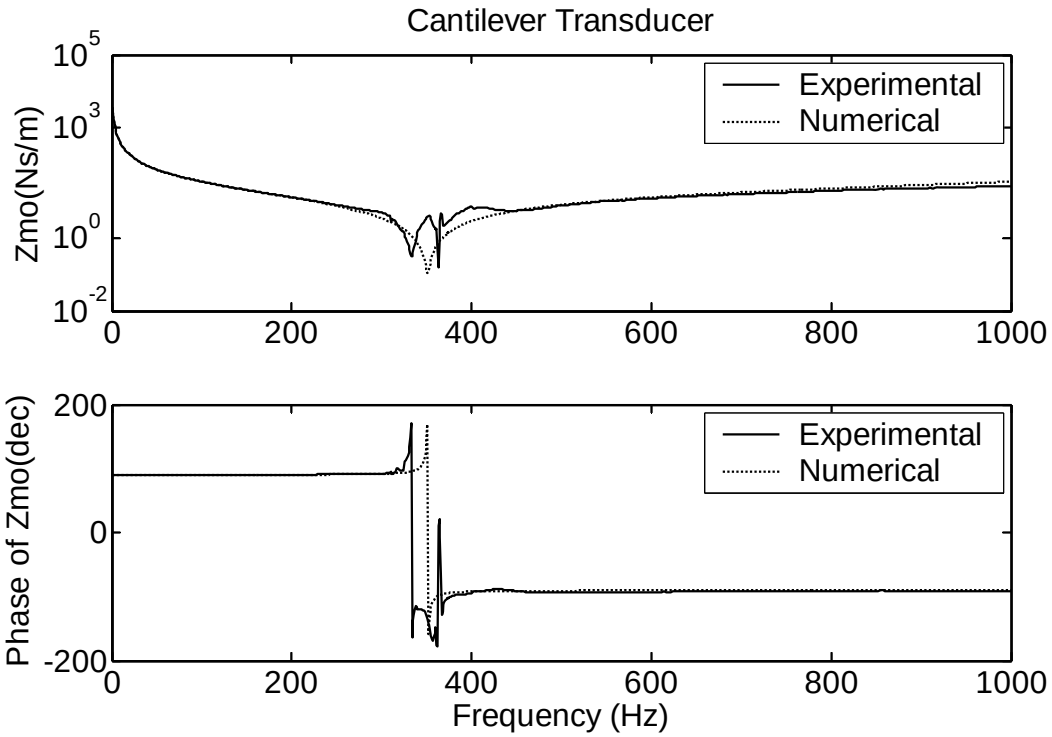

Fig. 5.13 Comparison of Z_{mo} between numerical (dash) and experimental (solid) results

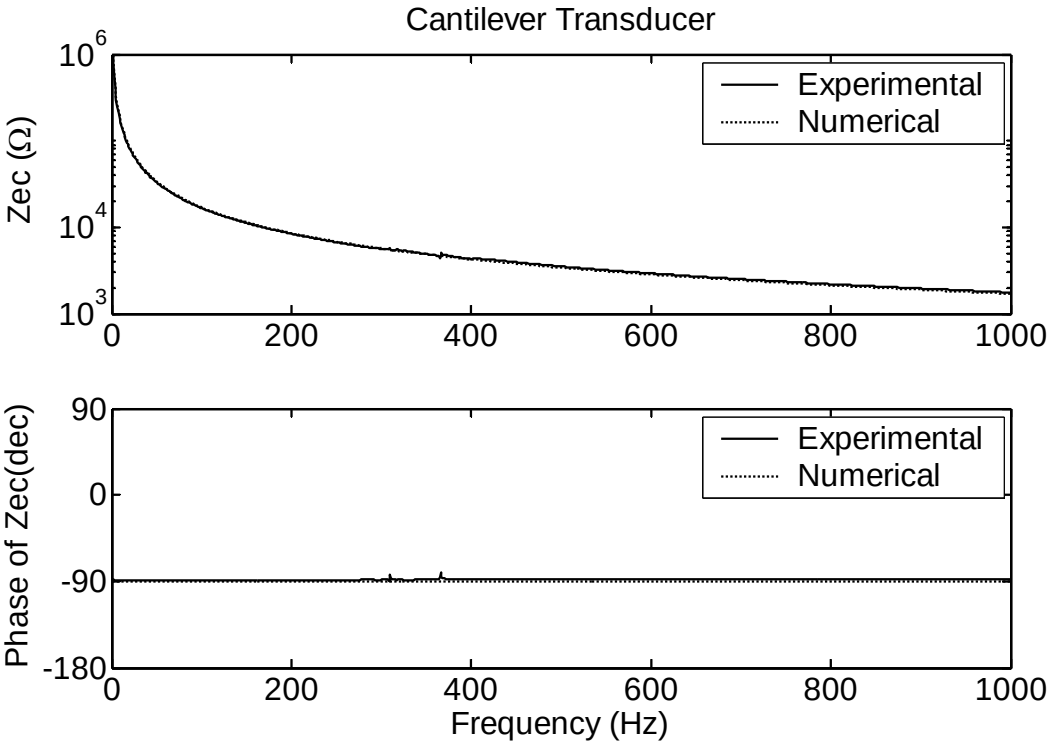

Fig. 5.14 Comparison of Z_{ec} between numerical (dash) and experimental (solid) results

After that, mechanical impedance of the tip can be derived by using Eq. (5.7), since the electrical impedance of the cantilever transducer with the tip is measured and transduction elements of the transducer are calibrated. Experimental results and numerical results are compared in Figure 5.15. Here, the tip is regarded as a mass, so that mechanical impedance of the tip is $j \cdot m\omega$, where ω is the working frequency. From the figure, it is concluded that the mechanical impedance of the tip at the output port is successfully detected.

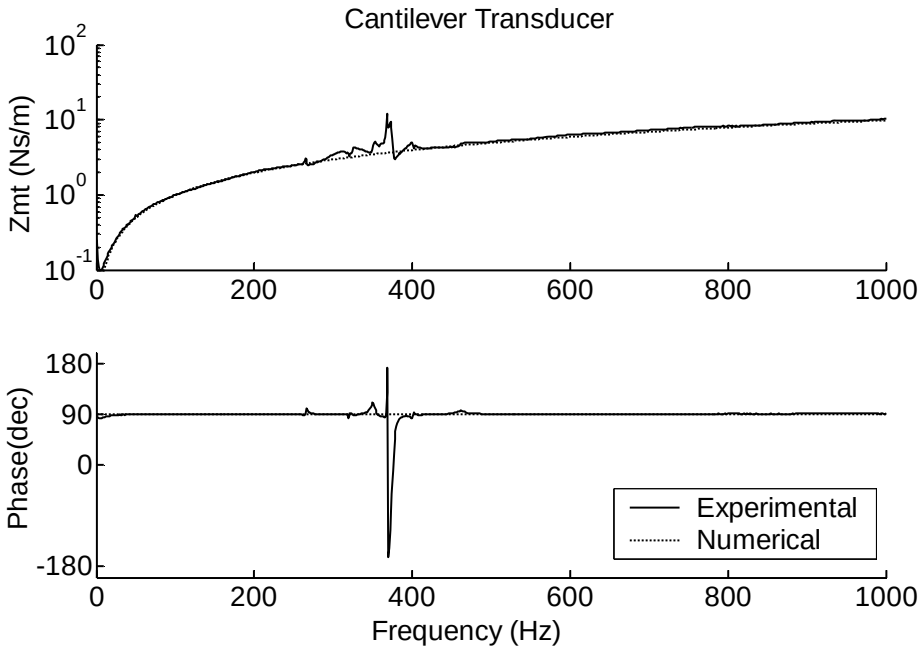

Fig. 5.15 Comparison of mechanical impedance of the tip

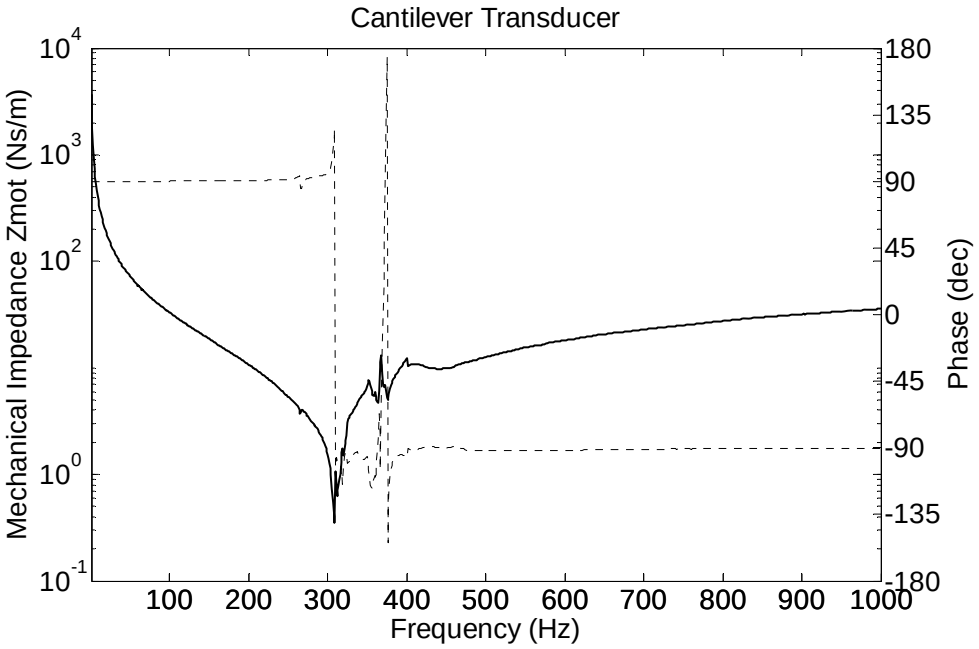

Fig. 5.16 Experimental evaluation results of Z_{mot}

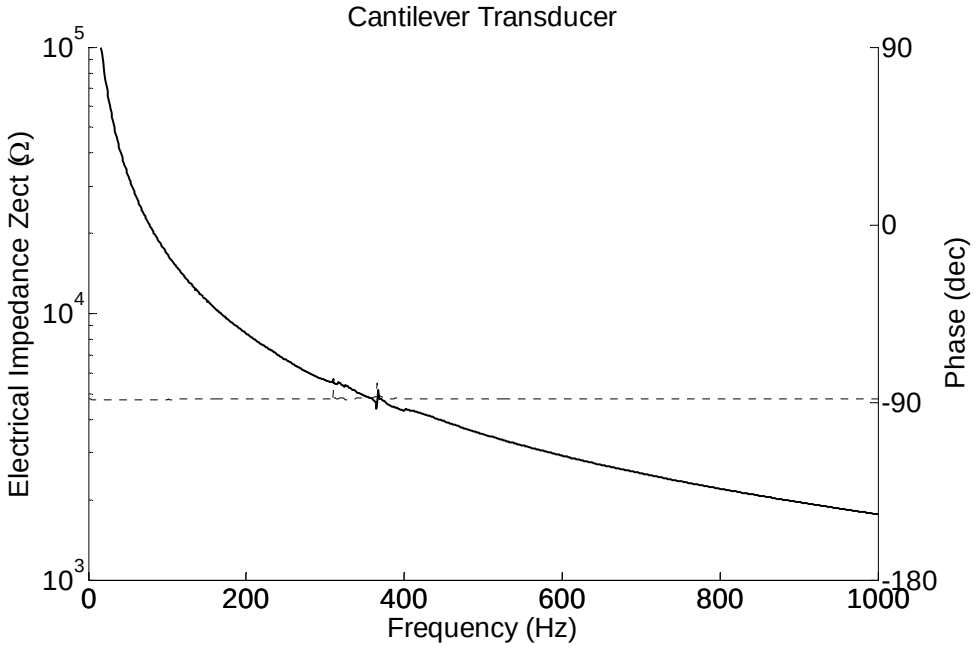

Fig. 5.17 Experimental evaluation results of Z_{ect}

Figures 5.16 and 5.17 show the results of frequency response functions Z_{mot} and Z_{ect} evaluated by using Eq. (5.8) and (5.9) respectively. Since the transduction properties of the whole system is fully known; in the following section, case studies including measuring mechanical impedance of rigid blocks and a beam structure will be carried out to verify the feasibility of the optimized cantilever transducer in the measurement of mechanical impedance.

5.3 Measurement of the Mechanical Impedance of Rigid Blocks

Since the intrinsic impedances Z_{mo}, Z_{ec} and Z_{ef} of the cantilever transducer have been calibrated, the mechanical impedance of load, can be calculated from the corresponding electrical input impedance of the actuator by using Eq. (5.1). Three metal cylinders shown in Figure 5.18 weighing 0.25g, 0.73g and 1.46g respectively are utilized as rigid blocks under testing.

Fig. 5.18 Picture of testing cylinders

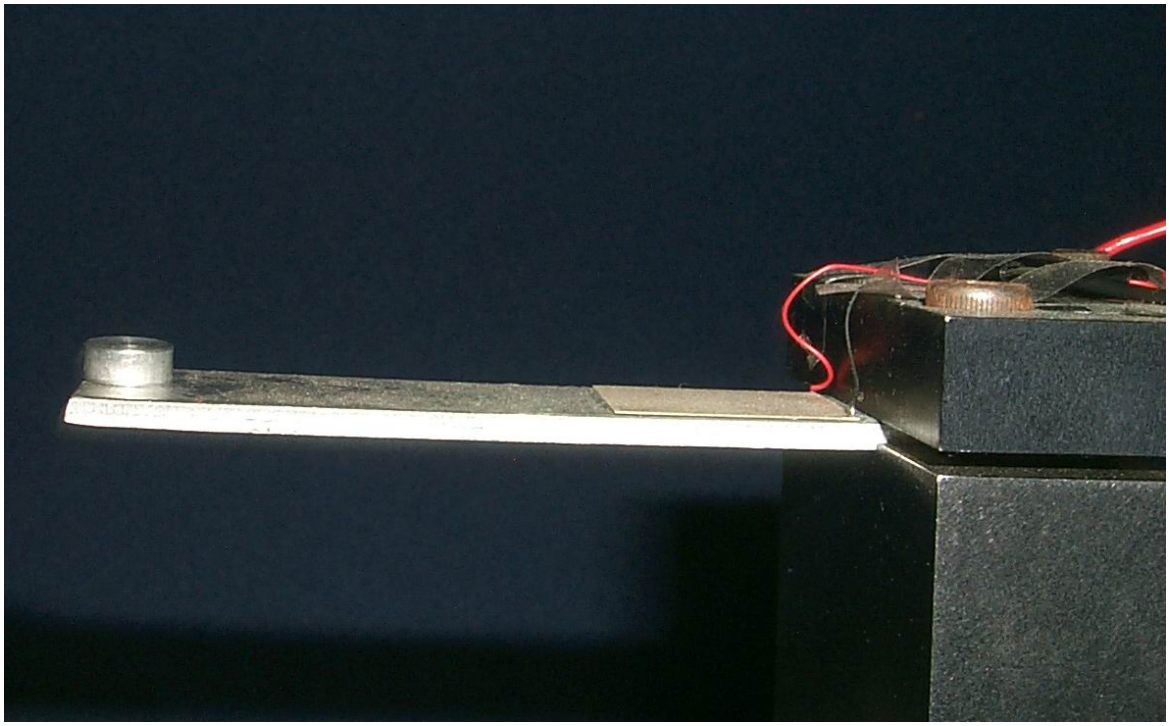

Fig. 5.19 Picture of the measurement system for rigid block

These cylinders are attached at the output port of the transducer serving as an external load to the transducer. Figure 5.19 shows the picture of the measurement system. The responding electrical impedances of cylinders are obtained at the input port and shown in Figure 5.20. The enlarged view of the responses is shown in Figure 5.21. Using the proposed method, mechanical impedance of the cylinders is calculated from the corresponding electrical impedance of the transducer.

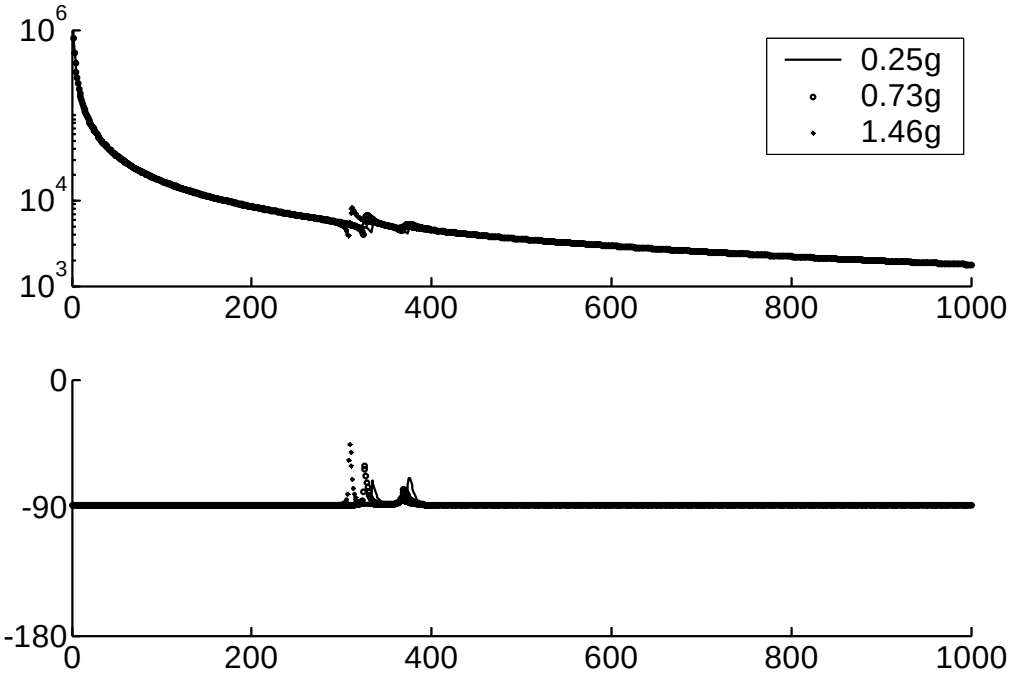

Fig. 5.20 Input electrical impedance of transducer with different rigid blocks

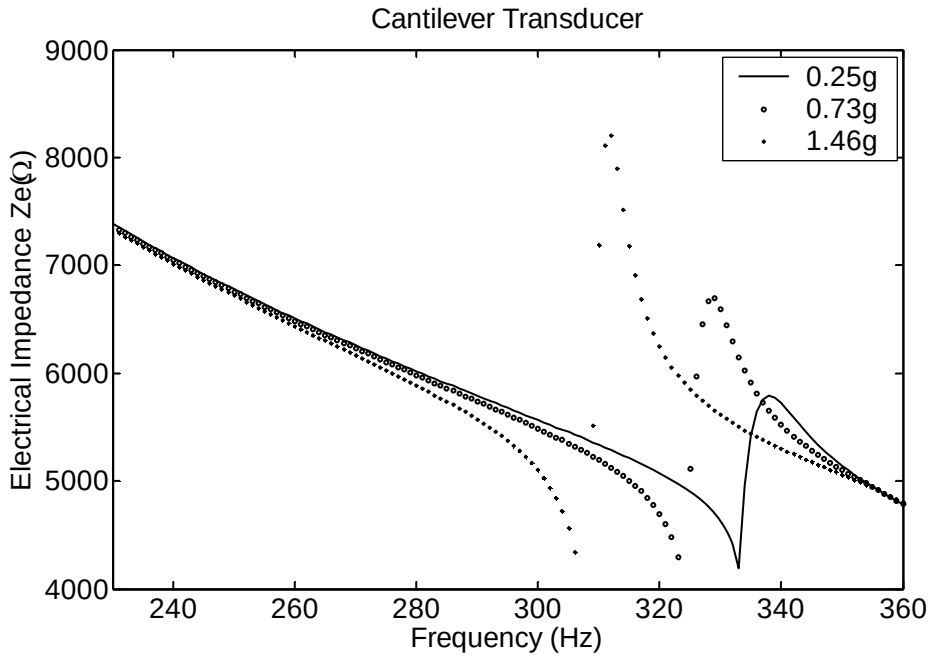

Figure 5.21 Enlarged view of electrical response

Compared with the long thin cantilever, the cylinder can be treated as an ideal rigid body with mass M. Its mechanical impedance at any frequency is known as:

$$Z_m^c = j \cdot 2\pi f M \tag{5.10}$$

Therefore the mass of the cylinders could be calculated from the mechanical impedance evaluated by the cantilever transducer.

$$M = \frac{Z_m^c}{j \cdot 2\pi f} \tag{5.11}$$

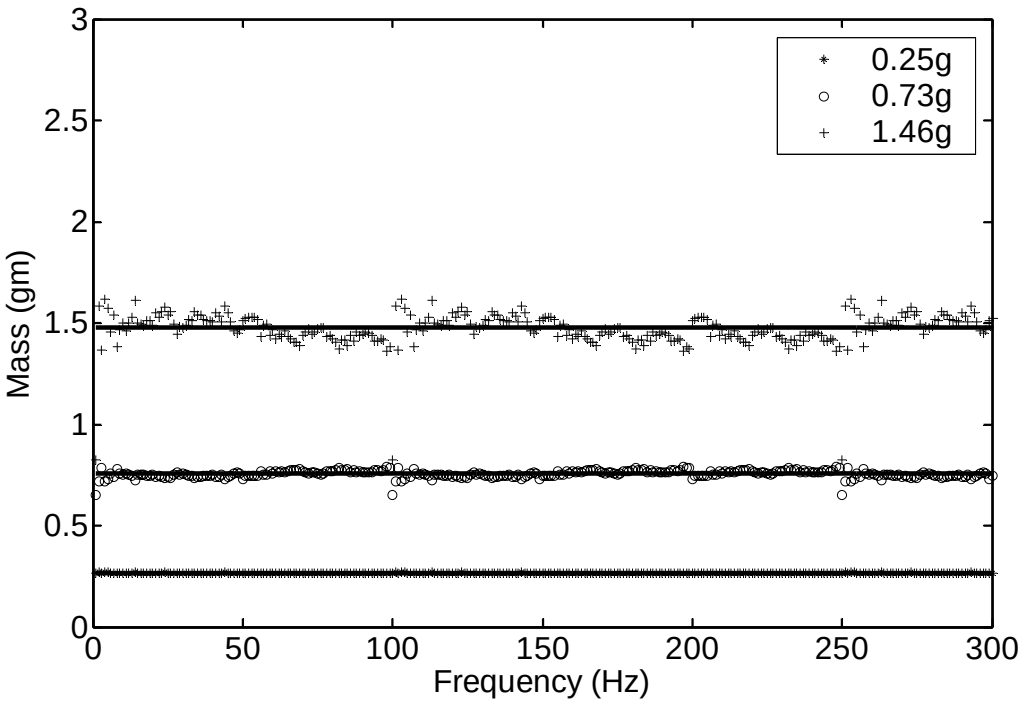

Fig. 5.22 Comparison of the block mass evaluated via cantilever transducer and true value

In comparing this calculated mass with the true mass, a very good correlation is found for each of the three blocks (Figure 5.22). The calculated values totally coincide with the true values, which verifies the effectiveness of the new cantilever transducer.

5.4 Measurement of Mechanical Impedance of a Beam Structure

Fig. 5.23 Picture of a beam structure for measurement

In this section, a one-dimensional beam, 100mm in length, 19.68mm in width and 0.48mm in thickness, is utilized as a sample to further examine the feasibility of the new transducer in mechanical impedance measurement. One end of the beam is clamped to a heavy supporting fixture (Figure 5.23) to achieve a fixed boundary condition. The other end is free. First of all, equations of mechanical impedance of a beam structure will be obtained by solving the governing equation of the system in close-form. After that, mechanical impedance of the beam will be experimentally detected via the cantilever transducer. The numerical results and experimental results will then be compared in one

figure to further validate the feasibility of the cantilever transducer in measuring mechanical impedance.

The governing equation of a beam structure, when an external force is applied on the beam, can be derived from generalized Hamilton's principle. Using the Rayleigh-Ritz method to remove the space dependence of the derived equations, the following ordinary differential equation is obtained:

$$[M_s]\{\ddot{r}\}+[K_s]\{r\}=[B_f]\{F\} \tag{5.12}$$

where $[M_s]$, $[K_s]$ are the mass and stiffness matrices for the structure.

$$M_s = \int_0^L A_s \Psi_r^T \rho_s \Psi_r dx \tag{5.13}$$

$$K_s = \int_0^L I_s (\Psi_r'')^T \hat{c}_s (\Psi_r'') dx \tag{5.14}$$

Obviously all the matrices characterizing the system are functions of the assumed modes $\psi_n(x)$ used in the Rayleigh-Ritz method as well as the physical properties such as density, Young's modulus, etc.

By solving the eigenvalue problem of Eq. (5.12) together with boundary conditions at the clamped and free end of the cantilever, the generalized coordinate $\{r\}$ can be easily obtained as (damping is also considered in the equation). To avoid lengthy duplications, derivation details similar to those which appeared in Chapter 3 are not repeated here.

$$\{r\} = [\Phi] \begin{bmatrix} \ddots & & 0 \\ & \dfrac{1}{\omega_n^2 + 2j\xi_n\omega_n\omega - \omega^2} & \\ 0 & & \ddots \end{bmatrix} [\Phi]^T [B_f] F \tag{5.15}$$

Assuming the excitation force is harmonic, the velocity distribution along the cantilever is

$$v(x,t) = [\Psi]\{\dot{r}\} = [\Psi][\Phi] \begin{bmatrix} \ddots & & 0 \\ & \dfrac{1}{\omega_n^2 + 2j\xi_n\omega_n\omega - \omega^2} & \\ 0 & & \ddots \end{bmatrix} [\Phi]^T [B_f] F \cdot j\omega \tag{5.16}$$

Thus, mechanical impedance of the beam structure at the exciting point can be calculated by the following equation.

$$Z_m = \frac{1}{[\Psi][\Phi] \begin{bmatrix} \ddots & & 0 \\ & \dfrac{1}{\omega_n^2 + 2j\xi_n\omega_n\omega - \omega^2} & \\ 0 & & \ddots \end{bmatrix} [\Phi]^T [B_f] \cdot j\omega} \tag{5.17}$$

Figures 5.24 and 5.25 show the experimental setup for the mechanical impedance measurement of the beam structure. When AC power is applied, the cantilever transducer shown in the right side of Figure 5.24 exerts an exciting force to drive the testing beam through the tip, at the same time; the electrical impedance at the input port is measured by the SI Impedance Analyzer.

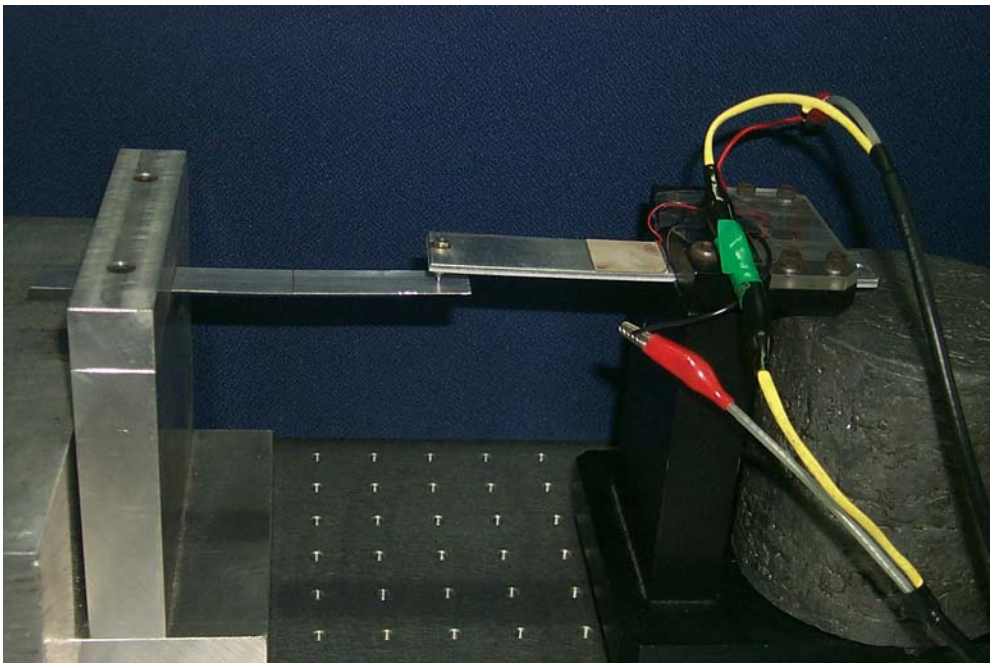

Fig. 5.24 Picture of the measurement system

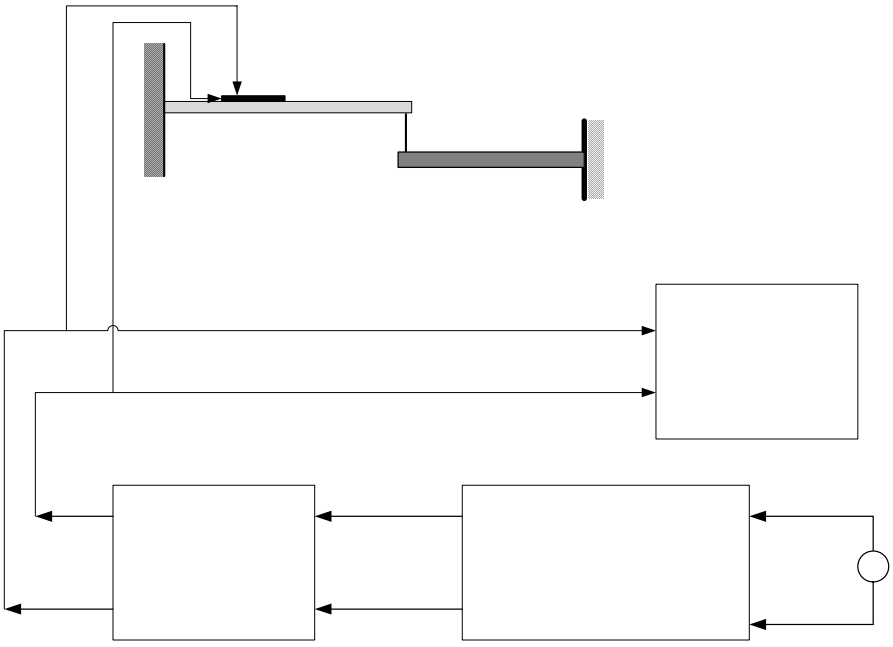

Fig. 5.25 Schematic of the experimental setup

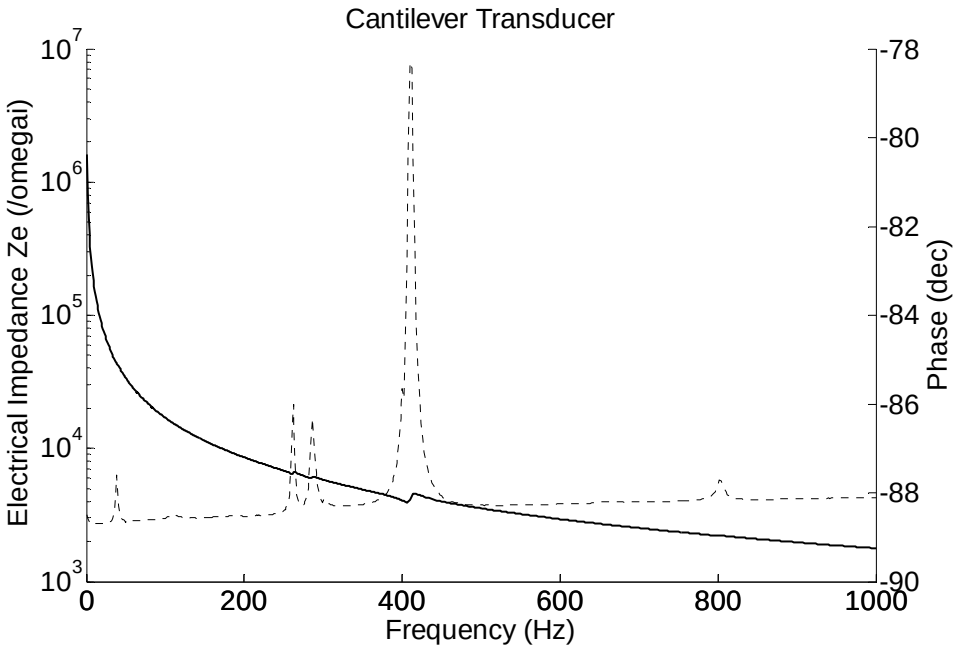

Fig. 5.26 Input electrical impedance of transducer with beam

Figure 5.26 shows the input electrical impedance of the transducer, where the solid line is magnitude and the dashed line is phase. Mechanical impedances of the beam structure are obtained from two methods, which are compared in the Figure 5.27. A good correlation is found between the curves in the low frequency. However, in the frequency range more than 300Hz, there is a big discrepancy between the experimental and numerical results. This may be due to: (1) a low sensitivity of the cantilever transducer in the high frequency; (2) a connection problem between the cantilever transducer and beam structure; (3) measurement errors.

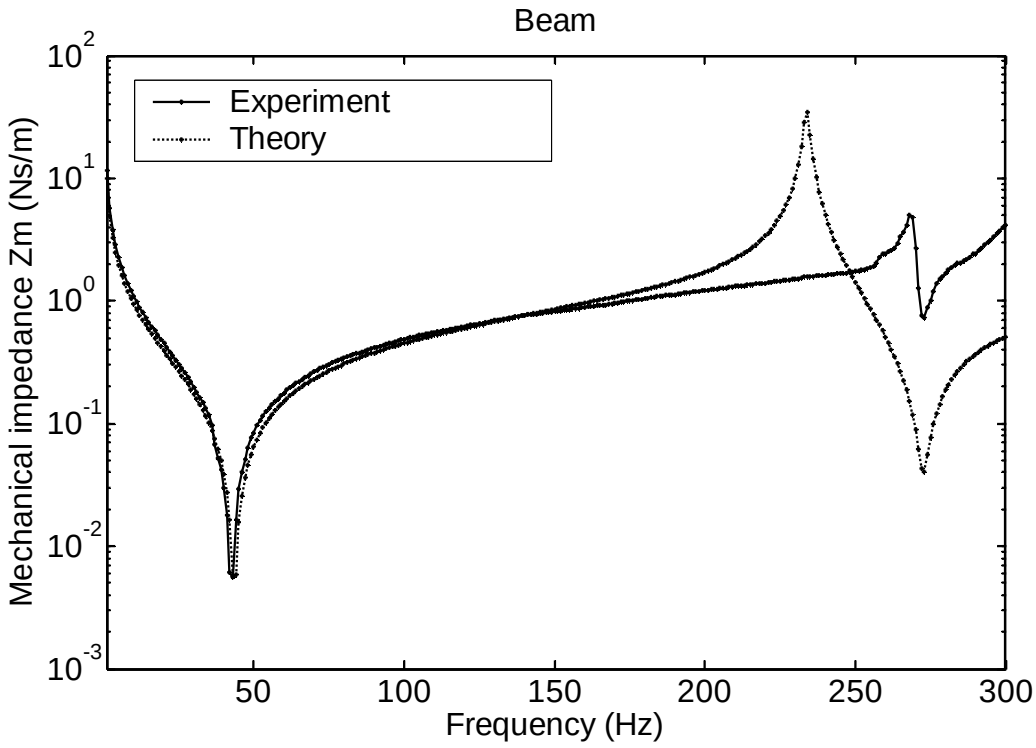

Fig. 5.27 Mechanical impedance of a beam

The resonances of the beam structure are also obtained from the experiment. An additonal accurate way is to use the LDV to measure the resonance when a hammer strikes on the testing beam structure. A comparison of resonance of the beam structure is listed in Table 5.4. Good agreement is found between these three results. The feasibility of the cantilever transducer for the measurement is confirmed.

Table 5.4 Comparison of the resonance of the beam structure

	Experiment	Numerical	LDV
1st resonance	42.5	43.0	40.9
2nd resonance	273	270	266

5.5 Summary

In this chapter, a PZT-coated cantilever has been designed and utilized as a SSA transducer for mechanical impedance measurement to further validate the proposed optimization strategy. Before the measurement, calibration of the cantilever transducer is necessary and a method, which selects several rigid masses as the load of the cantilever transducer, is proposed to calibrate the intrinsic attributes Z_{mo}, Z_{ec} and Z_{ef}.

In the calibration, Z_{ef} is measured directly from the SI Impedance Analyzer, when the transducer is under free condition. The other two impedances Z_{mo} and Z_{ec} are also evaluated by the proposed method using Eq. (5.2) and all these experimental results have been compared with the numerical results. A good correlation of the two results shows that the numerical prediction is accurate and the practicability of the present calibration method using adding masses is also confirmed. After the derivation of Z_{mo}, Z_{ec} and Z_{ef}, the transduction functions of the cantilever transducer with the tip are also acquired using Eq. (5.8) and Eq. (5.9). The mechanical impedance of the tip is detected experimentally and a comparison between experimental results and numerical results shows that the detection is successful and the cantilever transducer is suitable for mechanical impedance measurement.

After the calibration of the cantilever transducer, case studies including rigid blocks and a beam structure are carried out to further verify the feasibility of the designed cantilever

transducer in mechanical impedance measurement and the validity of the optimization strategy. It is found that the calculated masses of rigid blocks correspond perfectly with the true values, which verifies the effectiveness of the new cantilever transducer in mechanical impedance measurement. A good relationship in values is also found between the experimental results and numerical results of the beam structure in the low frequency. However, in the frequency range more than 300Hz, there is big discrepancy between the experimental and numerical results. This may be due to: (1) a low sensitivity of the cantilever transducer in the high frequency; (2) a connection problem between the cantilever transducer and beam structure; (3) measurement errors. In general, the designed cantilever transducer is capable of simultaneously sensing and actuating dynamic systems and the optimization strategy for designing the cantilever transducer for SSA is successful.

CHAPTER 6

TESTING OF A MINIATURE BEAM

As mentioned above, the method has been established for the design of a cantilever transducer with balanced sensing and actuating capability. Numerical simulation and experimental studies, which utilize the designed cantilever transducer to drive a dynamic system and sense its mechanical impedance, validate the proposed optimization.

To further explore the concept of using simultaneous sensing and actuating methods for testing miniature structures, in this chapter, a miniature PZT-coated cantilever is realized, using the same optimization strategy and utilized to drive and sense mini dynamic systems. Firstly, dimension and system parameters of a cantilever transducer will be obtained through the optimization. In turn, numerical simulation will be carried out to analyze the performances of the designed transducer. Since then, the transducer will be calibrated experimentally. There will be a contrast between the transduction matrix of the cantilever transducer calibrated experimentally and that obtained by the numerical methods. After the transduction functions of the proposed transducer have been fully

known, the feasibility of the proposed transducer for mechanical impedance measurement of mini structures will be validated experimentally.

6.1 An Optimized Miniature Cantilever Transducer

In this optimization, the cantilever transducer is expected to drive and sense the suspension beam of a hard disk drive. The optimization strategy is the same as that mentioned in Chapter 4. In this optimization, the cantilever transducer is proposed to be feasible for measuring mechanical impedance of a miniature beam below 4000Hz. Thus, the design parameter is given as: $f^* = 4000$; $k^* = 1$; $\psi^* = 40\%$. The design variables include length of the aluminum beam L_s; length of the PZT patch L_p; width of the cantilever beam (PZT patch) W; thickness of the cantilever beam T_s; thickness of the PZT patch T_p; position of the PZT patch x_1.

The PZT patch is FUJI Ceramics C-82 and the cantilever beam is ASTM 5052 aluminum. The material properties of the PZT patch and the aluminum beam are shown in Table 6.1.

After the optimization, the dimensions of the optimized mini cantilever transducer have been obtained and the results have been shown in Table 6.2.

Table 6.1 Material properties of piezoelectric material and beam

Category	Unit	Beam (Aluminum)	PZT (FUJI C-82)
Density	(kg/m^3)	2700	7500
Poisson's Ratio		0.34	0.34
Elastic Modulus	$(\times 10^9\ N/m^2)$	71	$c_{11}^E = 62$ $c_{33}^E = 51$ $c_{55}^E = 22$
Piezoelectric Constants	$(\times 10^{-12}\ m/V)$		$d_{31} = -266$ $d_{33} = 600$ $d_{15} = 781$
Relative Dielectric Constants			$\varepsilon_{11}^T / \varepsilon_0 = 3090$ $\varepsilon_{33}^T / \varepsilon_0 = 3650$

Table 6.2 Dimensions of the mini cantilever transducer

Component	Length (*mm*)	Width (*mm*)	Thickness (*mm*)	Position (*mm*)
Cantilever	21	6	2.5	
PZT	15.6	6	1	0

The cantilever transducer is made by FUJI CERAMICS CORPORATION, Japan. For the convenience of fabrication, the total length of the aluminum beam is set to be 40*mm*. Figure 6.1 illustrates the PZT-coated aluminum beam. The hole, 1.1*mm* in diameter, is designed to install a nut as an output tip and then the tip can connect to the testing dynamic system. The diameter of the nut is 1.0*mm*.

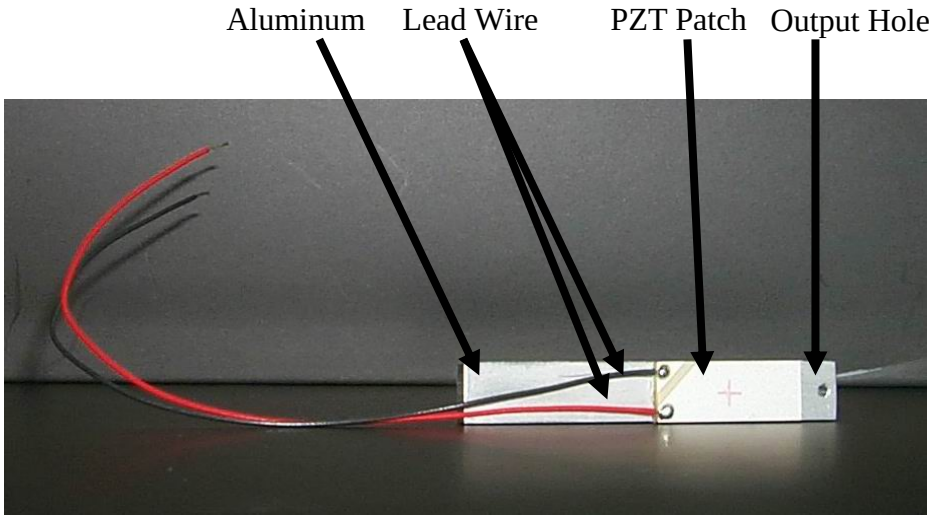

Fig. 6.1 Picture of a PZT-coated aluminum beam

6.2 Numerical Evaluation of Transduction Functions

Based on the determined dimensions of the mini cantilever transducer, a numerical simulation has been carried out to calculate the transduction functions of the optimized cantilever. Four transduction elements of the cantilever transducer were calculated using Eqs. (3.54—3.57) and the numerical results are shown in Figures 6.2—6.5. Also the determinant of the transduction matrix was calculated and the numerical results are shown in Figure 6.6, in which the reciprocity theorem also exists. In the following figures, the solid line is the magnitude of the variable and the dashed line is the phase of the variable.

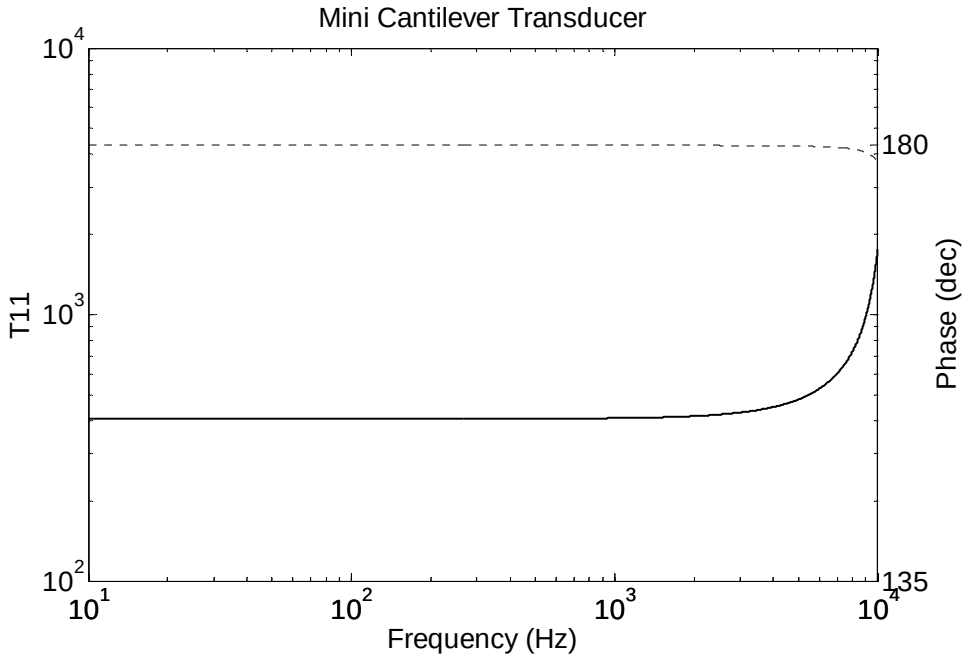

Fig. 6.2 Numerical results of transduction element t_{11}

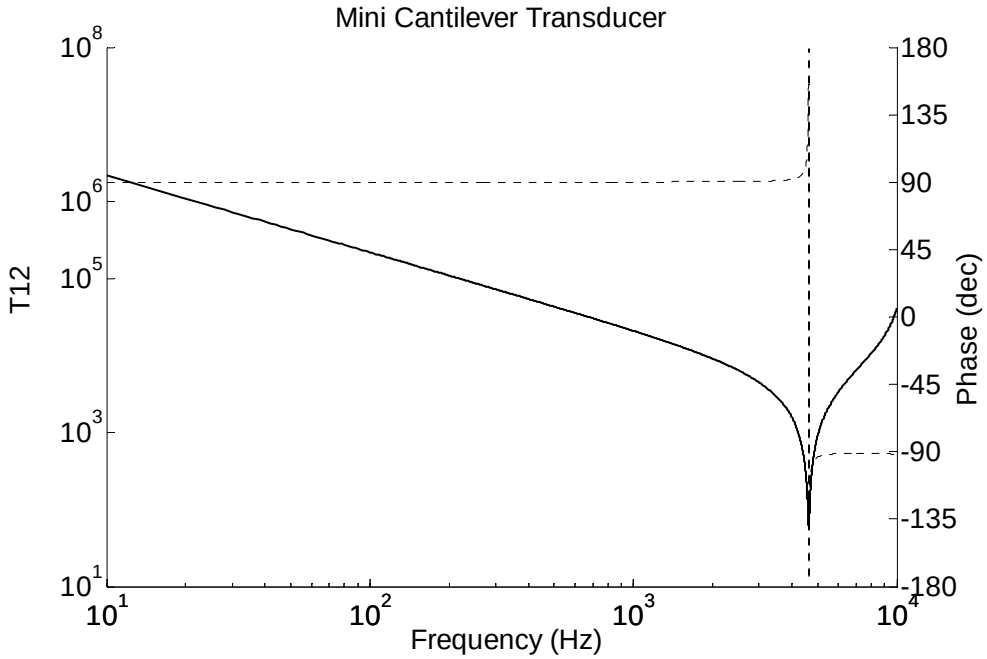

Fig. 6.3 Numerical results of transduction element t_{12}

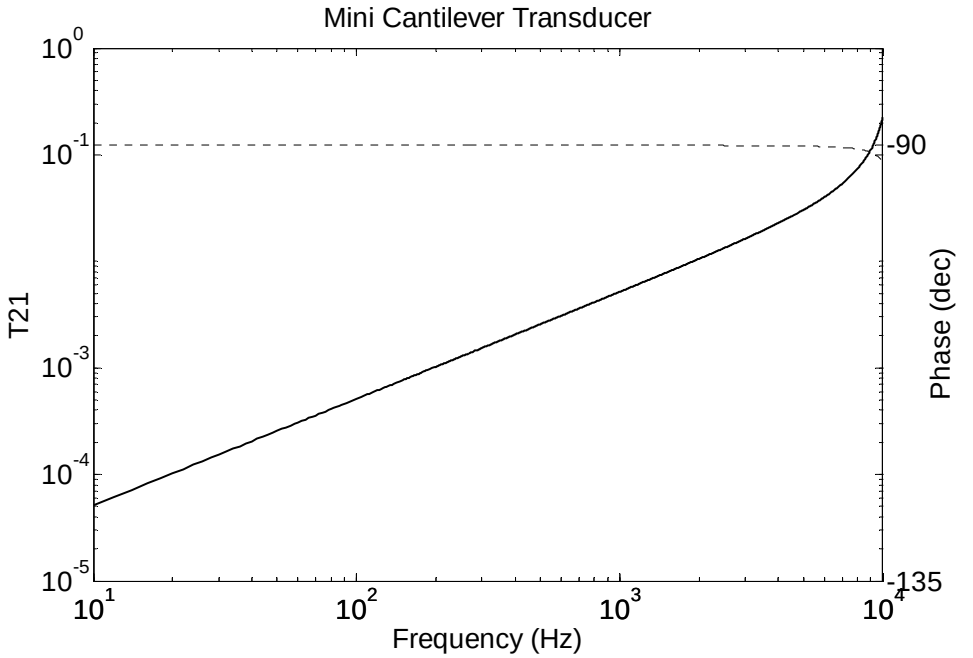

Fig. 6.4 Numerical results of transduction element t_{21}

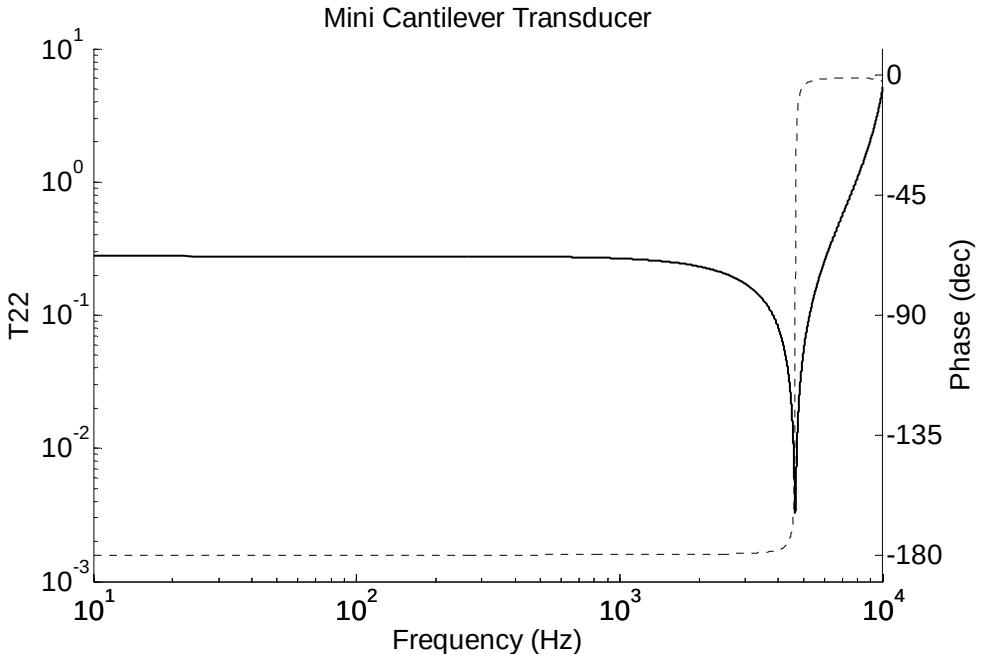

Fig. 6.5 Numerical results of transduction element t_{22}

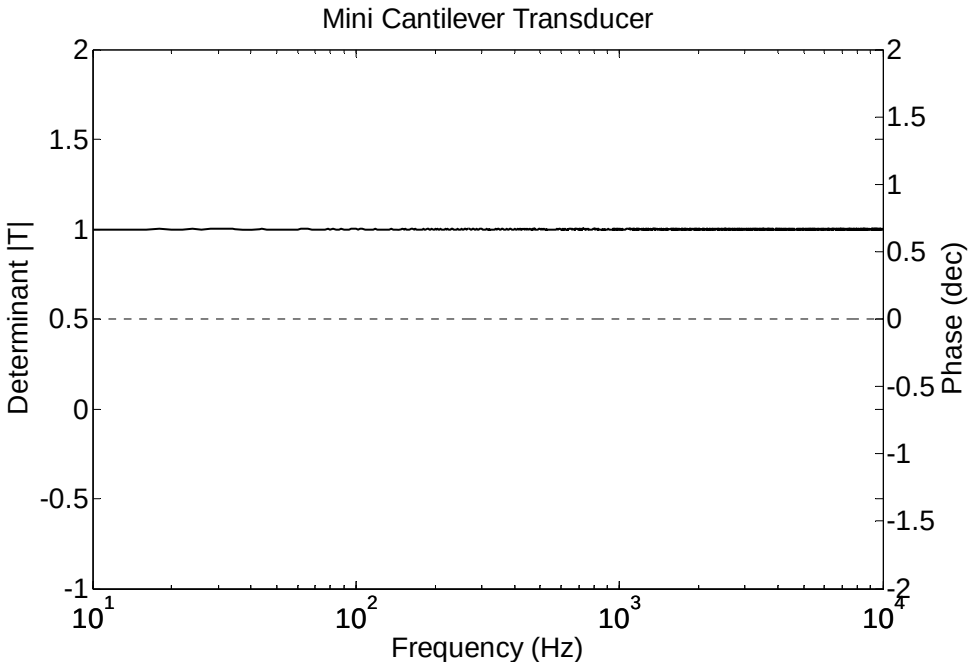

Fig. 6.6 Numerical results of determinant $|T|$

After the derivation of the four transduction elements, three intrinsic impedance Z_{mo}, Z_{ec} and Z_{ef} can also be calculated using Eq. (3.60) and the numerical results will be compared with the experimental results in the next section.

6.3 Experimental Calibration of Transduction Functions

6.3.1 Experimental Setup

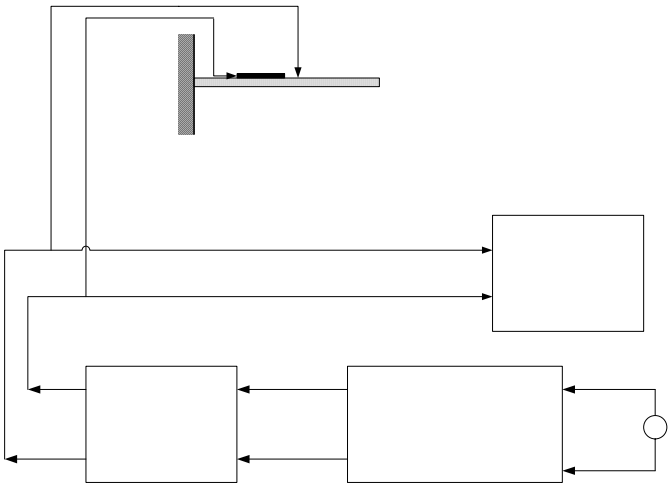

Fig. 6.7 Experimental setup for the miniature cantilever transducer

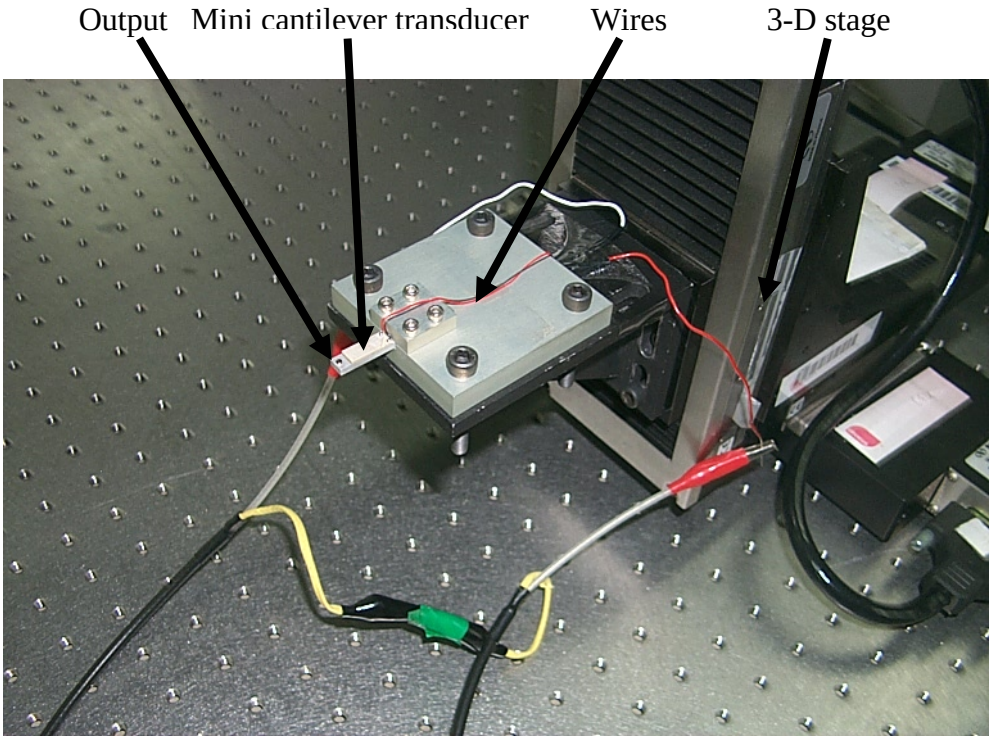

Fig. 6.8 Picture of the mini cantilever transducer

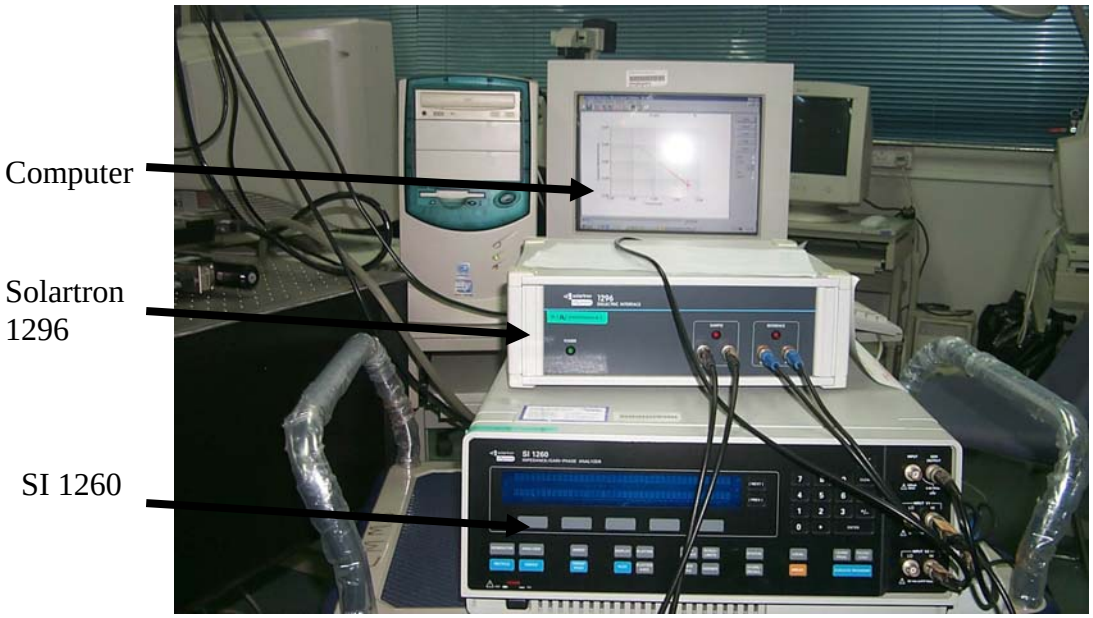

Fig. 6.9 Picture of the impedance analyzer device

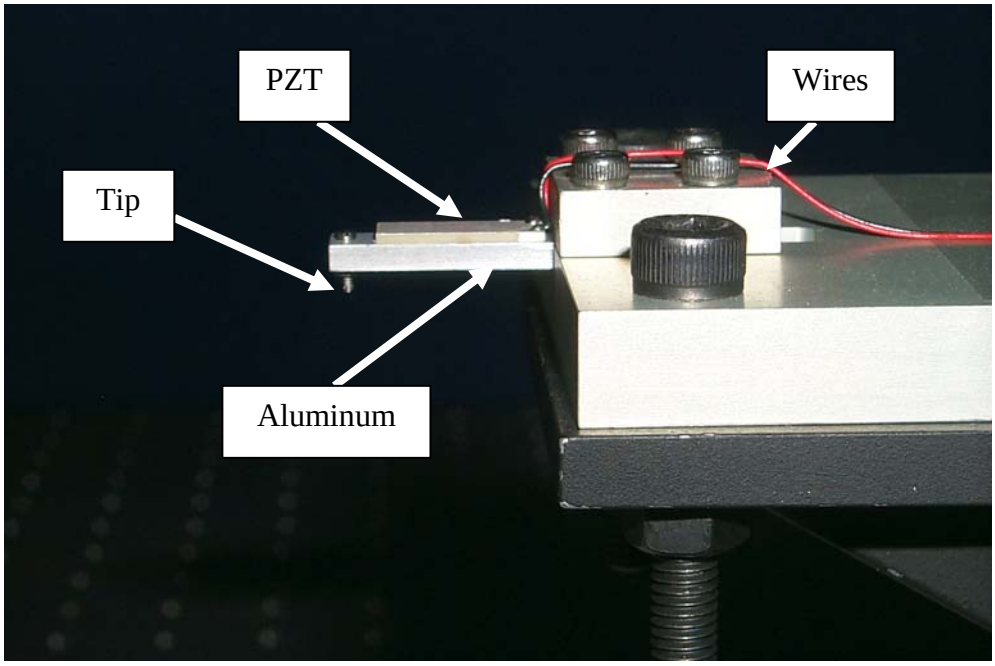

Fig. 6.10 Enlarged view of the mini cantilever transducer

Figure 6.7 shows the experimental setup of the miniature cantilever transducer. When AC power is applied, the SI 1260 Impedance Analyzer generates a signal of voltage onto the input port of mini cantilever transducer. The mini cantilever transducer can exert a mechanical force to the test structure onto the output port because of the electromechanical interaction; simultaneously, the current signal, reflecting the backward sensing, is also measured by the impedance analyzer. Both the voltage and current signals are then analyzed by impedance measurement software to obtain the input electrical impedance. In this experiment, the input voltage is set to be 1 Volt and the working frequency range is from 10*Hz* to 5000*Hz* with an interval of 2*Hz*.

The photograph of the mini cantilever transducer installed on a 3-D stage, which is used to control the universal motion of the transducer, is shown in Figure 6.8. The parameters of the cantilever beam and PZT patch are listed in Table 6.1 and the dimensions of the cantilever components have been listed in Table 6.2. The diameter and position of the hole, which are suitable for the M1 screw, are1.1*mm* and 20.28*mm* respectively. Figure 6.9 and 6.10 show the picture of the impedance analyzer device and the enlarged view of the mini transducer respectively.

After the mini cantilever transducer is fabricated, the electrical impedance of the transducer without a tip can be obtained using the impedance analyzer mentioned above. The experimental results are shown in Figures 6.11 and 6.12, in which the solid line is magnitude and the dashed line is phase. The natural frequencies of the mini transducer at first and second mode are also derived from these results. In Figure 6.12, an extra resonant

is found at 28.7 *kHz*, which is due to the torsion of the mini transducer. This resonant can be found in the finite element analysis using ANSYS.

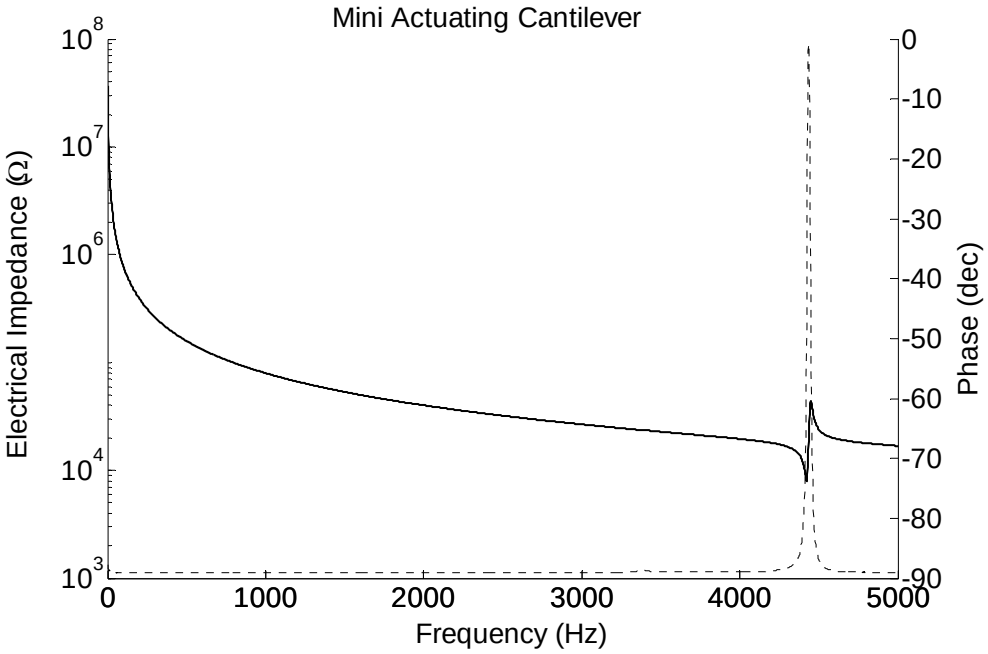

Fig. 6.11 Electrical impedance of the mini transducer at 1st mode

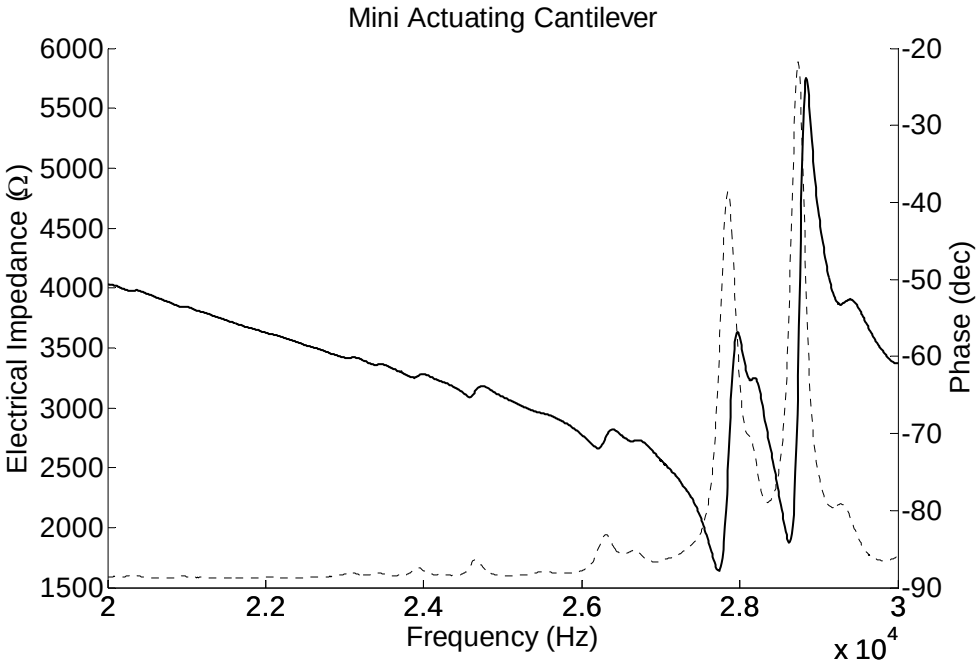

Fig. 6.12 Electrical impedance of the mini transducer at 2nd mode

Also by solving the associated eigenvalue problem of Eq. (3.44) in Chapter 3 together with the boundary conditions at the clamped and free end of the cantilever, the natural frequencies ω_n of the system are calculated. The results from the experiment and close-form analysis will be compared with the corresponding natural frequency of the transducer, calculated through finite element modal analysis. The comparison results have been presented in Table 6.3. A very small discrepancy has been found between these results obtained from the experiment, finite element analysis and close-form analysis.

Table 6.3 Natural frequency of mini cantilever transducer

Natural Frequency	Experiment	Finite Element Model	Close-Form Analysis
1^{st} mode (*kHz*)	4.436	4.486	4.630
2^{nd} mode (*kHz*)	27.85	26.35	27.95

6.3.2 Measurement of Z_{ef}

To identify the frequency response function Z_{ef}, the cantilever transducer works under a free condition, as illustrated in Figure 6.8. An excitation voltage with the amplitude of 1 Volt is applied to the PZT of the cantilever transducer by the SI 1260 Impedance Analyzer. The input electrical impedance Z_{ef} is measured at the same time. From the definition of Z_{ef}, the numerical results of Z_{ef} are also calculated using Eq. (6.4) since the four transduction elements have been determined numerically. In Figures 6.13 and 6.14, the amplitude and phase characteristics of the experimentally determined Z_{ef} are compared with the numerical results. Although the peak values and resonant frequency have an insignificant difference between the results of the two methods due to the damping of the

system. In general, a close agreement among these results in both amplitude and phase is found.

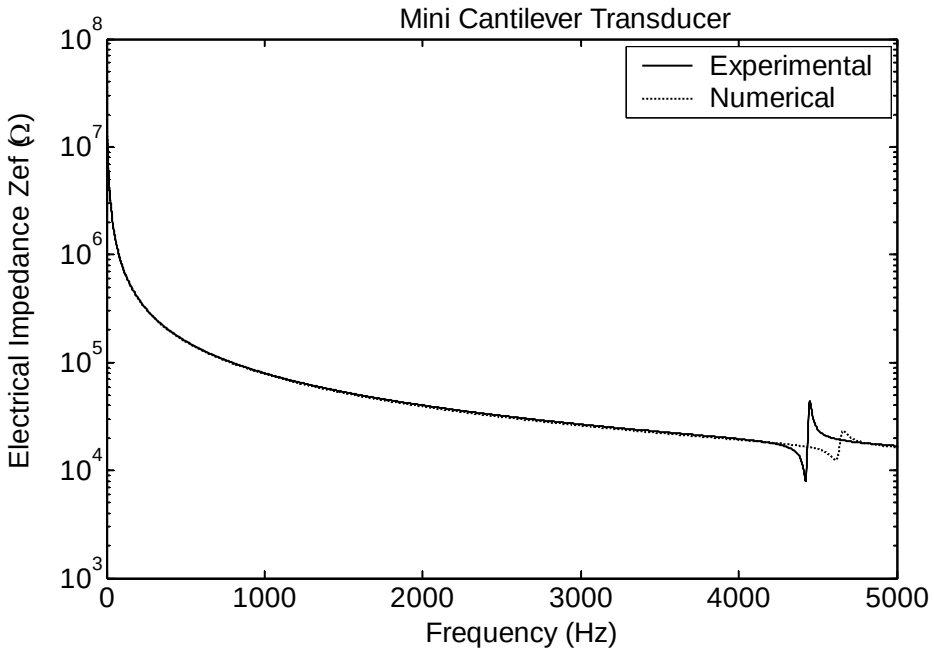

Fig. 6.13 Magnitude of Z_{ef} between numerical (dash) and experimental (solid) results

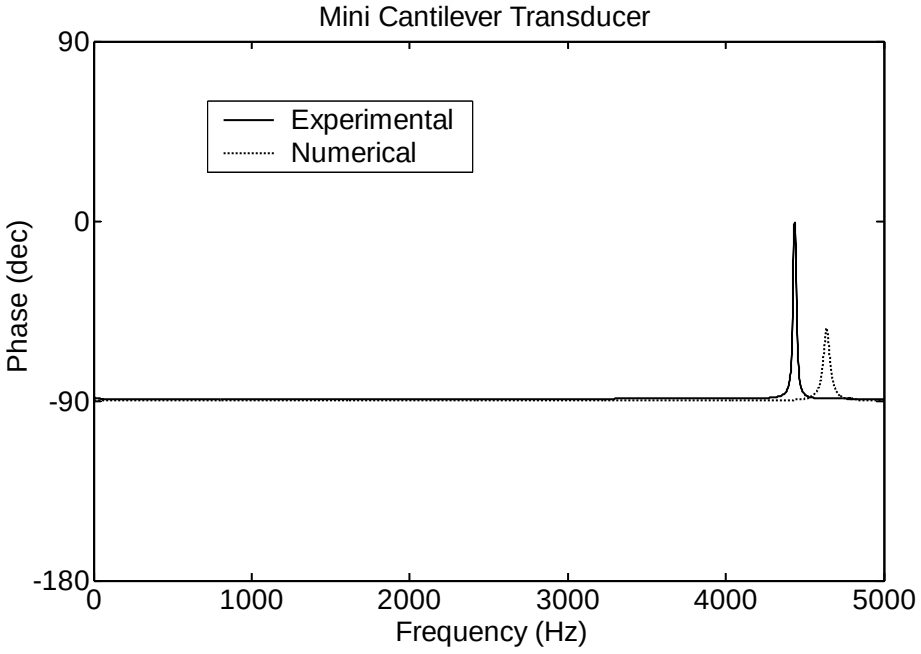

Fig. 6.14 Phase of Z_{ef} between numerical (dash) and experimental (solid) results

6.3.3 Experimental Evaluation of Z_{ec} and Z_{mo}

As mentioned in Section 3.5, in order to calibrate Z_{ec} and Z_{mo} of the cantilever transducer, several masses are needed as loads applied to the transducer for the calibration. After deriving the input electrical impedance responses under these loads, Z_{mo} and Z_{ec} can be identified by solving over-determined simultaneous equations Eq. (3.63). The selected masses (nuts) and tips (screw) are shown in Figure 6.15 and the parameters of the masses are listed in Table 6.4.

Table 6.4 Selected masses for the calibration

Symbol	Free	I	II	III	IV
Load		A+B	A+B+C	A+B+C+D	A+B+C+D+E
Mass (*mg*)	0	61.53	87.20	112.76	139.24

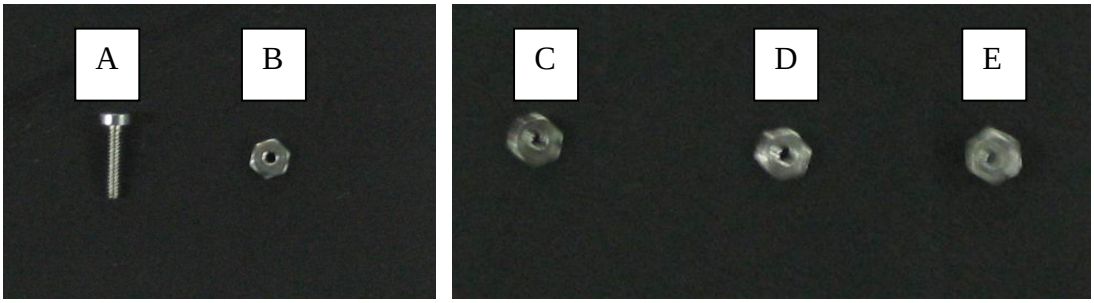

Fig. 6.15 Picture of the calibration masses

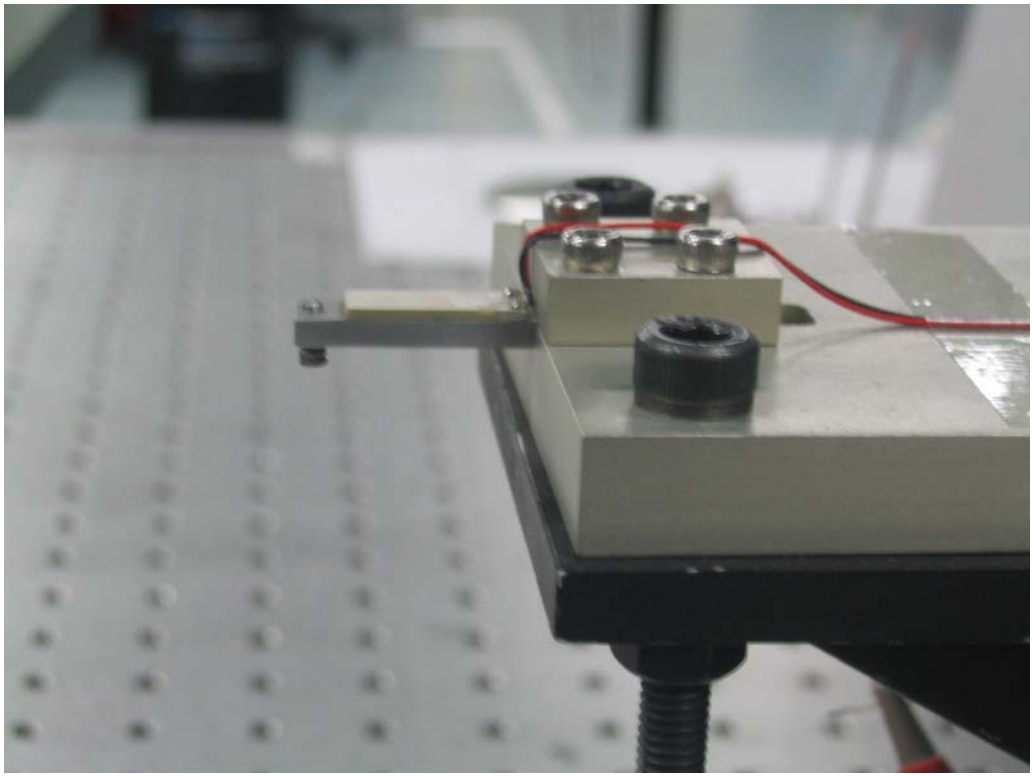

Fig. 6.16 Picture of the experimental setup for the evaluation of Z_{ec} and Z_{mo}

In the calibration, the screw shown in Figure 6.15 is tightened by a nut through the hole in the transducer and in the measurement. It will connect to the sample as an output port of the cantilever transducer. After AC voltage with the same amplitude and phase is supplied to the cantilever transducer, the electrical impedance Z_e^m is measured by the SI Impedance Analyzer. The four loads shown in the following table are employed to experimentally determine Z_{mo} and Z_{ec}. For each mass, testing illustrated in Figure 6.16 is carried out. The measured electrical impedance corresponding to each calibration mass is overlay vs. frequency in Figure 6.17. The enlarged figure around resonance is depicted in

Figure 6.18. In the figure, from the left to the right, each curve represents the electrical impedance of the cantilever transducer when it is loaded with a different mass. It is found that Z_e^m directly reflects the properties of the mechanical load attached to the transducer. The greater the calibration mass, the lower the resonance.

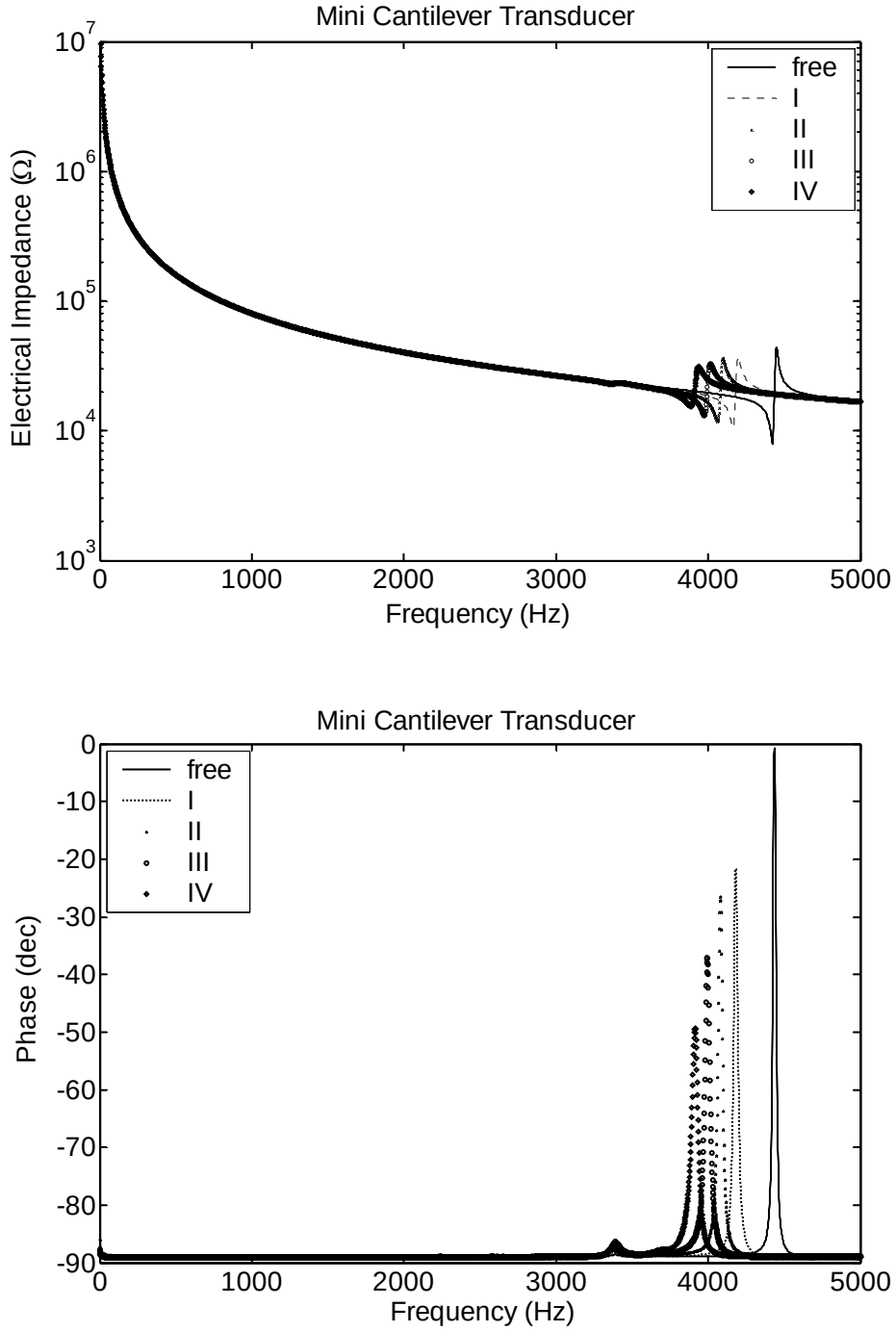

Fig. 6.17 Electrical impedance corresponding to different loads

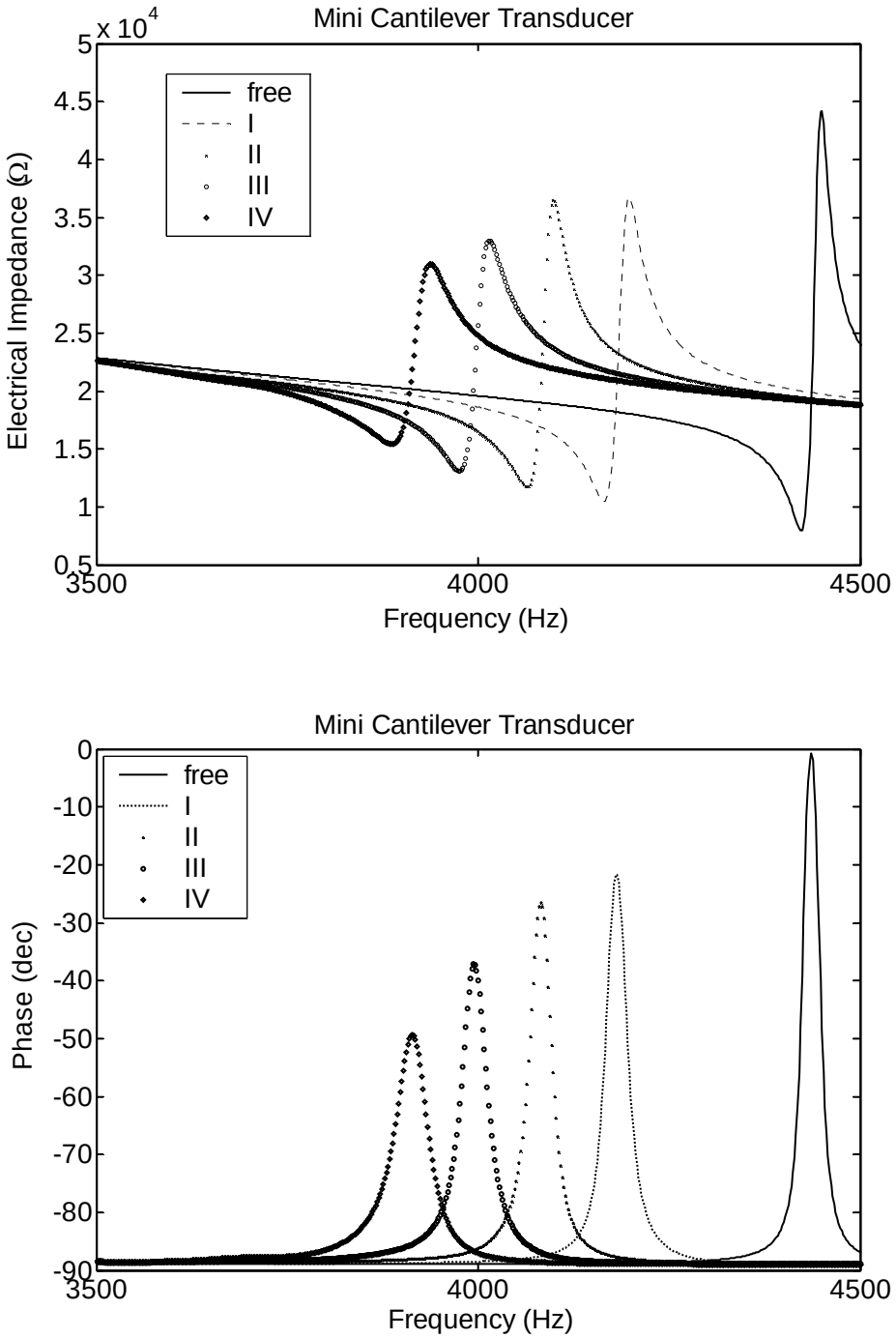

Fig. 6.18 Electrical impedance responses around 1st resonance

From the measured electrical impedance Z_e^m, the frequency response functions Z_{mo} and Z_{ec} can be easily calculated. These experimentally determined Z_{mo} and Z_{ec} are then compared with the numerical results and a comparison of these results are shown in Figures 6.19—6.22. It is observed that Z_{mo} and Z_{ec}, which are determined via two calibration methods, are comparable. There is a small discrepancy between the experimental and numerical results due to the fact that the numerical studies are based on ideal conditions; while the experimental results are affected by the fabrication of the cantilever transducer and calibration masses, which are not absolutely ideal. Nevertheless, the confirmation of the theoretical predictions by the experimental results is quite clear. Two unexpected protuberances are evident in Figures 6.21 and 6.22, which are due to the manufactured problem of the cantilever transducer. If the electrical impedance of the cantilever transducer under a free condition as shown in Figure 6.17 is enlarged, the protuberances are also found.

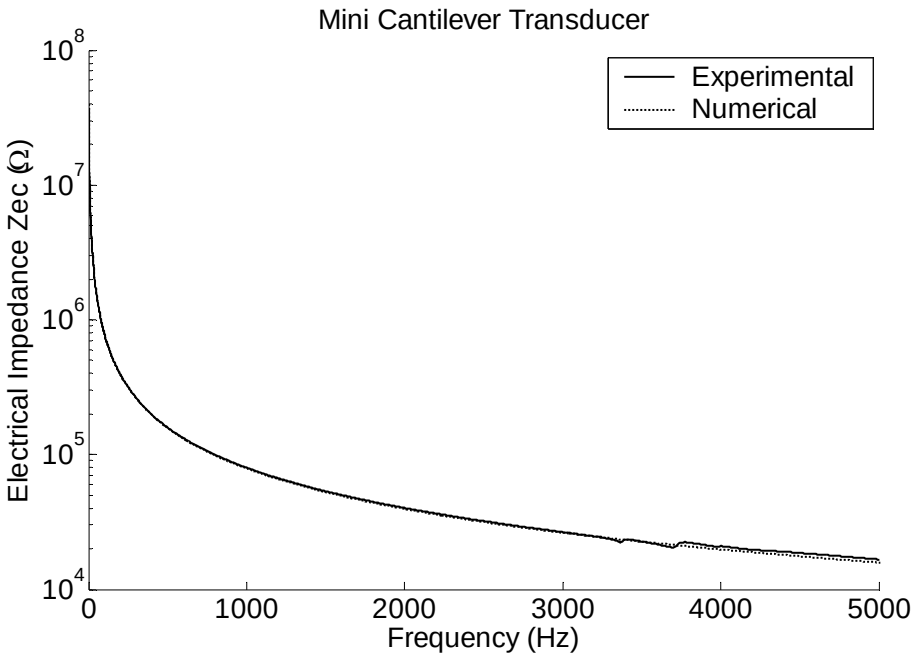

Fig. 6.19 Magnitude of Z_{ec} between numerical (dash) and experimental (solid) results

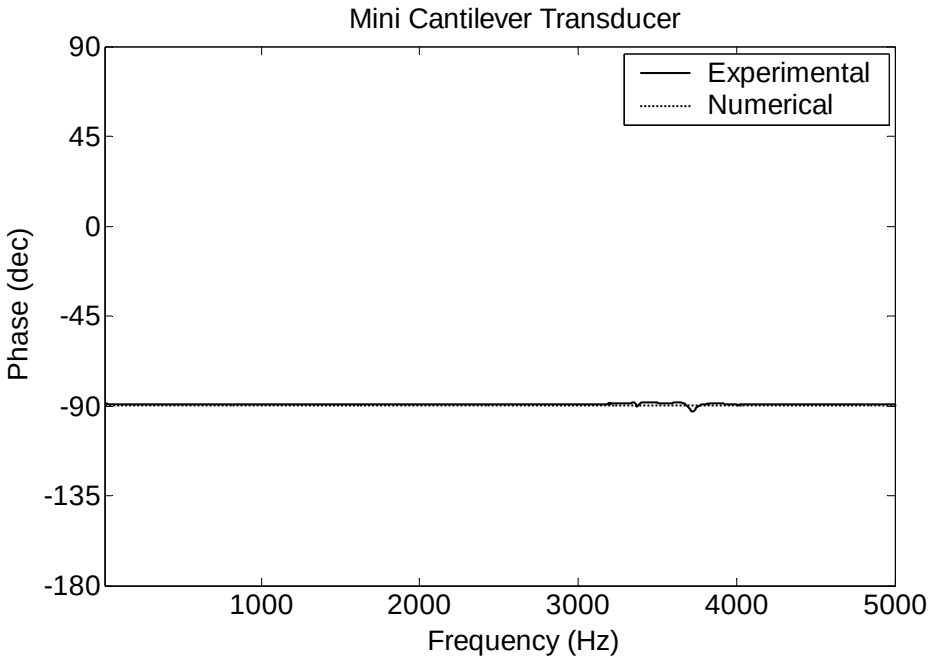

Fig. 6.20 Phase of Z_{ec} between numerical (dash) and experimental (solid) results

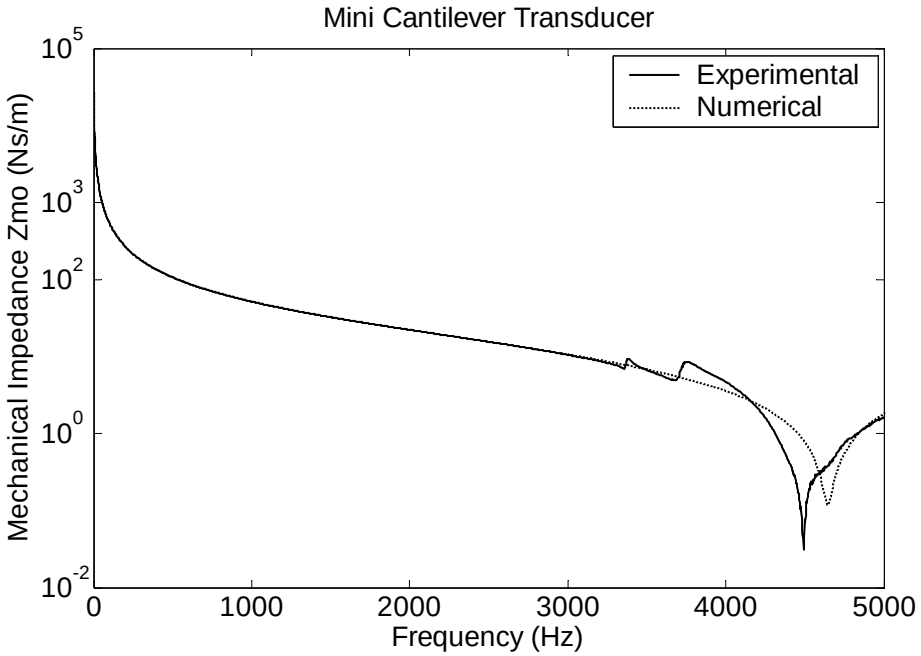

Fig. 6.21 Magnitude of Z_{mo} between numerical (dash) and experimental (solid) results

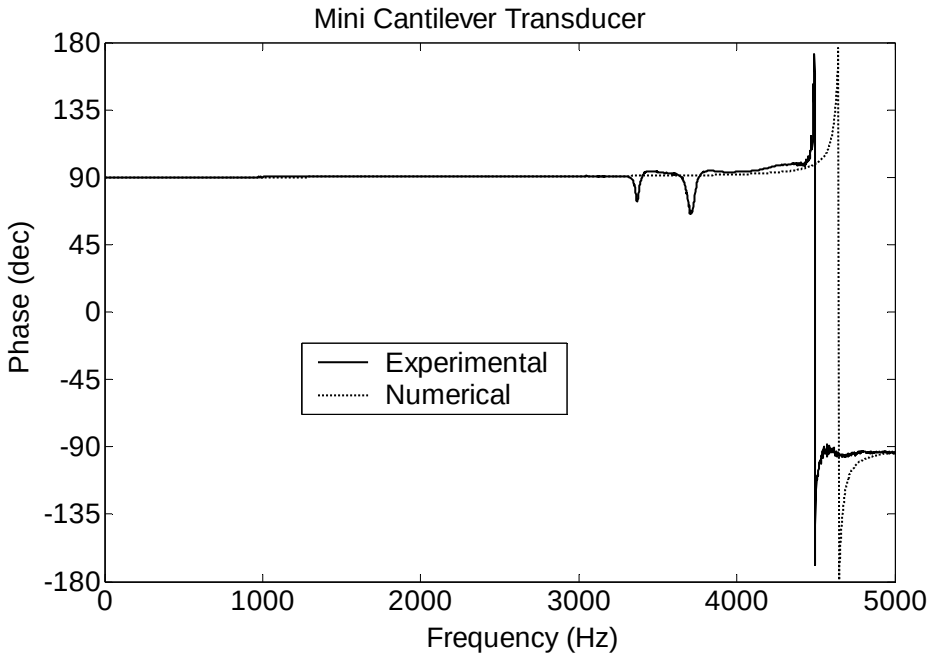

Fig. 6.22 Phase of Z_{mo} between numerical (dash) and experimental (solid) results

In the following section, the transducer will serve as an actuator and a sensor simultaneously to validate its potential application experimentally. Since the transduction functions of the cantilever transducer have been determined, a case study using a miniature beam as a load onto the transducer will be carried out to further examine the feasibility of the designed cantilever transducer in the measurement of mechanical impedance of miniature dynamic systems.

6.4 Detection of Mechanical Impedance of a Miniature Beam

Figure 6.23—6.25 show the different view of the experimental setup, in which a one-dimensional miniature suspension beam is utilized as a sample, which is added onto the cantilever transducer. One end of the test beam is clamped to a heavy supporting fixture to achieve a fixed boundary condition by using super glue; the other end is connected to the cantilever transducer through a mini screw. Figure 6.26 shows the experimental layout for the mechanical impedance measurement. When AC power is applied, the cantilever transducer shown in the right side of Figure 6.23 exerts an exciting force to drive the testing beam through the connection point, while, the electrical impedance at the input port is measured by the SI Impedance Analyzer.

Fig. 6.23 Top view of the experimental setup

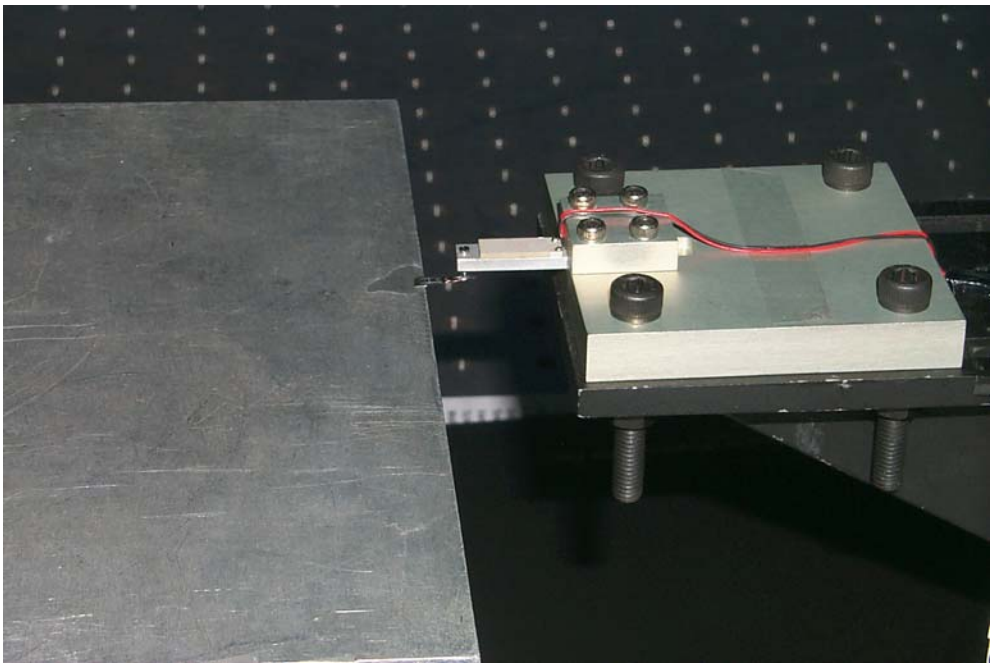

Fig. 6.24 Main view of the experimental setup

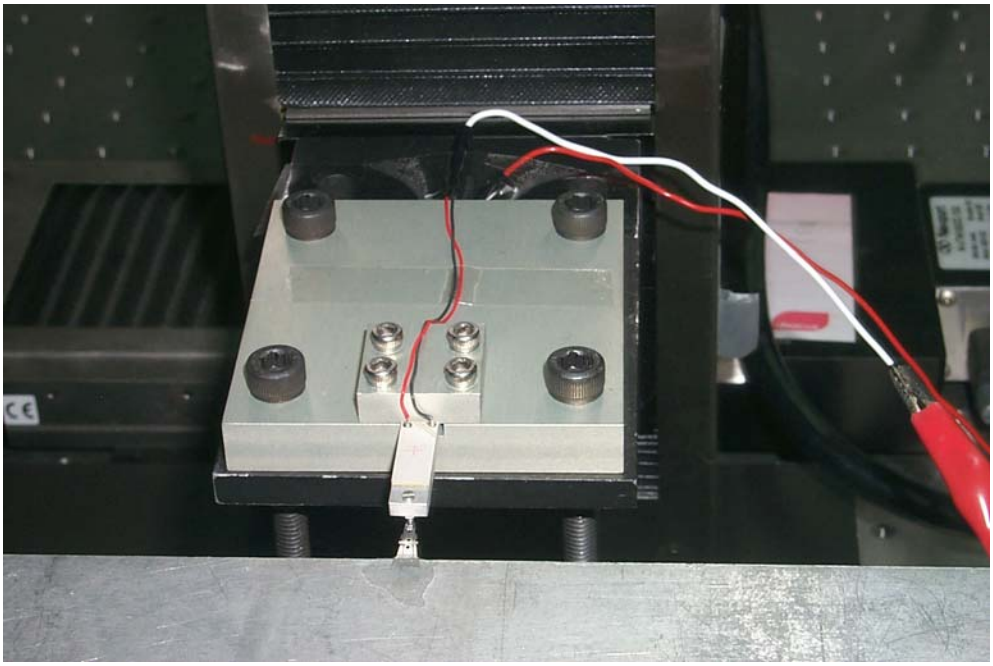

Fig. 6.25 Right view of the experimental setup

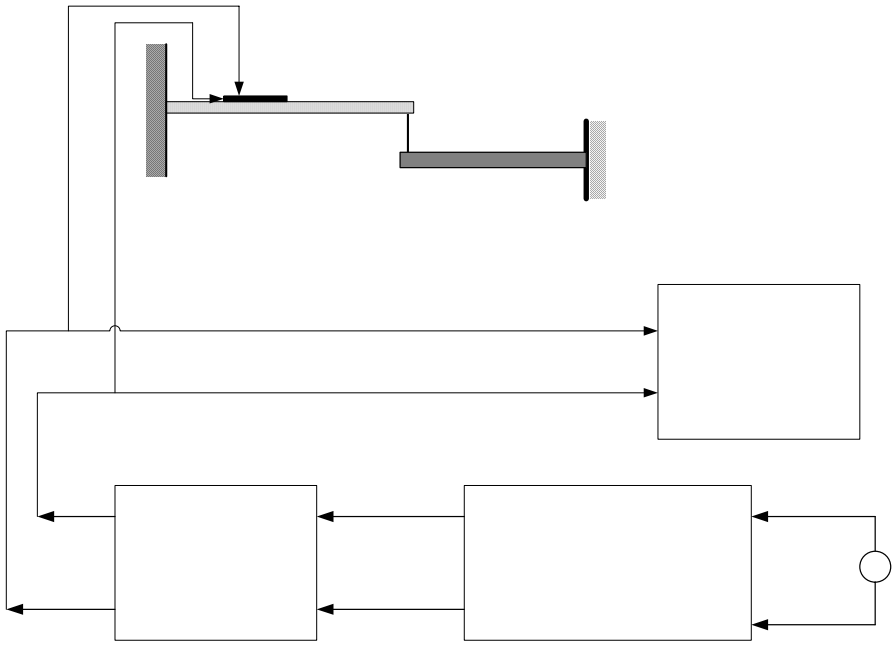

Fig. 6.26 Layout of the experimental setup

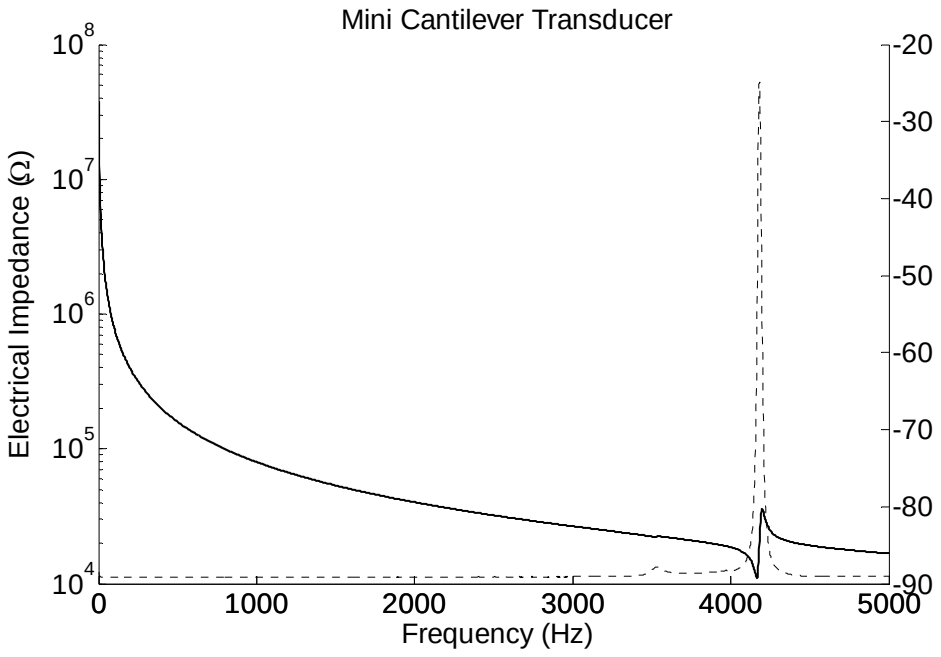

Fig. 6.27 Electrical impedance response for the mini sample beam

Since the transduction functions of the cantilever transducer were fully calibrated in the last section, the mechanical impedance of testing an object at the driving point can be calculated by the input electrical impedance of the cantilever transducer using the proposed transduction matrix. Figure 6.27 shows the input electrical impedance of the transducer, in which solid line is magnitude and the dashed line is phase. Finally, the mechanical impedance of the mini sample beam is obtained experimentally.

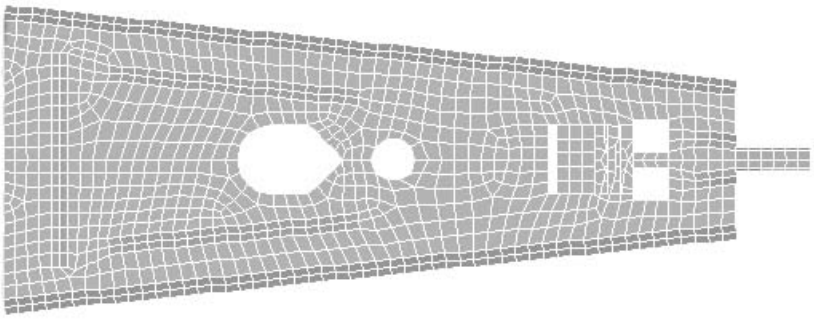

Fig. 6.28 FEM model of the mini sample beam

A comparison between experimental results and FEM analysis results of the mechanical impedance of the mini sample beam has been done. The model of the mini sample beam in FEM analysis is shown in Figure 6.28, where the element type of the model is solid 45 and aluminium material is selected for the beam element. The left end of the beam is clamped and the right end is free for the boundary condition in the analysis.

The mechanical impedances of the beam structure were obtained using two methods. They are compared in Figures 6.29 and 6.30. The three unexpected resonances around 3000—4500 can be found, one of which is due to the resonance of the mini cantilever transducer. The others are due to the unexpected protuberance that occurred in the calibration described in the last section. In general, the experimental results agree well with the numerical results. The top three resonances of the mini sample beam are found in the experimental results, especially in the phase. However, at the third resonance, large differences between the experimental and the numerical results occur due to the low sensitivity when the cantilever transducer is used out of the dynamic frequency range.

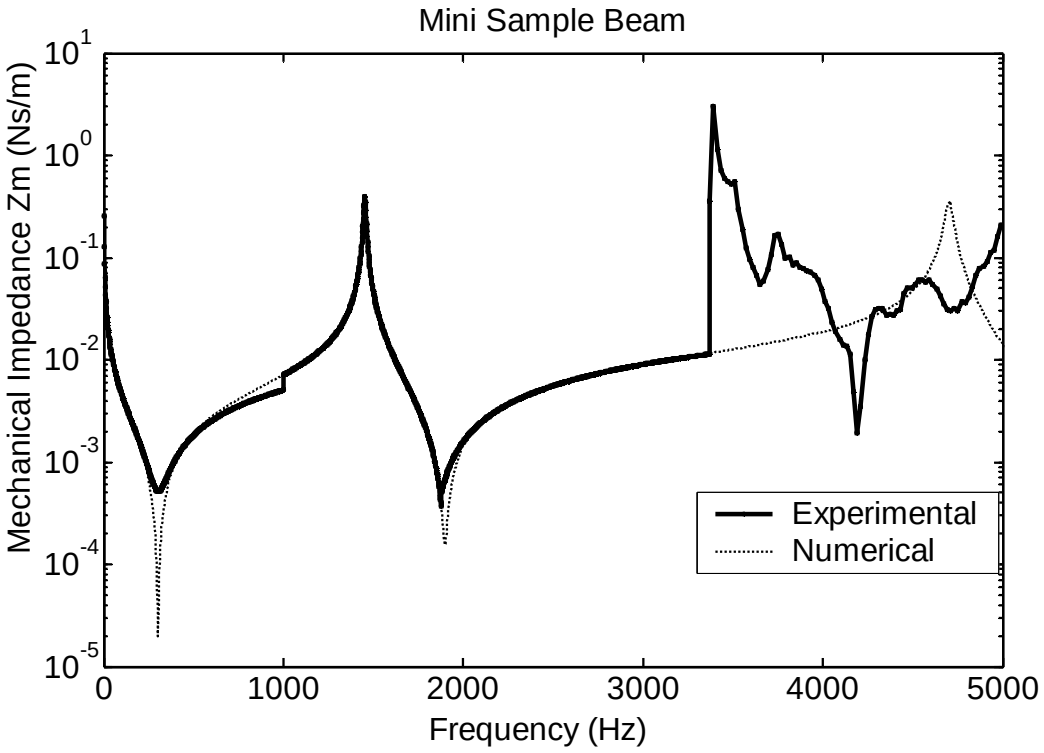

Fig. 6.29 Magnitude of mechanical impedance of the mini sample beam

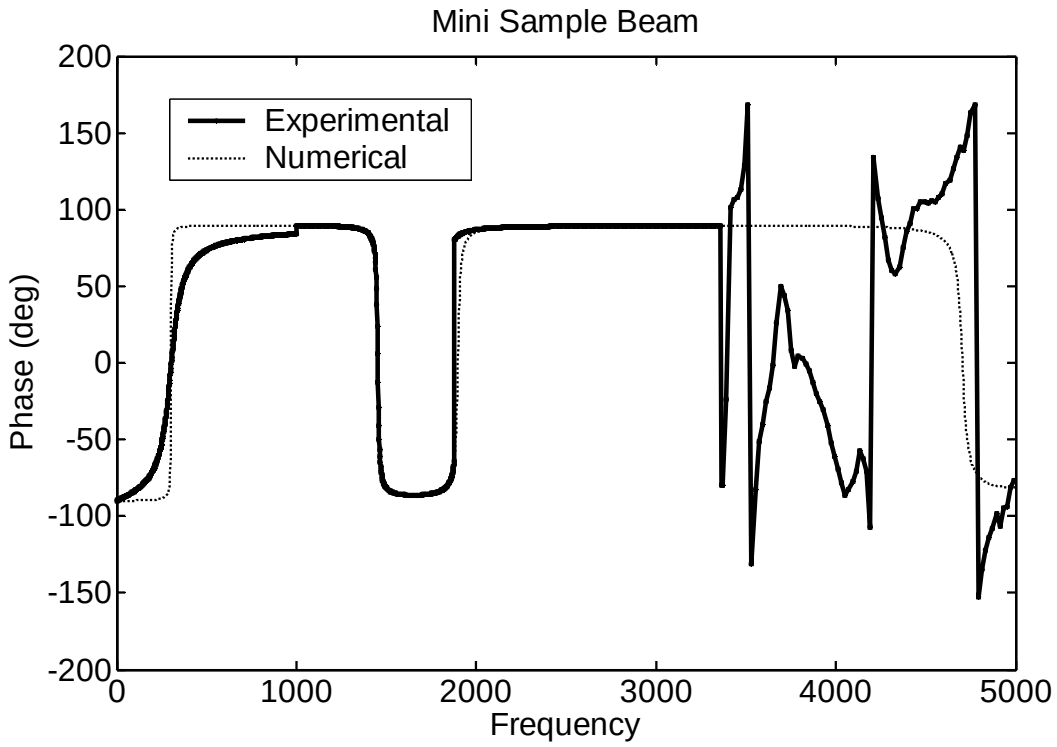

Fig. 6.30 Phase of mechanical impedance of the mini sample beam

6.5 Summary

In this chapter, a miniature PZT-coated cantilever is realized using the optimization developed in the last chapter and utilized to drive and sense mini dynamic systems. The newly designed cantilever transducer is then utilized to confirm its potential application after it is fully calibrated. In the calibration, Z_{ef} is measured directly from the SI Impedance Analyzer, when the transducer works under a free condition. The other two intrinsic impedances Z_{mo} and Z_{ec} are also evaluated by the proposed calibration method

and all these experimental results have been compared with the numerical results. A good correlation is found between the two types of results.

After the transduction functions of the proposed transducer have been fully known, the feasibility of the designed transducer for mechanical impedance measurement of mini structures is also validated experimentally. The mini cantilever transducer is utilized to drive a suspension beam taken from a hard disk drive and to detect its mechanical impedance by measuring input electrical impedance through the obtained transduction functions. The experimental results coincide well with the impedance directly calculated by finite element simulation. Thus, the applicability of the optimization has been successfully examined.

CHAPTER 7

CONCLUSION AND RECOMMENDATION

7.1 Conclusion

7.1.1 Dynamics of a PZT-Coated Cantilever

In this thesis, the dynamics of the PZT-coated cantilever have been thoroughly studied and the possibility of the cantilever transducer for dynamic measurement is validated. It founds the theoretical basis to develop the method for the design of the SSA device. Supplied with electricity, the cantilever vibrates and exerts forces to test structure connected to its tip. Due to the load from the test structure, the PZT patch of the cantilever undergoes variations of input electrical impedance. Probing the input electrical impedance quantitatively detects the mechanical impedance imposed at the output port of the cantilever transducer provided that its transduction matrix is known. Transduction matrix is defined to characterize the forward actuating and backward sensing capability of an

electro-mechanical transducer. It is a two by two matrix consisting of four frequency response functions between the input electrical voltage and current and the output force and velocity of the transducer. The four components can be evaluated analytically, numerically or experimentally following different boundary conditions. The determinant of the matrix was proved to be unity as it should be for linear and reciprocal systems without internal energy generation and consumption. After it was made available, the mechanical impedance at the output port of an electromechanical transducer was evaluated from the electrical impedance actually measured at the input port through it. In this step, in order to be more generally useful for future studies, they were evaluated in close form by solving the governing equations of the PZT driven cantilever. After it had been made available, the matrix was exploited in a numerical experiment for measuring mechanical impedance of simple beam structure. Good coincidence was found between the experimental results and numerical results obtained by finite element simulation and possibility of cantilever transducer for dynamic measurement was confirmed.

7.1.2 Optimization of the PZT-Coated Cantilever

Moreover, an optimization strategy is successfully created and utilized in our study to decide the dimensions and system parameters of the transducer, which provides the optimal compromise between the sensing and actuating capability. As we known, a cantilever transducer which supplies more power for excitation is usually less sensitive to the load imposed at its tip. By comparing performance of new cantilever with that of original cantilever, it was seen that the effective frequency range is greatly increased and

sensitivity is also enough to sense the load. More importantly, the actuating capability of transducer is strongly emphasized. Numerical simulation shows that the designed cantilever transducer is a good actuator with relative high sensitivity, which the feasibility of optimization is examined.

7.1.3 Experimental Investigation of the PZT-Coated Cantilever

Furthermore, experimental studies verify the validity of the proposed optimization and the developed method is feasible to design the SSA device. Before the measurement, calibration of cantilever transducer is necessary and a method, which selects several rigid masses as the load of cantilever transducer, is proposed to calibrate the intrinsic attributes Z_{mo} , Z_{ec} and Z_{ef} . In the calibration, Z_{ef} is measured directly from the SI Impedance Analyzer, when the transducer is under free condition. The other two impedances Z_{mo} and Z_{ec} are also evaluated by the proposed method and all these experimental results have been compared with the numerical results obtained by the equations derived in Chapter 3. Comparison of two results shows that the numerical prediction is accurate and the proposed calibration method also works as roles. After the calibration of the cantilever transducer, case studies including rigid block and beam structure are carried out to further verify the feasibility of the designed cantilever transducer in mechanical impedance measurement and the validity of the optimization method. It is found that the calculated masses of rigid block totally coincide with the true values, which confirms the effectiveness of the new cantilever transducer in mechanical impedance measurement. Good agreement is also found between the experimental results

and numerical results of beam structure in a frequency range. In general, the designed cantilever transducer is capable of simultaneously sensing and actuating dynamic systems and the optimization is successful.

7.1.4 Application of the PZT-Coated Cantilever

To further explore the applicability of the optimization, finally, a mini cantilever is designed and utilized to drive and sense mini dynamic systems. Firstly, dimension and system parameters of cantilever transducer are derived through optimization. Followed, numerical simulation has been carried out to analyze the performance of designed transducer and the transducer is calibrated experimentally. After the transduction functions of the proposed transducer have been fully known, the feasibility of the proposed transducer for mechanical impedance measurement of mini structures is demonstrated experimentally. The detected experimental results agree well with the numerical results obtained by the finite element simulation, which examines the applicability of the design method.

7.2 Recommendation

From the work done in the thesis, it is seen that although the optimization works as proposed, several shortness also exist. In the previous study, for the convenience, only size optimization is considered and the optimization algorithm relies on the closed-form analytical solutions of the structural performance. This means that for structures having

complex geometry, the present algorithm is not applicable. In future work, the applicability of this design method in complex system should be studied using finite element analysis. This work can be easily finished since the criterion defining optimal performance of transducers has been found and well accepted. For the same reason, topological optimization can be done simply as well.

After the effectiveness of method for designing optimal transducers with optimal balanced sensing and actuating capabilities has been thoroughly investigated, it is necessary to apply this method to other existing SSA transducers, such as Piezoceramic Inertial Actuator (PIA), electromagnetic shaker, Bimorph Impedance Transducer (BIT) and so on. In literature review, it's known that Piezoceramic Inertial Actuator (PIA) was designed to measure mechanical impedance and monitor structural integrity without involving conventional sensors like accelerometers, load cells or impedance heads. Also an electromagnetic shaker together with an indenter has been successfully taken to for characterize soft incompressible viscoelastic materials. Furthermore, the effectiveness of BIT in measuring translational and rotational impedance has been thoroughly investigated. For these SSA devices, in their works, nothing has been done to examine the possibility of improving theirs actuating and sensing performance. However, now, the design method provides a straight valid way to improve the actuation efficiency and sensing capability of transducers.

Besides, since the proposed cantilever transducer has been proved to be a good tool for mechanical impedance measurement in dynamic systems and is technically feasible to fabricating a PZT driven cantilever with precise dimensions in mini or micro scale, it can

be widely applied into the fields of mechanics, dynamics, chemistry, biomedicine and so on. In a preliminary study, a cantilever transducer has been used to measure fluid viscosity. Viscosity of several familiar fluids has been successfully determined (Publication 2). For a further study, the research can focus on the design of portable viscometer or micro viscometer to measure the blood viscosity of human. Moreover, further study has been in progress to utilize micro cantilever transducer fabricated via MEMS technology to measure acoustic impedance of an acoustic wave. Last few decades have seen incremental improvements of microphone technology in measuring acoustic pressure. Compared with pressure measurement, advancement in technology for measuring particle velocity, acoustic impedance, a very critical piece of information describing acoustic field, was impossible to measure. In this new sensor, the PZT driven micro cantilever is employed to transducer the acoustic signals into electrical signals. The electrical-structural-acoustical interaction taken place in the sensor is modeled as a transduction matrix. Once the transduction matrix is characterized, acoustic impedance, pressure, and particle velocity can be conveniently detected by measuring the input electrical voltage and current.

REFERENCES

1. Cremer, L. and Heckl, M., *Structure-borne sound: structural vibrations and sound radiation at audio frequencies*. 2nd ed., Berlin; New York--Springer-Verlag (1988): 573.
2. Harris, C.M. and Piersol, A.G., *Harris' shock and vibration handbook*. 5th ed., New York--McGraw-Hill (2002): 1 v. (various pagings).
3. Cawley, P., "The sensitivity of the mechanical impedance method of non-destructive testing", *NDT Int.*, **20**(4) (1987): 209-215.
4. Ewins, D.J., *Modal testing: theory, practice, and application*. 2nd ed., Taunton, Somerset, England and New York--Research Studies Press; Wiley (2000): 562.
5. Liang, C., Sun, F.P., and Rogers, C.A., "Electro-mechanical impedance modeling of active material systems", *Smart Materials & Structures*, **5**(2) (1996): 171-186.
6. Liang, C., Sun, F.P., and Rogers, C.A., "An impedance method for dynamic analysis of active material systems", *Journal of Intelligent Material Systems and Structures*, **8**(4) (1997): 323-334.

7. Zhou, S.W., Liang, C., and Rogers, C.A., "An impedance-based system modeling approach for induced strain actuator-driven structures", *Journal of Vibration and Acoustics-Transactions of the Asme*, **118**(3) (1996): 323-331.
8. Yin, Y., Ling, S.-F., and Liu, Y., "A dynamic indentation method for characterizing soft incompressible viscoelastic materials", *Materials Science and Engineering A*, **379**(1-2) (2004): 334-340.
9. Ling, S.F. and Xie, Y., "Monitoring structural integrity using a piezoelectric inertial actuator cum sensor", *Journal of Sound and Vibration*, **247**(4) (2001): 731-737.
10. Ling, S.F. and Xie, Y., "Detecting mechanical impedance of structures using the sensing capability of a piezoceramic inertial actuator", *Sensors and Actuators a-Physical*, **93**(3) (2001): 243-249.
11. Ian, R.S., *Sensors and transducers*. 3rd ed. --Newnes, Oxford Auckland Bostion Johannesburg Melbourne New Delhi (2001).
12. Busch-Vishniac, I.J., "Spatially distributed transducers: part I--Coupled two-port models", *Journal of dyanic systems, measurement and control, Transactions of the ASME*, **112** (1990): 372-380.
13. Busch-Vishniac, I.J., "Bond graph models of sound and vibration systems", *J. Acoust. Soc. Am.*, **85** (1989): 1750.
14. Busch-Vishniac, I.J., *Electromechanical sensors and actuators*. New York--Springer (1999): xvi, 341.
15. Sinclair, I.R., *Sensors and transducers*. 3rd ed., Oxford--Newnes (2001): 306.
16. Babuska, V. and O'Donnell, R.P., "Self-sensing actuators for precision structures", in: *Aerospace Conference, 1998. Proceedings., IEEE*, **1** (1998): 179-187.
17. Guran, "Structronic systems: smart structures, devices and systems", in: *Series on stability, vibration, and control of systems*, World Scientific, Singapore, **4** (1998).

18. Jones, L., Garcia, E., and Waites, H., "Self-sensing control as applied to a PZT stack actuator used as a micropositioner", *Smart Materials & Structures*, **3** (1994): 147-156.

19. Lee, C.K., O'Sullivan, T.C., and Chaing, W.W., "Piezoelectric strain rate sensor and actuator designs for active vibration control," in: *Proceedings of the 32nd AIAA/ASME/ASCE/AHS Structures Structural Dynamics and Materials Conference*, Baltimore, MD(1991): 2197-2207.

20. Yellin, J.M. and Shen, I.Y., "A self-sensing active constrained layer damping treatment for a Euler-Bernoulli beam", *Smart Materials & Structures*, **5**(5) (1996): 628-637.

21. Takigami, T., Oshima, K., and Hayakawa, Y., "Application of self-sensing actuator to control of a cantilever beam", in: *Proceedings of the American Control Conference*, Albuquerque, New Mexico(1997).

22. Sermoneta, A., Liang, C., et al., "Dynamic analysis of active structures under multiple actuators excitations using an impedance approach", in: *Proceedings of smart structures and integrated systems, SPIE*, USA, **2443** (1995).

23. Liang, C., Sun, F.P., and Rogers, C.A., "An impedance method for dynamic analysis of active material systems", *Journal of Intelligent Material Systems and Structures*, **8**(4) (1997): 323-334.

24. Sun, F.P., Liang, C., and Rogers, C.A., "Structural modal analysis using collocated piezoelectric actuator/sensors- an electormechanical approach", in: *Smart Structures and Intelligent Systems, SPIE*, Orlando, **2190** (1994).

25. Lalande, F., Chaudhry, Z., and Rogers, C.A., "Impedance-based modelling of actuators bonded to shell structures", in: *The international society for optical engineering smart structure and intelligent systems, SPIE*, **2443** (1995): 396-408.

26. Lalande, F., Chaudhry, Z., and Rogers, C.A., "Impedance-based modelling of induced strain actuators bonded on ring structures", *Journal of Sound and Vibration*, **201**(2) (1997): 169-187.
27. Chen, Y.-C., Wu, S., and Chen, P.-C., "The impedance-matching design and simulation on high power elctro-acoustical transducer", *Sensors and Actuators A: Physical*, **115**(1) (2004): 38-45.
28. Daugela, A., Fujii, H., and Misaki, A., "Nondestructive mechanical contact impedance and compliance testing of rubberlike materials", *Jsme International Journal Series a-Mechanics and Material Engineering*, **39**(4) (1996): 640-648.
29. Bamnios, Y., Douka, E., and Trochidis, A., "Crack identification in beam structures using mechanical impedance", *Journal of Sound and Vibration*, **256**(2) (2002): 287-297.
30. Gardonio, P. and Brennan, M.J., "On the origins and development of mobility and impedance methods in structural dynamics", *Journal of Sound and Vibration*, **249**(3) (2002): 557-573.
31. Crawley, E.F. and Javier, d.L., "Use of piezoelectric actuators as elements of intelligent structures", in: *Structural dynamics and materials conference*, American, **25** (1987): 1373-1385.
32. Rossi, A., Liang, C., and Rogers, C.A., "A coupled electromechanical analysis of PZT actuator driven structures-an application to cylindrical structures", in: *34th SDM Conference*, LaJolla, CA(1993).
33. Linjama, J. and Lahti, T., "Measurement of bending wave reflection and impedance in a beam by the structural intensity technique", *Journal of Sound and Vibration*, **161**(2) (1993): 317-331.

34. Zeng, Q.H. and Bogy, D.B., "Experimental modal analysis technique, system and application for miniature structures", in: *Proc. of the 15th IMAC*(1997): 1731-1738.

35. Zeng, Q.H. and Bogy, D.B., "Dynamic characteristics of a suspension assembly part 1: modal experiment", *Advances in Information Storage Systems*, **8** (1998): 105-120.

36. Tabib-Azar, M., *Microactuators : electrical, magnetic, thermal, optical, mechanical, chemical & smart structures*. Boston--Kluwer Academic (1998): 287.

37. Skitek, G.G. and Marshall, S.V., *Electromagnetic concepts and applications*. Englewood Cliffs, N.J.--Prentice-Hall (1982): xvii, 510.

38. Paul, C.R. and Nasar, S.A., *Introduction to electromagnetic fields*. New York--McGraw-Hill (1982): xv, 567.

39. Englemann, R.H., *Static and rotating electromagnetic device*. New York--M. Dekker (1982).

40. Hanson, B. and Levesley, M., "Self-sensing applications for electromagnetic actuators", *Sensors and Actuators A: Physical*, **In Press, Corrected Proof** (2004).

41. Bruant, I., Coffignal, G., et al., "A methodology for determination of piezoelectric actuator and sensor location on beam structures", *Journal of Sound and Vibration*, **243**(5) (2001): 861-882.

42. Chen, S.H. and Cao, Z.J., "A new method for determining locations of the piezoelectric sensor/actuator for vibration control of intelligent structures", *Journal of Intelligent Material Systems and Structures*, **11**(2) (2000): 108-115.

43. Tan, C.H., *A study of piezoelectric material in mechanical impedance control*. Singapore--School of Mechanical and Production Engineering Nanyang Technological University (1996): 1 v. (various pagings).

44. Wang, X.M., Ehlers, C., and Neitzel, M., "Dynamic analysis of piezoelectric actuator bonded on beam", in: *Proceedings of the third international conference on intelligent materials*, Lyon, France(1996).

45. Wang, B.T. and Chen, R.L., "The use of piezoceramic transducers for smart structural testing", *Journal of Intelligent Material Systems and Structures*, **11**(9) (2000): 713-724.

46. Cudney, H.H., Inman, D.J., and Oshman, Y., "Distributed structural control using multilayered piezoelectric actuators", in: *Proceedings of the AIAA/ASME/ASCE/AHS/ASC 31st structural dynamics and materials conference*, Ling Beach, CA.(1990).

47. Newnham, R.E., "Piezoelectric sensors and actuators: smart materials", in: *Frequency Control Symposium, . 46th., Proceedings of the 1992 IEEE*, Hershey, PA , USA(1992): 513-524.

48. de Vera, C.P. and Guemes, J.A., "Embedded self-sensing piezoelectric for damage detection", *Journal of Intelligent Material Systems and Structures*, **9**(11) (1998): 876-882.

49. Sirohi, J. and Chopra, I., "Fundamental behavior of piezoceramic sheet actuators", *Journal of Intelligent Material Systems and Structures*, **11**(1) (2000): 47-61.

50. Ritdumrongkul, S., Abe, M., et al., "Quantitative health monitoring of bolted joints using a piezoceramic actuator-sensor", *Smart Materials & Structures*, **13**(1) (2004): 20-29.

51. Lu, P. and Lee, K.H., "An alternative derivation of dynamic admittance matrix of piezoelectric cantilever bimorph", *Journal of Sound and Vibration*, **266**(4) (2003): 723-735.

52. Lesieutre, G.A., Rusovici, R., et al., "Modelling and characterization of a piezoceramic inertial actuator", *Journal of Sound and Vibration*, **261**(1) (2003): 93-107.

53. Hanagud, S., Obal, M.W., and Calise, A.J., "Optimal vibration control by the use of piezoceramic sensors and actuators", in: *28th AIAA/ASME/ASCE/AHS Structures Structural Dynamics and Materials Conference*, Monterey, CA,(1987): 987-997.

54. Smits, J.G. and Ballato, A., "Dynamic admittance matrix of piezoelectric cantilever bimorphs", *Microelectromechanical Systems, Journal of*, **3**(3) (1994): 105-112.

55. Sunar, M. and Rao, S.S., "Recent advances in sensing and control of flexible structures via piezoelectric materials technology", in: *ASME Applied Mechanics Reviews*, **52** (1999): 1-16.

56. Chaudhry, Z., Joseph, T., et al., "Local-area health monitoring of aircraft via piezoelectric actuator/sensor patches", in: *Proceedings of SPIE, North American Conference on Smart Structures and Materials*, Sun Diego, CA(1995): 268-276.

57. Chaudhry, Z., Sun, F.P., and Rogers, C.A., "Health monitoring of space structures using impedance measurements", in: *Fifth International Conference on Adaptive Structures*, Sendai, Japan(1994): 584-591.

58. Zhou, S.W., Liang, C., and Rogers, C.A., "A dynamic model of piezoelectric actuator-driven thin plates", in: *Proceeding of the Smart Structures and Materials Conference, SPIE*, Orlando, **2190** (1994): 550-562.

59. Liang, C., Sun, F.P., and Rogers, C.A., "Investigation of the energy transfer and consumption of adaptive structures", in: *Proceedings of the 31st conference on decision and control*, Tucson, Arizona(1992).

60. Liang, C., Sun, F.P., and Rogers, C.A., "Dynamic output characteristics of piezoceramic actuators", in: *Proceedings of Smart Structures and Intelligent Systems, SPIE,* Albuquerque, NM, **1817** (1993).

61. Liang, C., Sun, F.P., and Rogers, C.A., "Determination of Design of Optimal Actuator Location and Configuration Based on Actuator Power-Factor", *Journal of Intelligent Material Systems and Structures*, **6**(4) (1995): 456-464.

62. Liang, C., Sun, F.P., and Rogers, C.A., "Determination of design of optimal actuator location and configuration based on actuator power factor", *Journal of intelligent material systems and structures*, **8** (1997): 344-352.

63. Wilson, C.J. and Bogy, D.B., "An experimental modal analysis technique for miniature structures", *Journal of Vibration and Acoustics-Transactions of the Asme*, **118**(1) (1996): 1-9.

64. Jones, L.A. and Lang, J.H., "A state observer for permanent-magnet synchronous motor", *IEEE Transactions on Industrial Electronics*, **36**(3) (1989): 374-382.

65. Li, X.L., "On-line detection of the breakage of small diameter drills using current signature wavelet transform", *Int. J. Mach. Tools Manufact.*, **39** (1999): 157-164.

66. Corley, M.J. and Lorenz, R.D., "Rotor position and velocity estimation for a salient-pole permanent magnet synchronous machine at standstill and high speeds", *Industry Applications, IEEE Transactions on*, **34**(4) (1998): 784-789.

67. Choi, C. and Park, K., "Self-sensing magnetic levitation using a LC resonant circuit", *Sensors and Actuators a-Physical*, **72**(2) (1999): 169-177.

68. Hanson, B. and Levesley, M., "Self-sensing applications for electromagnetic actuators", *Sensors and Actuators a-Physical*, **116**(2) (2004): 345-351.

69. Vischer, D. and Bleuler, H., "Self-sensing active magnetic levitation", *Magnetics, IEEE Transactions on*, **29**(2) (1993): 1276-1281.

70. Sivadasan, K.K., "Analysis of self-sensing active magnetic bearings working on inductance measurement principle", *Magnetics, IEEE Transactions on*, **32**(2) (1996): 329-334.

71. Bai, M.R. and Wu, H.P., "Robust control of a sensorless bass-enhanced moving-coil loudspeaker system", *Journal of the Acoustical Society of America*, **105**(6) (1999): 3283-3289.

72. Leo, D.J. and Limpert, D., "A self-sensing technique for active acoustic attenuation", *Journal of Sound and Vibration*, **235**(5) (2000): 863-873.

73. Guckel, H., Earles, T., et al., "Electromagnetic linear actuators with inductive position sensing", *Sensors and Actuators a-Physical*, **53**(1-3) (1996): 386-391.

74. Hagood, N.W. and Anderson, E.H., "Simultaneous Sensing and Actuation Using Piezoelectric Materials", in: *Active and Adaptive Optical Components*, **1543** (1991): 409-421.

75. Hagood, N.W., Chung, W., and A.., v.F., "Modelling of piezoelectric actuator dynamics for active structural control," *Journal of Intelligent Material Systems and Smart Structures*, **1**(3) (1990): 327-354.

76. Hagood, N.W. and von Flotow, A., "Damping of structural vibrations with piezoelectric materials and passive electrical networks", *Journal of Sound and Vibration*, **146**(2) (1991): 243-268.

77. Anderson, E.H. and Hagood, N.W., "Simultaneous Piezoelectric Sensing/Actuation: Analysis And Application To Controlled Structures", *Journal of Sound and Vibration*, **174**(5) (1994): 617-639.

78. Hou, X., "A new transducer for measuring mechanical impedance", Ph.D thesis, School of Mechanical & Aerospace Engineering, Nanyang Technological University (2004).

79. Hou, X. and Ling, S.F., "A sensing cum actuating transducer for detecting rotational mechanical impedance of structures", in: *First International Conference on Structural Health Monitoring and Intelligent Infrastructure*, Tokyo, Japan(2003): 893-897.

80. Ling, S.F. and Lu, B., "Modeling of a PZT-driven cantilever actuator", in: *Proceedings of SPIE - The International Society for Optical Engineering*, **4753 I** (2002): 724-730.

81. Ling, S.F. and Tang, Y.J., "A new modal testing technique for miniature structures", in: *Proceedings of the international modal analysis conference - IMAC-XIX*, Kissimmee, USA(2001): 1478-1482.

82. Ling, S.F. and Xie, Y., "Mechanical impedance detection utilizing sensing capability of piezoceramic inertial actuator", in: *Proceedings of the 18th international modal analysis conference - IMAC*, San Antonio, TX, USA, **2** (2000): 1901-1905.

83. Ling, S.F. and Xie, Y., "Modeling and identification of a piezoceramic sensor cum actuator", in: *Proceedings of 2001 SEM Annual Conference*, Portland, Oregon, USA(2001): 145-148.

84. Luan, J., "Modeling and monitoring of ultrasonic welding of thermoplastics", Ph.D thesis, School of Mechanical & Aerospace Engineering, Nanyang Technological University (2002).

85. Li, X.C., Ling, S.-F., and Sun, Z., "Dynamic modulus measurement of thermoplastics under a ultrasonic welding system", in: *Symposium I, International Conference on Materials for Advanced Technologies*, Singapore(2003).

86. Li, X.C., Ling, S.F., and Sun, Z., "Heating mechanism in ultrasonic welding of thermoplastics", in: *The international Conferences on the Joining of Materials*, Helsingor, Denmark(2003).

87. Li, X.C., "Process and mechanism of ultrasonic welding of thermoplastics", Ph.D thesis, School of Mechanical & Aerospace Engineering, Nanyang Technological University (2005).

88. Yin, Y., "A new method for testing mechanical properties of viscoelatic materials", Ph.D thesis, School of Mechanical & Aerospace Engineering, Nanyang Technological University (2005).

89. Ying, M., Ling, S.F., et al., "Horn design for minimal input impedance of ultrasonic welding systems", in: *The IIW Asian pacific international congress 2002*, Singapore(2002).

90. Yin, Y., "A novel method for testing mechanical properties of viscoelastic materials", First year report in fulfillment for the requirement of Ph.D, School of Mechanical & Aerospace Engineering, Nanyang Technological University (2002).

91. Xie, Y. and Ling, S.F., "Study on tuning mechanical impedance of inertial actuator with passive shunt circuits", in: *Proceedings of the Asia-Pacific vibration conference*, Singapore(1999): 129-133.

92. Zhang, D., "Study of mechanism of ultrasonic wire bonding process", Ph.D thesis, School of Mechanical & Aerospace Engineering, Nanyang Technological University (2001).

93. Zhang, D. and Ling, S.F., "Detecting force and velocity at wire bonding interface", in: *The IIW Asian pacific international congress*, Singapore(2002): 29-31.

94. Ling, S.-F., Hou, X., and Xie, Y., "Decoupling loading effect in simultaneous sensing and actuating for dynamic measurement", *Sensors and Actuators A: Physical*, **120**(1) (2005): 257-265.

95. Xie, Y. and Ling, S.F., "Material characterization by depth sensing impedance measurement", in: *Proceedings of 2001 SEM annual conference*, Portland, Oregon, USA(2001): 215-218.

96. Ling, S.F. and Wan, L.X., "Monitoring and diagnosing a spot welding process via electrical input impedance", in: *SEM IX International Congress*, Orlando, Florida(2000).

97. Zhang, D. and Ling, S.F., "Monitoring wire bonding via time-frequency analysis of horn vibration", *IEEE Transactions on Electronics Packaging Manufacturing*, **26**(3) (2003): 216-220.

98. Ling, S.F., Luan, J., et al., "Input electrical impedance as signature for nondestructive evaluation of weld quality during ultrasonic welding of plastics", *NDT & E International*, **(accepted)** (2005).

99. Fu, L., Ling, S.F., and Tseng, C.-H., "On-line breakage monitoring of small drills with input impedance of driving motor", *Mechanical Systems and Signal Processing*, **(in press)** (2005).

100. Fu, L.Y., Ling, S.-F., and Liang, F.G., "Application of wavelet and Hilbert transform in sensing cum actuating technology", in: *ICITA*, Australia(2002): 369-371.

101. Xiao, Z.Y. and Ling, S.F., "The Application of fuzzy reasoning system in monitoring EDM", in: *Knowledge-Based Intelligent Information and Engineering Systems: 7th International Conference*, KES 2003 Oxford, UK, **2773** (2003): 699 - 706.

102. Harman, W.W. and Lytle, D.W., *Electrical and Mechanical Networks*. New York--McGraw-Hill (1962).

103. Wang, D., "Sensing capability of an actuating cantilever", First year report in fulfillment for the requirement of Ph.D, School of Mechanical & Aerospace Engineering, Nanyang Technological University (2002).

104. Ling, S.-F., D. Wang, and B. Lu, Dynamics of a PZT-coated cantilever utilized as a transducer for simultaneous sensing and actuating. Smart Materials and Structures, 14(2005): p. 1127-1132.

105. Singh, G.K. and Kazzaz, S., "Induction machine drive condition monitoring and diagnosis research—a survey", *Electrical Power System Research*, 6**4** (2003): 145-158.

106. Xie, J., Hu, M., et al., "Fabrication and characterization of piezoelectric cantilever for micro sensors and actuators", in: 3*rd International Conference on Experimental Mechanics, ICEM 2004*, Singapore(2004).

107. Rozvany, G.I.N., *Optimal design of flexural systems : beams, grillages, slabs, plates, and shells*. 1st ed., Oxford ; New York--Pergamon Press (1976): xvi, 297.

108. Bunday, B.D., *Basic optimisation methods*. London ; Baltimore--Edward Arnold (1984): vi, 128.

109. Greig, D.M., *Optimisation*. London ; New York--Longman (1980): xi, 179.

110. Papalambros, P.Y. and Wilde, D.J., *Principles of optimal design : modeling and computation*. Cambridge ; New York--Cambridge University Press (1988): xxi, 416.

111. Liu, G.P., Yang, J.-B., and Whidborne, J.F., *Multiobjective optimisation and control*. Philadelphia, Pa.--Research Studies Press (2002): 320.

112. MathWorks-Inc., *Optimization toolbox user's guide-for use MATLAB Computation, Visualization, Programming*. 2nd ed. --The MathWorks, Inc (2000).

113. Xu, B. and Liu, Z., *Usage of MatLab into engineering mathematic*. --Qinghua University of China (2000).

114. Perriard, Y. and Nguyen, V., "Transducer design with global parametric optimization", in: *IEEE Transactions on Magnetics*, **39** (2003): 1019-1025.

115. Stender, J., Hillebrand, E., and Kingdon, J., *Genetic algorithms in optimisation, simulation and modelling*. Amsterdam, Tokyo--IOS Press, Ohmsha (1994): 261.

116. Yi, J.W., Shih, W.Y., and Shih, W.H., "Effect of length, width, and mode on the mass detection sensitivity of piezoelectric unimorph cantilevers", *Journal of Applied Physics*, **91**(3) (2002): 1680-1686.

117. Valch and Jiri., *Computerized approximation and synthesis of linear networks*. New York, Wiley (1969).

118. Jimmie, J.C., *Electricmachines-Analysis and design applying MATLAB*. New York--McGraw-Hill Higher Education (2001).

119. Meirovitch, L., *Fundamentals of vibrations*. Boston--McGraw-Hill (2001): xviii, 806.

120. Fox, R. and M. Kapoor, *Rate of change of eigenvalues and eigenvectors.* AIAA Journal, **6**(1968): p. 2426-2429.

121. Nelson, R., *Simplied calculations of eigenvector derivatives.* AIAA Journal, **14**(1976): p. 1201-1205.

APPENDIX A

RECIPROCITY THEOREM

For the reciprocity theorem in this thesis, suppose the transducer is passive where the one energy can flow in either direction, i.e., which can function as either a sensor or an actuator. Such a transducer can be regarded as a reciprocal transducer. As we know, for the linear system, the relationships between the input variables e_{in} and f_{in} and the output variables e_{out} and f_{out} can be written as

$$\begin{Bmatrix} e_{out} \\ f_{out} \end{Bmatrix} = \begin{bmatrix} b_{11} & -b_{12} \\ b_{21} & -b_{22} \end{bmatrix} \begin{Bmatrix} e_{in} \\ f_{in} \end{Bmatrix} \tag{a1}$$

where, the matrix containing b_{11}, $-b_{12}$, b_{21} and $-b_{22}$ is the transduction matrix of the transducer.

Selecting the output port of the transducer as the input port and the input port as the output port, and then rewriting the above equation, we have the following equations:

$$\begin{aligned}\begin{Bmatrix} e_{in} \\ f_{in} \end{Bmatrix} &= \begin{bmatrix} a_{11} & -a_{12} \\ a_{21} & -a_{22} \end{bmatrix} \begin{Bmatrix} e_{out} \\ f_{out} \end{Bmatrix} \\ &= \begin{bmatrix} a_{11} & -a_{12} \\ a_{21} & -a_{22} \end{bmatrix} \begin{bmatrix} b_{11} & -b_{12} \\ b_{21} & -b_{22} \end{bmatrix} \begin{Bmatrix} e_{in} \\ f_{in} \end{Bmatrix} \\ &= \begin{bmatrix} a_{11}b_{11} - a_{12}b_{12} & -a_{11}b_{12} + a_{12}b_{22} \\ a_{21}b_{11} - a_{22}b_{21} & -a_{21}b_{12} + a_{22}b_{22} \end{bmatrix} \begin{Bmatrix} e_{in} \\ f_{in} \end{Bmatrix}\end{aligned} \tag{a2}$$

Identify the last matrix in the above equation as the identity matrix leads to the following relations:

$$\begin{aligned} a_{11}b_{11} - a_{12}b_{12} &= 1, \\ -a_{11}b_{12} + a_{12}b_{22} &= 0, \\ a_{21}b_{11} - a_{22}b_{21} &= 0, \\ -a_{21}b_{12} + a_{22}b_{22} &= 1. \end{aligned} \tag{a3}$$

The relations might seem difficult to solve, being a set of four nonlinear algebraic equations in eight unknowns. However, there is a unique, easily verified solution, which is given below:

$$\begin{aligned} a_{11} &= b_{22} = A \\ a_{12} &= b_{12} = B \\ a_{21} &= b_{21} = C \\ a_{22} &= b_{11} = D \end{aligned} \tag{a4}$$

According to the above relations, the elements of the transduction matrix are not independent, and related by the following equation:

$$AD - BC = 1 \tag{a5}$$

The above equation is called the reciprocity relation, which is the characteristic of the reciprocity.

APPENDIX B

SQP ALGORITHM

1. Optimization Process

   ⇨ Initialize;

   ⇨ Solve the QP sub problem to determine a search direction s_k;

   ⇨ Minimize a merit function along s_k to determine a step length α_k;

   ⇨ Set $x_{k+1} = x_k + \alpha_k s_k$;

   ⇨ Check for termination. Go to 2 if not satisfied.

2. Quadratic Programming Solution

A final question is how to solve efficiently the quadratic programming sub problem. For example, at each major iteration of the SQP method a QP problem is solved of the form where A_i refers to the i[th] row of the m-by-n matrix A.

$$\text{minimize } q(x) = \frac{1}{2} x^T H x + c^T x$$

$$A_i x = b_i \qquad i = 1 \cdots m_e \tag{b1}$$

$$A_i x \le b_i \qquad i = m_e + 1 \cdots m$$

The method used in the Optimisation Toolbox is an active set strategy. It has been modified for both Linear Programming (LP) and Quadratic Programming (QP) problems.

The solution procedure involves two phases: the first phase involves the calculation of a feasible point (if one exists), the second phase involves the generation of an iterative sequence of feasible points that converge to the solution. In this method an active set is maintained, $\overline{A}_k$, which is an estimate of the active constraints (i.e., which are on the constraint boundaries) at the solution point. Virtually all QP algorithms are active set methods. This point is emphasized because there exists many different methods that are very similar in structure but that are described in widely different terms. $\overline{A}_k$ is updated at each iteration, *k*, and this is used to form a basis for a search direction $\hat{x}_k$. Equality constraints always remain in the active set, $\overline{A}_k$. The notation for the variable, $\hat{x}_k$, is used here to distinguish it from x_k in the major iterations of the SQP method. The search direction, $\hat{x}_k$, is calculated and minimizes the objective function while remaining on any active constraint boundaries. The feasible subspace for $\hat{x}_k$ is formed from a basis, Z_k whose columns are orthogonal to the estimate of the active set $\overline{A}_k$ (i.e., $\overline{A}_k Z_k = 0$). Thus a search direction, which is formed from a linear summation of any combination of the columns of Z_k , is guaranteed to remain on the boundaries of the active constraints.

The matrix Z_k is formed from the last *m*-*l* columns of the QR decomposition of the matrix $\overline{A}_k^T$, where *l* is the number of active constraints and $l < m$. That is, Z_k is given by

$$Z_k = Q[:, l+1 : m] \tag{b2}$$

where

$$Q^T \overline{A}_k^T = \begin{bmatrix} R \\ 0 \end{bmatrix} \tag{b3}$$

Having found Z_k , a new search direction $\hat{x}_k$ is sought that minimizes $q(x)$ where $\hat{x}_k$ is in the null space of the active constraints, that is, $\hat{x}_k$ is a linear combination of the columns of Z_k : $\hat{x}_k = Z_k p$: for some vector *p*.

Then if we view our quadratic as a function of *p*, by substituting for $\hat{x}_k$, we have

$$q(p) = \frac{1}{2} p^T Z_k^T H Z_k p + c^T Z_k p \tag{b4}$$

Differentiating this with respect to *p* yields

$$\nabla q(p) = Z_k^T H Z_k p + Z_k^T c \tag{b5}$$

$\nabla q(p)$ is referred to as the projected gradient of the quadratic function because it is the gradient projected in the subspace defined by Z_k. The term $_k^T HZ_k$ is called the projected Hessian. Assuming the Hessian matrix *H* is positive definite (which is the case in this implementation of SQP), then the minimum of the function *q(p)* in the subspace defined by Z_k occurs when $\nabla q(p) = 0$, which is the solution of the system of linear equations.

$$Z_k^T H Z_k p = -Z_k^T c \tag{b6}$$

A step is then taken of the form

$$x_{k+1} = x_k + \alpha \hat{x}_k \quad \text{where } \hat{x}_k = Z_k^T p \tag{b7}$$

At each iteration, because of the quadratic nature of the objective function, there are only two choices of step length α. A step of unity along $\hat{x}_k$ is the exact step to the minimum of the function restricted to the null space of $\overline{A}_k$. If such a step can be taken, without violation of the constraints, then this is the solution to QP (Eq. b2). Otherwise, the step along $\hat{x}_k$ to the nearest constraint is less than unity and a new constraint is included in the active set at the next iterate. The distance to the constraint boundaries in any direction $\hat{x}_k$ is given by

$$\alpha = \min_i \left\{ \frac{-(A_i x_k - b_i)}{A_i \hat{x}_k} \right\}, \quad (i = 1,...,m) \tag{b8}$$

which is defined for constraints not in the active set, and where the direction $\hat{x}_k$ is towards the constraint boundary, i.e., $A_i \hat{x}_k > 0, \ i = 1,...,m$.

When *n* independent constraints are included in the active set, without location of the minimum, Lagrange multipliers, λ_k are calculated that satisfy the non-singular set of linear equations

$$\overline{A}_k^T \lambda_k = c \tag{b9}$$

If all elements of are positive, x_k is the optimal solution of QP (Eq. b2). However, if any component of λ_k is negative, and it does not correspond to an equality constraint, then the corresponding element is deleted from the active set and a new iterate is sought.

Initialisation

The algorithm requires a feasible point to start. If the current point from the SQP method is not feasible, then a point can be found by solving the linear programming problem

$$\begin{aligned} &\underset{\gamma\in\mathrm{R},\, x\in\mathrm{R}^n}{\text{minimize}}\ \gamma \\ &A_i x = b_i \qquad i = 1\cdots m_e \\ &A_i x - \gamma \le b_i \qquad i = m_e + 1,\cdots m \end{aligned} \tag{b10}$$

The notation A_i indicates the ith row of the matrix *A*. A feasible point (if one exists) to Eq. b10 can be found by setting *x* to a value that satisfies the equality constraints. This can be achieved by solving an under- or over-determined set of linear equations formed from the set of equality constraints. If there is a solution to this problem, then the slack variable is set to the maximum inequality constraint at this point.

The above QP algorithm is modified for LP problems by setting the search direction to the steepest descent direction at each iteration where g_k is the gradient of the objective function (equal to the coefficients of the linear objective function).

$$\hat{x}_k = -Z_k Z_k^T g_k \tag{b11}$$

If a feasible point is found using the above LP method, the main QP phase is entered. The search direction is initialized with a search direction $\hat{x}_k$ found from solving the set of linear equations

$$H\hat{x}_1 = -g_k \tag{b12}$$

where g_k is the gradient of the objective function at the current iterate x_k (i.e., $Hx_k + c$).

If a feasible solution is not found for the QP problem, the direction of search for the main SQP routine $\hat{x}_k$ is taken as one that minimizes γ.

3. Line Search and Merit Function

The solution to the QP sub problem produces a vector s_k, which is used to form a new iterate

$$x_{k+1} = x_k + \alpha s_k \tag{b13}$$

The step length parameter α_k is determined in order to produce a sufficient decrease in a merit function. The merit function used by Han and Powell of the form below has been used in this implementation.

$$\Psi(x) = f(x) + \sum_{i=1}^{m_e} r_i \cdot g_i(x) + \sum_{i=m_e+1}^{m} r_i \cdot \max\{0, g_i(x)\} \tag{b14}$$

Powell recommends setting the penalty parameter

$$r_i = (r_{k+1})_i = \max_i \left\{ \lambda_i \cdot \frac{1}{2}((r_k)_i + \lambda_i) \right\}, \quad i = 1,...,m \tag{b15}$$

This allows positive contribution form constraints that are inactive in the QP solution but were recently active. In this implementation, initially the penalty parameter r_i is set to

$$r_i = \frac{\|\nabla f(x)\|}{\|\nabla g_i(x)\|} \tag{b16}$$

where $\| \ \|$ represents the Euclidean norm.

This ensures larger contributions to the penalty parameter from constraints with smaller gradients, which would be the case for active constraints at the solution point.

PUBLICATIONS

1 Shih-Fu Ling, Deyang Wang and Bei Lu (2005). Dynamics of PZT-Coated Cantilever Utilized as a Transducer for Simultaneous Sensing and Actuating, *Smart Materials and Structures*, **14**:1127-1132.

2 Shih-Fu Ling, Deyang Wang (2006). Optimization of a PZT-coated cantilever for best simultaneous sensing and actuating, submitted to *13th International Congress on Sound and Vibration*, Viena 2006.

3 Shih-Fu Ling, Deyang Wang and Soon Jeffrey (2006). Development of a Novel Viscosity Measuring Technique, submitted to *13th International Congress on Sound and Vibration*, Viena 2006.

4 Wang Deyang, Shih-Fu Ling (2006). Experimental study on sensing capability of a PZT-coated cantilever, ready for sumbittion.

5 Wang Deyang, Shih-Fu Ling (2006). Dynamic testing of a miniature beam utilizing a PZT-coated cantilever as a sensor cum actuator, in preparation.